Chapter 15

Linking Weather and Climate

RANDALL M. DOLE

NOAA/Earth System Research Laboratory, Boulder, Colorado

(Manuscript received 1 March 2006, in final form 14 September 2006)

Dole

ABSTRACT

Historically, the atmospheric sciences have tended to treat problems of weather and climate separately. The real physical system, however, is a continuum, with short-term (minutes to days) ''weather'' fluctuations influencing climate variations and change, and, conversely, more slowly varying aspects of the system (typical time scales of a season or longer) affecting the weather that is experienced. While this past approach has served important purposes, it is becoming increasingly apparent that in order to make progress in addressing many socially important problems, an improved understanding of the connections between weather and climate is required.

This overview summarizes the progress over the last few decades in the understanding of the phenomena and mechanisms linking weather and climate variations. The principal emphasis is on developments in understanding key phenomena and processes that bridge the time scales between synoptic-scale weather variability (periods of approximately 1 week) and climate variations of a season or longer. Advances in the ability to identify synoptic features, improve physical understanding, and develop forecast skill within this time range are reviewed, focusing on a subset of major, recurrent phenomena that impact extratropical wintertime weather and climate variations over the Pacific–North American region. While progress has been impressive, research has also illuminated areas where future gains are possible. This article concludes with suggestions on near-term directions for advancing the understanding and capabilities to predict the connections between weather and climate variations.

1. Introduction

Through his research and teaching, Professor Fred Sanders has contributed greatly to advancing our understanding and predictions of a broad range of atmospheric phenomena. Although most noted for his work on meso- and synoptic-scale phenomena, Professor Sanders also helped to stimulate new research linking slowly varying features of the planetary circulation with changes in synoptic-scale storm activity. This overview summarizes major developments in this area from early work (some of which was guided by Professor Sanders) through to our present understanding. A major underlying theme is the value of both synoptic and general circulation research methods in developing an understanding of how weather and climate phenomena are related, and how this knowledge can be used to improve forecasts.

In approaching this broad problem, it is useful to consider three related subquestions. First, how do climate variations affect weather phenomena? Second, how do weather phenomena affect climate variations?

Corresponding author address: Randall M. Dole, NOAA Eartn System Research Laboratory, Boulder, CO 80305.
E-mail: randall.m.dole@noaa.gov

And third, what are key phenomena and processes that bridge the time scales between synoptic-scale weather variability and climate variations of a season or longer? As one example of the first question, we might ask: How do climate variations influence hurricane behavior? Individual hurricanes evolve on weather time scales and cannot be predicted, say, a month or season in advance. However, climate phenomena such as El Niño–Southern Oscillation (ENSO), the quasi-biennial oscillation (QBO), and slowly evolving tropical ocean conditions have been shown to alter the probability that a given hurricane season will be more or less active (e.g., Gray 1984a,b; Bove et al. 1998; Vitart and Stockdale 2001). Because of such relationships, skillful seasonal hurricane activity outlooks can be made months and even seasons in advance (e.g., Owens and Landsea 2003; Klotzbach and Gray 2003, 2004).

As an example of the second question, we might ask: What are the effects of hurricanes on the climate system? Hurricanes clearly impact the atmospheric heat budget through the transfer of heat from the tropical oceans into the tropical upper atmosphere and to higher latitudes. More subtly, by altering the upper-ocean heat balance hurricanes can change the ocean thermohaline circulation, and thereby induce longer-term climate variations (Emanuel 2001, 2002). As another example, modeling studies show that transient eddy fluxes associated with synoptic-scale disturbances play a major role in determining the extratropical response to ENSO (Kok and Opsteegh 1985; Held et al. 1989; Hoerling and Ting 1994). More generally, many hydrological processes, such as clouds, moist convection, and water vapor transports operate on fast ''weather'' time scales, and yet also profoundly impact climate variations.

While we will touch on these first two questions, our main emphasis will be on the third question. More specifically, we will focus on key phenomena and processes that operate on time scales longer than typical synoptic-scale periods but less than a season, with a primary emphasis on understanding extratropical flow variations between approximately 1 week and a few months. On these time scales, initial conditions and boundary variations can each play important roles, and hence both need to be considered in attempts to advance predictive skill. Because of the vast body of related literature, we cannot hope to cover all relevant topics. Rather, our primary intent is to expose future researchers, and especially current students, to some key concepts and scientific steps that have led to progress in advancing understanding and predictions at the interface between weather and climate, and to suggest promising directions for future progress.

Some basic questions can be motivated by examining Fig. 1. This figure shows daily time series of precipitation in Los Angeles for two winters in which sea surface temperatures (SSTs) in the central and eastern equatorial Pacific were anomalously warm (El Niño conditions), and a third winter in which SSTs in the same region were anomalously cold (La Niña conditions). It is immediately apparent that the seasonal-average rainfall is greater in the two El Niño years than in the La Niña year. More comprehensive statistical analyses show a significantly increased probability of above-normal precipitation during El Niño years over much of southern California and the southwestern United States (Schonher and Nicholson 1989; Cayan et al. 1999), although it should be noted that El Niño conditions are neither necessary nor sufficient for wet conditions to occur in this region (Schonher and Nicholson 1989). The seasonal averages themselves, however, provide only bland characterizations of the season as a whole. In particular, they do not reveal important differences in temporal behavior that occur within the seasons, the *intraseasonal variability* that is our primary focus here.

For example, even during the El Niño years there are extended periods of up to a month in which no rainfall occurs. While this behavior is well known to meteorologists, this knowledge has not always been conveyed adequately to the public, as evidenced by frequent comic references to ''El No-Show'' when midwinter 1997/98 was relatively dry in southern California despite official seasonal forecasts for abnormally wet wintertime conditions (which subsequently materialized in late January). Interspersed with these extended dry regimes are periods of several days to a few weeks in which the rainfall shows multiple peaks separated by a few days, the peaks being reflective of individual synoptic storms, which would be a primary focus for short-range forecasters. The longer-period organization of storm tracks is a crucial problem that we need to consider.

There are also indications of other differences that are highly relevant to emergency planning and resource management; for example, more frequent rainy days and more extreme rainfall events in the El Niño years, relationships that again appear in more detailed studies (Gershunov and Barnett 1998; Cayan et al. 1999; Gershunov and Cayan 2003; Andrews et al. 2004). While the extreme events themselves are clearly manifestations of individual weather events, how climate variability and change affect the likelihood of their occurrence is clearly a question of major societal significance. From a forecast perspective, we need to consider to what extent these probability shifts might be predictable, how they might be forecasted, how to identify the maximal time limits of predictability, and how to determine the factors that presently limit forecast skill.

This overview will begin with an informal, personal synopsis of the situation circa 1980, a time when the present author was a graduate student under Professor Sanders's guidance. Several major developments that occurred around and shortly after this time were vital to advancing our understanding of relationships between weather and climate variations. In the spirit of Professor Sanders's research and teaching, we will then turn our attention to describing key phenomena that bridge the time scales between weather and climate, and our

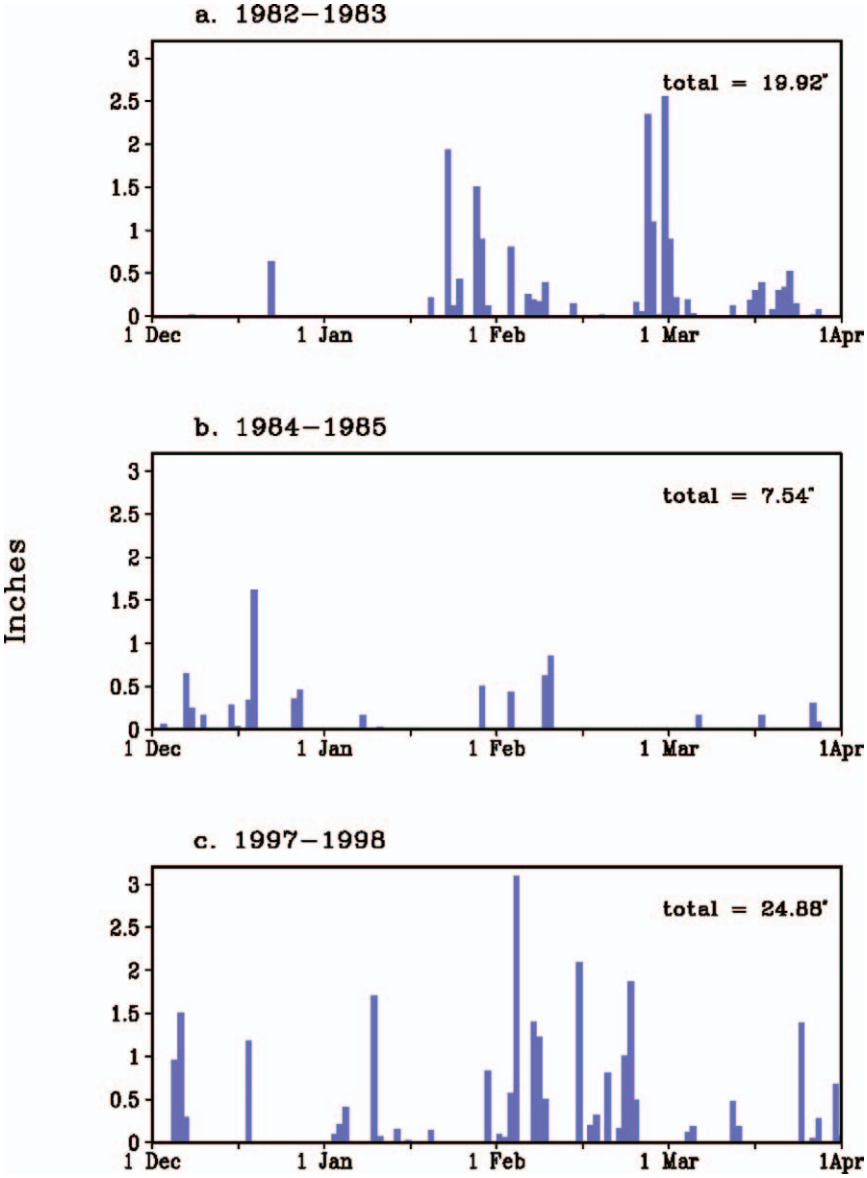

FIG. 1. Daily precipitation at Los Angeles airport for three extended winter seasons (December–April) associated with either El Niño (EN) or La Niña (LN) conditions: (a) 1982/83 EN, (b) 1984/85 LN. and (c) 1997/98 EN.

emerging understanding of the associated dynamical mechanisms. This will be followed by a discussion on the advances in forecast skill and analyses of potential predictability. We conclude with an outlook on prospects and potential directions for further progress in this area.

2. Background

A fundamental problem in meteorology is to advance the lead time of skillful weather forecasts. Sanders (1979), in an update of an earlier study (Sanders 1973), assessed weather forecast skill up to 1978. This assessment was confined to temperature and precipitation forecasts for a single station (Logan Airport in Boston) produced by a relatively small sample of forecasters, which consisted of the Massachusetts Institute of Technology (MIT) faculty (including Sanders) and students (including myself for a time). Despite the limited scope of the study, the results appear broadly representative of what was then the state of the art. Put simply, by lead times of 4 days, skill in temperature forecasts, as measured relative to the baseline forecast of climatological-mean values, was marginal, while skill in precipitation forecasts relative to that same baseline was nonexistent. Furthermore, trends in forecast skill evaluated over the period 1966–78 were very small, and in most cases not statistically significant.

Thus, in 1980 forecasts beyond a few days were effectively in the ''extended range.'' While the U.S. National Weather Service did provide outlooks in the form of forecast maps for days 3, 4, and 5, the skill in these products was also limited, in agreement with Sanders's results. Among some MIT forecasters these maps were referred to whimsically as ''5-day fantasy charts,'' in part because in wintertime they had a tendency to show strong cyclogenesis occurring near the East Coast by day 5, with implied major snowstorms for Boston and much of the Northeast corridor that usually failed to materialize.

The status of climate forecasting circa 1980 was, if anything, less advanced. As discussed by Gilman (1985) climate forecasts were at the time largely an empirical art, with no usable, quantitative theory underlying the forecasts, nor any guidance from dynamical model projections. Forecasts were based primarily on statistical relationships, such as linear correlations linking slowly varying oceanic and land surface boundary conditions with time-mean circulation anomalies. El Niño and its atmospheric counterpart, the Southern Oscillation, had attracted the interest of scientists for quite some time (Walker and Bliss 1932; Bjerknes 1969; Wyrtki 1975; Trenberth 1976). However, knowledge was limited and hence information on ENSO had yet to be effectively incorporated into climate forecasts. Indeed, in 1982, the development of one of the largest El Niño events of the century was not fully recognized while it was occurring, much less predicted (National Research Council 1996).

Thus, in the late 1970s, there was no significant forecast skill on time scales longer than a typical synoptic period (approxomately 3–5 days) and shorter than a season. There was, however, abundant observational evidence for recurrent flow patterns that persisted beyond the periods associated with synoptic-scale variability. The most commonly cited example was ''blocking,'' which is characterized by a quasi-stationary, persistent, and anomalously strong anticyclone located at mid- to high latitudes, often with a ''split'' westerly flow defined by separate, well-defined jet maxima located well to the north and south of the anticyclone center (e.g., Namias 1947; Elliott and Smith 1949; Rex 1950a,b; Sumner 1954). Once established, blocking can last for weeks or longer, with the associated persistent flow patterns appearing to divert (block) migratory storm systems far north and south of their normal tracks (Berggren et al. 1949; Petterssen 1956).

Blocking clearly had major implications for extended range forecasting and, indeed, has long been a focus for prediction efforts at the European Centre for Medium-Range Weather Forecasts (ECMWF) and other major operational forecast centers. By 1980, the problem of explaining blocking characteristics, including typical structures, geographical locations, and persistence, had also attracted substantial attention from dynamicists (Green 1977; Charney and DeVore 1979; Tung and Lindzen 1979a,b; McWilliams 1980). Thus, several factors appeared favorable for advancing our understanding of blocking, and thereby potentially improving lead times for extended-range forecasts.

A question remained, however, as to whether blocking was unique, or rather part of a broader class of recurrent phenomena that had time scales longer than typical synoptic periods. If so, could such features be identified and described within a more general and systematic framework? Furthermore, could relationships between the persistent flow anomalies and changes in synoptic-scale storm activity be more rigorously established, and fundamental dynamical mechanisms identified? These were the primary problems considered by myself in my thesis research guided by Professor Sanders. Subsequent progress on these and related questions will be discussed in the remainder of this overview.

3. Major phenomena and mechanisms

To keep the discussion reasonably compact, we will focus on a subset of major, recurrent phenomena that impact extratropical wintertime weather and climate variations over the Pacific–North American region. The characteristic features described here illustrate more general processes that also affect other regions and seasons.

a. Teleconnections and persistent anomalies

We begin by considering the question of whether early studies on blocking could be placed within a more general and systematic framework. Progress in this area has benefited from research that has approached this question from two fronts, one from the ''weather side out,'' and the other from the ''climate side in.'' The former has focused more on initial conditions and details of evolution out to a few weeks, often using synoptic analysis methods, while the latter has placed more emphasis on the effects of boundary conditions and used methods commonly applied in climate and general circulation studies.

The major foundations for identifying systematic behaviors of variability between a week and a season were laid in the late 1970s through pioneering studies of the Northern Hemisphere general circulation led by Blackmon, Lau, and colleagues (Blackmon 1976; Blackmon et al. 1977, 1979; Lau 1978, 1979; Lau and Wallace 1979). Blackmon (1976) described the spatial and temporal characteristics of wintertime variability in the Northern Hemisphere 500-hPa time field. He apportioned the temporal variance into three spectral bands: 1) periods of less than 2 days (high-pass variability); 2) periods between 2.5 and 6 days (bandpass variability); and 3) periods between 10 and 90 days (intraseasonal low-frequency variability), the latter being the time scales of most direct interest here.

Blackmon's analyses of low-frequency variability showed three major regional maxima, with the primary

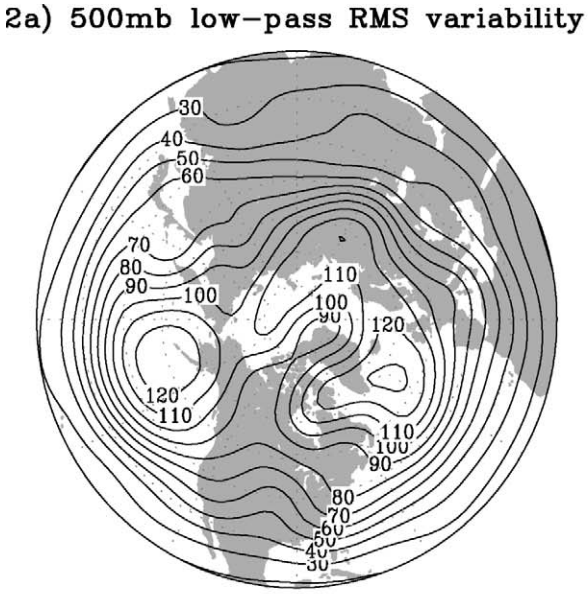

FIG. 2. Winter (DJF) root-mean-square variability of 500-hPa geopotential height fields for (a) low-pass-filtered data and (b) bandpass-filtered data, using the Blackmon (1976) time filters applied to NCEP–NCAR reanalysis data for the years 1950–2004.

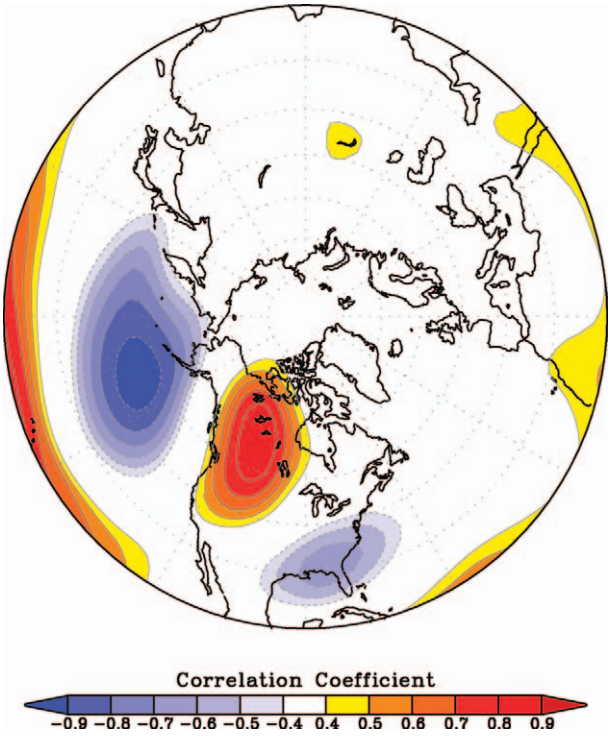

FIG. 3. Winter (DJF) correlations between the 300-hPa geopotential height field and the PNA index of Barnston and Livezey (1987), derived from the NCEP–NCAR reanalysis data for the same period as in Fig. 2.

centers located over the North Pacific to the south of the Aleutians, over the eastern North Atlantic to the southeast of Greenland, and over northwest Russia (Fig. 2a). The two oceanic low-frequency maxima were centered in the climatological-mean jet exit regions downstream of maxima in bandpass variability (Fig. 2b). Blackmon (1976) and subsequent studies showed that the bandpass variations were associated with migratory synoptic-scale storm systems, with maximum variance occurring near the locations of mean storm tracks described in earlier synoptic climatology studies (Petterssen 1956; Palmen and Newton 1969). The bandpass variations exhibited westward phase shifts with height (Blackmon et al. 1979), consistent with the interpretation that they were produced by baroclinic growth processes (Charney 1947; Eady 1949). In contrast, the low-frequency variations had a more equivalent-barotropic structure, with little or no phase tilt with height throughout the troposphere (Blackmon et al. 1979; Schubert 1986).

The early studies by Blackmon, Lau, and collaborators established important characteristics of low-frequency variability, but did not specifically consider associated spatial patterns. Wallace and Gutzler (1981, hereafter WG81) provided a major step forward in this area in their landmark study on ‘‘teleconnections,’’ which are defined by significant contemporaneous correlations of a given variable (e.g., 500-hPa heights or sea level pressure) occurring at widely separated geographical locations. While there had been considerable prior research on teleconnections, including monumental efforts on the Southern Oscillation by Walker and Bliss (1932), the WG81 study was particularly significant in providing a simple, objective, and systematic means of identifying major teleconnection patterns, in their study derived from Northern Hemisphere 500-hPa geopotential height and sea level pressure fields. Figure 3 shows one example of a teleconnection pattern dis-

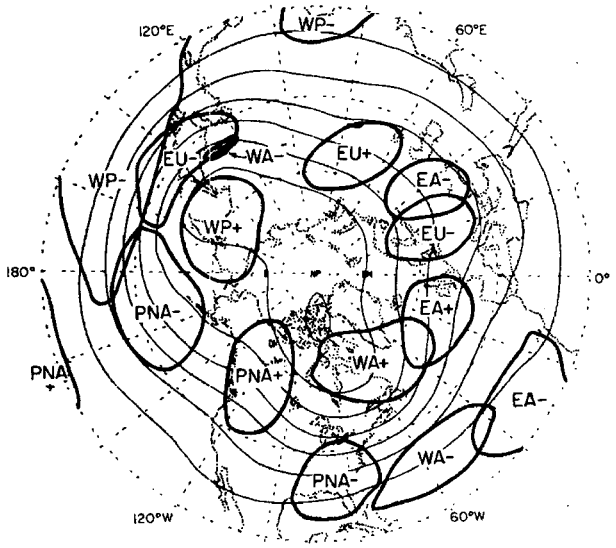

FIG. 4. Schematic of major teleconnection patterns, from Wallace and Gutzler (1981). The map shows ±0.6 isopleths of correlation coefficient for each of the five teleconnection pattern indices and local 500-hPa geopotential heights (heavy lines), superimposed on wintertime mean 500-hPa contours (lighter lines). The contour interval is 120 m.

cussed in detail by WG81, the Pacific–North American (PNA) pattern, as obtained from more recent data. Because of the importance of the PNA pattern for weather and climate variability, as well as its implications for extended-range predictability, we will later discuss this pattern and related dynamical mechanisms in more detail.

WG81 focused on teleconnections in extratropical Northern Hemisphere monthly-average 500-hPa data for three winter months (December–February). They described several strong teleconnection patterns (Fig. 4), many of which had been identified in earlier investigations. These were the western Pacific (WP) and western Atlantic (WA) patterns, which WG81 related to the North Pacific Oscillation (NPO) and North Atlantic Oscillation (NAO) patterns identified previously by Walker and Bliss and analyzed in more detail later by van Loon and Rogers (1978) and Rogers (1981); the PNA pattern, also evident in earlier studies (Klein 1952; Dickson and Namias 1976); an eastern Atlantic (EA) pattern that resembled a pattern described by Sawyer (1970); and a Eurasian pattern (EU). While WG81 did not perform detailed theoretical comparisons, they noted that several of the patterns strongly resembled Rossby wave trains obtained in linearized models on a sphere forced by steady, localized heating or topography (Egger 1977; Hoskins et al. 1977; Opsteegh and Van Den Dool 1980; Hoskins and Karoly 1981; Webster 1981).

Wallace and Gutzler's study presents an important example of what we have termed a climate approach to the problem, with its emphasis on the use of statistical techniques (linear correlations) applied to monthly-average height anomalies. Such approaches have the capability of identifying major recurrent features, with measures of reproducibility being provided through the estimated statistical significance of the relationships. Furthermore, the use of temporal averaging removes ''noise'' produced by higher-frequency fluctuations that are not of proximate interest. At the same time, potentially important information may be lost; for example, on how the associated flow patterns develop and evolve in time.

Dole (1982, 1983), influenced by Professor Sanders's synoptic methods, used an alternative approach for identifying persistent features that enabled a more detailed analysis of temporal evolution. Dole defined a ''persistent anomaly'' event for a given location whenever a 500-hPa height anomaly at that location exceeded a threshold value for longer than a specified duration (e.g., a 500-hPa anomaly of greater than 100 m for more than 10 consecutive days). In common with WG81, an important aspect of this method is that specific patterns are not defined a priori but, rather, are determined through subsequent data analyses. In this aspect, WG81's and Dole's approaches differed substantially from early studies of blocking, in which predefined flow patterns constituted the primary basis for case identification. This enabled WG81 and Dole to address the more general question of whether, and to what extent, blocking patterns were part of a broader class of recurrent low-frequency phenomena.

Dole and Gordon (1983, hereafter DG83) described the geographical distribution and regional persistence characteristics of persistent anomalies. In common with Blackmon (1976), DG83 identified three major regions of frequent occurrence: the North Pacific to the south of the Aleutians, the North Atlantic to the southeast of Greenland, and the region over northern Asia extending northeastward to the Arctic Ocean. While some of the cases identified in DG83 were clearly associated with blocking events, many others were not. For example, DG83's persistent negative anomaly cases over both the Pacific and Atlantic were associated with the persistent, abnormally strong cyclonic circulations in these regions, with intense, eastward-extended jets on their southern flanks. The persistence characteristics of anomalies in each of the regions broadly resembled those seen in a red noise process, with some modest deviations from red noise behavior for large magnitude events, as well as some apparently modest differences between positive and negative anomalies for the strongest events. DG83 also considered temporal characteristics of two primary regional patterns of variability, one essentially identical to the PNA pattern and the other to the EA pattern, but could find no compelling evidence for either strongly preferred durations or the existence of multiple equilibria (Charney and DeVore 1979).

More detailed analyses of persistent anomaly life cycles were provided in the following studies (Dole 1983, 1986a, 1989; Dole and Black 1990, hereafter DB90).

These studies indicated that the events often developed rapidly (a time scale of less than a week), and could break down similarly rapidly, with a typical life cycle from development through decay occurring within a month (for a more recent analysis of temporal characteristics, see Feldstein 2000). Despite the relatively rapid developments, once such events are established, they could project strongly on monthly and, in some cases, even seasonal mean variability, and strongly alter synoptic-scale storm tracks.

Figure 5 illustrates systematic features during development for persistent negative anomaly cases over the central North Pacific (centered near 45°N, 170°W) analyzed by DB90 and Black and Dole (1993). As discussed in DB90, the developments are typically preceded by an intensifying upper-level trough and jet streak over eastern Asia and the far western Pacific 3–5 days before case onset (Figs. 5a,b). At these times, height anomalies over the central Pacific are weak and, if anything, of opposite sign to the subsequent developments. Between days −5 and −1 (Fig. 5c), the upper-level trough and jet maxima propagate eastward and continue to intensify, thereafter becoming quasi-stationary over the central North Pacific. Following this time, the main center continues to intensify, while an alternating series of ridges and troughs develop and amplify in sequence downstream from North America to the central Atlantic (Figs. 5d–f). Subsequent downstream developments can be traced across western Europe and Russia (not shown).

By the early 1980s, several potential mechanisms for low-frequency variability had been proposed. As noted by WG81, linearized dynamical models on a sphere forced by localized heat or topographic sources produced forced Rossby wave responses of approximately the right spatial scales and, for forcing in particular regions, patterns that at least qualitatively resembled the observed teleconnections. Indeed, in a major paper on ENSO, Horel and Wallace (1981, hereafter HW81), obtained highly statistically significant correlations between various ENSO indices and the PNA pattern. HW81's schematic illustration of the hypothesized upper-tropospheric response to tropical diabatic heating associated with ENSO (Fig. 6) shows an arching wave train broadly resembling that of the PNA pattern (cf. Fig. 3).

One clear difficulty in making a direct connection between PNA variability and ENSO was the mismatch between time scales. While strong PNA events could grow and decay within a month and events of opposite sign could occur within a given season (WG81; DG83), ENSO events evolved much more slowly, with typical periods of a few years or longer (Trenberth 1976). A second concern involved the amplitudes of the PNA events, which were much larger than what could be produced in simple models linearized about zonal-mean basic states and forced by realistic values of tropical heating. A third concern involved rather subtle differences in the height patterns over the North Pacific. To better appreciate this last issue and aid in our subsequent discussion of potential mechanisms, it is useful to review a few basic ideas from Rossby wave theory.

b. Potential mechanisms

1) ROSSBY WAVE ENERGY DISPERSION FROM STEADY, LOCALIZED SOURCES

As a simple starting point, consider the dispersion relation for Rossby waves in an unbounded, barotropic β-plane model linearized about a constant zonal-mean zonal flow U (e.g., Holton 2004):

$$\omega = Uk - \frac{\beta k}{K^2}. \tag{1}$$

Here, ω is the frequency; $\beta = df/dy$ is the meridional derivative of the Coriolis parameter f; and $K^2 = k^2 + l^2$ is the total wavenumber squared, where k $(=2\pi/L_x)$ and l $(=2\pi/L_y)$ are the zonal and meridional wavenumbers, respectively, and L_x and L_y the corresponding zonal and meridional wavelengths, respectively. Because $\omega = kc$, where c is the phase speed, Rossby waves always propagate westward relative to the zonal mean flow. The direction of energy dispersion is related to the group velocity, which is obtained by differentiating (1) with respect to wavenumber. The resulting x and y components of the group velocity are

$$c_{gx} = U + \frac{\beta(k^2 - l^2)}{K^2} \quad \text{and} \tag{2}$$

$$c_{gy} = \frac{\beta kl}{K^2}. \tag{3}$$

From (2), the zonal group speed may be either eastward or westward relative to the zonal mean flow, depending on the structure of the waves. In particular, for waves with $k^2 > l^2$, which appear synoptically as north–south-elongated waves, and is a structure typical of much synoptic-scale variability (Wallace and Lau 1985), the zonal group speed is greater than the mean flow and energy disperses rapidly eastward. Conversely, in zonally elongated waves, more characteristic of low-frequency variability (Wallace and Lau 1985), energy dispersion is westward relative to the zonal mean flow. The direction of meridional energy propagation is determined by the sign of the meridional wavenumber, l, with northward energy propagation when l is positive (northwest–southeast-oriented phase lines) and southward propagation for negative l (southwest–northeast-oriented phase lines).

A particularly interesting case is the wavenumber at which Rossby waves are stationary, as this is a favored response scale for excitation due to geographically fixed forcing (e.g., Holton 2004). The stationary wavenumber is obtained from (1) by setting $\omega = 0$, from which it can be seen that stationary Rossby waves can only exist

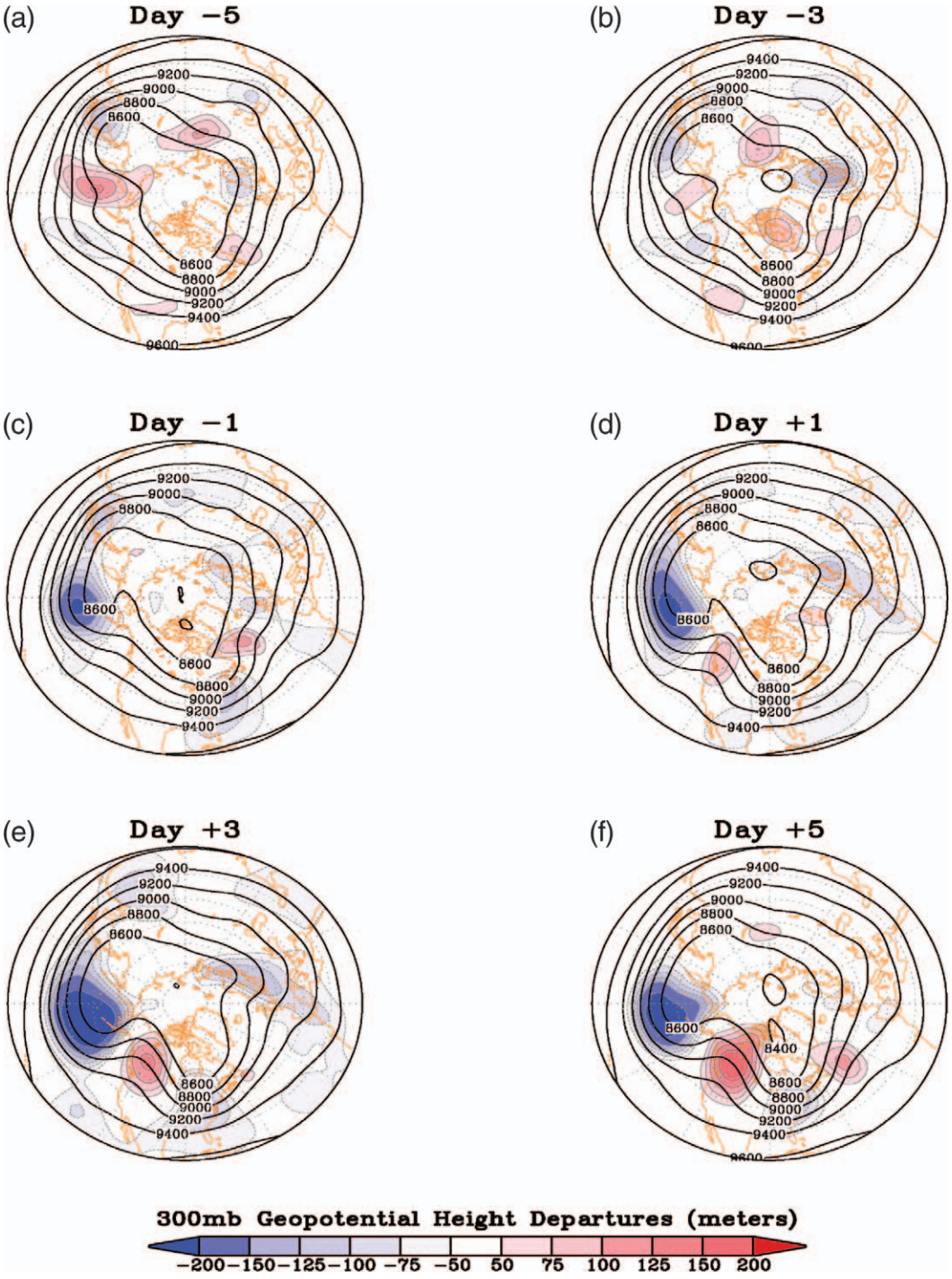

FIG. 5. Time evolution of composite 300-hPa heights (solid lines) and height anomalies (colors) for the 23 persistent negative height anomaly cases over the North Pacific analyzed in Dole and Black (1990), where time is relative to case onset, defined as day 0. For days (a) −5, (b) −3, (c) −1, (d) +1, (e) +3, and (f) +5.

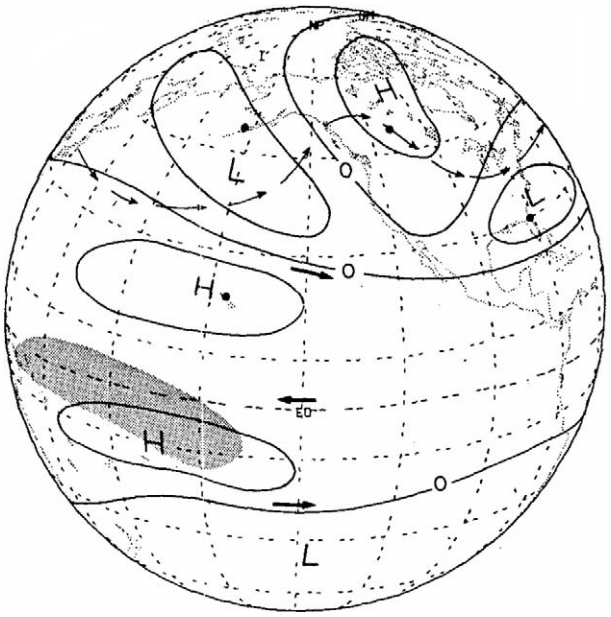

FIG. 6. Schematic illustration of the hypothesized global pattern of mid- and upper-tropospheric geopotential height anomalies (solid lines) during a Northern Hemisphere winter which falls within an episode of warm SSTs in the equatorial Pacific. The arrows in darker type reflect the strengthening of the subtropical jets in both hemispheres along with stronger easterlies near the equator during warm episodes. The arrows in lighter type depict a midtropospheric streamline as distorted by the anomaly pattern, with pronounced troughing over the central Pacific and ridging over western Canada. Shading indicates regions of enhanced cirriform cloudiness and rainfall. From Horel and Wallace (1981).

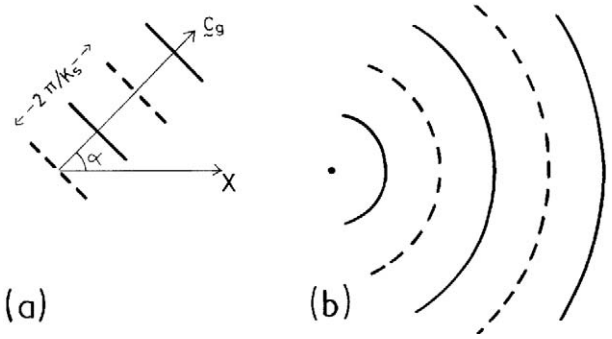

FIG. 7. (a) Stationary Rossby wave in a westerly flow on an infinite β plane with the crests (continuous lines) and troughs (dashed lines) making an angle α with the y axis. The wavelength is $2\pi/K_S$ and the group velocity relative to the ground is $c_g = 2\bar{u}\cos\alpha$. (b) A schematic illustration of the steady vorticity or height field waves forced from local source region on an infinite β plane in an atmosphere with a westerly flow $\bar{u}$ and wave dampening on a time-scale T. The wavelength in all directions is $2\pi/K_S$ and the wave train fills a circle with its center at $x = \bar{u}T$ and radius $\bar{u}T$. From Hoskins (1983).

when the mean flow is westerly. Combining this relation with (2) and (3), for stationary barotropic Rossby waves we obtain the following:

$$c_{gx} = \frac{2Uk^2}{K^2} \quad \text{and} \tag{4}$$

$$c_{gy} = \frac{2Ukl}{K^2}. \tag{5}$$

From (4), energy dispersion in stationary Rossby waves is always eastward and, in the limiting case of stationary waves that are infinitely elongated in the north–south direction, occurs at twice the speed of the mean zonal flow. In addition, (4) and (5) imply that for stationary Rossby waves the group velocity vector is perpendicular to the wave crests; for example, northwest–southeast-oriented stationary waves indicate northeastward energy dispersion. Figure 7 illustrates these basic relationships.

This simple barotropic model can be extended to incorporate additional factors such as meridional shear in the basic state or the effects of spherical geometry in modifying effective β. Hoskins et al. (1977) considered the latter case, and showed that in a constant angular velocity superrotation, which is the spherical analog to constant zonal mean flow, energy dispersion occurs along great circle ray paths. Figure 8 shows one example of energy dispersion on a sphere away from a fixed, localized source, in which the principal relationships discussed above are clearly evident. Inclusion of more realistic meridional shear results in refraction of the Rossby wave paths away from great circles as well as the formation of waveguides that preferentially organize energy dispersion (Hoskins and Ambrizzi 1993; Newman and Sardeshmukh 1998; Branstator 2002).

Returning to Fig. 6, it can be seen that the schematic ENSO pattern displays phase lines with a northwest–southeast orientation over the subtropical and midlatitude Pacific, consistent with northward energy dispersion by Rossby waves from a source in the tropical mid-Pacific (Hoskins et al. 1977; Plumb 1985). However, examination of the PNA pattern (Fig. 3) shows little evidence of systematic horizontal tilts that would suggest poleward energy propagation from this region. This discrepancy suggested a need for caution in interpreting the PNA pattern as a simple forced Rossby wave response to anomalous heating over the tropical mid-Pacific. However, for many years the terms ''ENSO pattern'' and ''PNA pattern'' were often used interchangeably. Mo and Livezey (1986) and Barnston and Livezey (1987) further clarified the observational distinctions between ENSO and PNA patterns, identifying a ''tropical Northern Hemisphere'' (TNH) pattern as being more directly related to ENSO. Straus and Shukla (2002) also showed that the midlatitude response to El Niño sea surface temperatures differs from the PNA pattern, which they identify as the leading structure of internal variability over the North Pacific in winter.

Despite these issues, it remained possible that ENSO, or other tropical forcing, could alter the likelihood of PNA pattern occurrence, essentially ''loading the climate dice'' so that events of a given type were more probable in a given year. A second possibility was that WG81's correlation analysis and Dole's use of com-

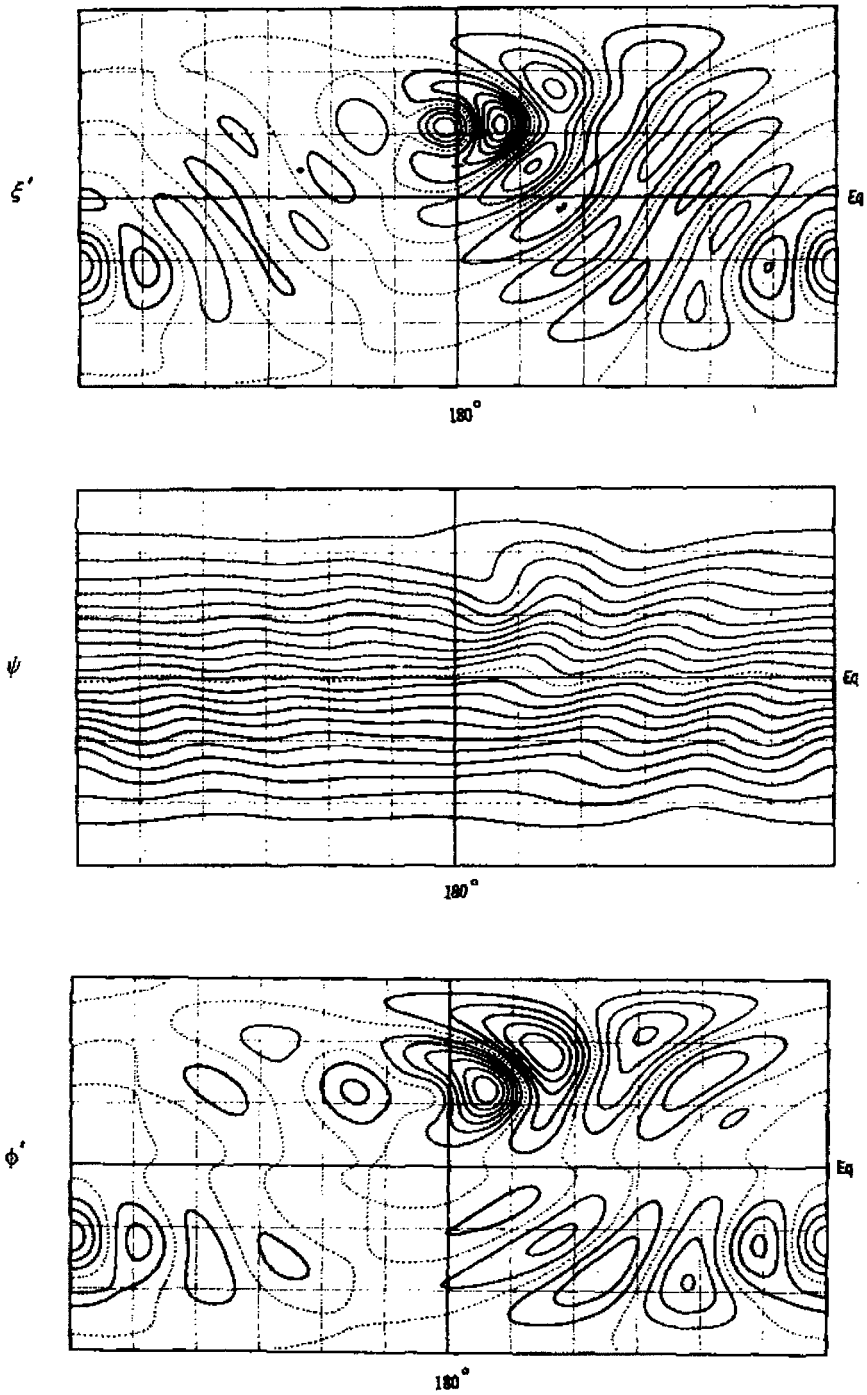

FIG. 8. Barotropic Rossby wave response on a sphere to forcing by a circular mountain located at 30°N in a uniform superrotation flow: (top) perturbation vorticity field, (middle) total streamfunction field, and (bottom) perturbation height field. From Grose and Hoskins (1979).

positing blurred any potential tropical signal, by including a mixture of events arising from both tropical and mid- or high-latitude sources. A third possibility hinged on the wave sources themselves. As noted by Sardeshmukh and Hoskins (1988), Rossby waves could be forced by the advection of vorticity by the divergent flow as well as by divergence acting on the rotational flow; that is,

$$S_{\mathrm{RW}} = -\mathbf{V}_\chi \cdot \nabla\eta - \eta\nabla \cdot \mathbf{V}, \tag{6}$$

where S_{RW} is the Rossby wave source, $\mathbf{V}_\chi$ is the divergent wind component, and η is the absolute vorticity. There-

fore, tropical convection could produce Rossby wave sources at latitudes well removed from where the convection itself was occurring; for example, through divergent outflow advecting absolute vorticity in the region of strong vorticity gradients associated with the subtropical jets. Thus, the potential role for tropical forcing remained open, although the simple interpretation of the PNA pattern as a stationary Rossby wave train forced from the tropical mid-Pacific appeared inadequate.

Despite this limitation, work during this period convincingly established the fundamental importance of Rossby wave dynamics for interpreting much low-frequency variability, and arching Rossby wave trains forced by local vorticity sources are now recognized as ubiquitous features in upper-level wind and potential vorticity analyses. As one indication of how our perspective had changed, it is interesting to recall an excellent earlier review on Rossby waves by Platzman (1968), in which he posed the provocative question: ''Have Rossby waves ever been observed in the atmosphere?'' While Platzman answers affirmatively, perhaps the clearest evidence he had at that time came from spherical harmonic decompositions of 24-h height field tendencies (e.g., Eliasen and Machenhauer 1965), an analysis technique that, while mathematically justified, is not as well-suited for synoptic interpretations of the Rossby wave trains described here, because of the broad band (high number) of individual wave modes required to adequately represent the evolution of observed teleconnection patterns.

2) Instabilities of zonally varying mean flows

A second proposed mechanism for producing the low-frequency variations was through the growth of unstable normal modes of the wintertime mean flow. Several candidates were suggested, including baroclinic instability (e.g., Frederiksen 1983) and barotropic instability (Simmons et al. 1983, hereafter SWB) of zonally varying basic states. The study by SWB was particularly noteworthy in showing how barotropic mechanisms could contribute to the development of flow patterns that strongly resembled the PNA and EA patterns. SWB interpreted the development of these patterns as a manifestation of the most rapidly growing mode associated with barotropic instability of the zonally varying climatological basic state (Fig. 9), since termed the SWB mode. To understand the essential development mechanism it is useful to consider the barotropic interactions between the time-mean flow and transient eddies for a mean flow that varies in both zonal and meridional directions.

To an accuracy of approximately 10%, the barotropic energy conversion from the zonally varying time-mean flow to the transient eddies is (Hoskins et al. 1983; SWB):

$$C(\overline{K}, K') \cong (\overline{v'^2} - \overline{u'^2})\frac{\partial \overline{u}}{\partial x} - \overline{u'v'}\frac{\partial \overline{u}}{\partial y}, \qquad (7)$$

where the overbars denote time averages, the primes departures from the time average, and

$$\overline{K} = \frac{\overline{u}^2 + \overline{v}^2}{2}$$

and

$$K' = \overline{\frac{u'^2 + v'^2}{2}}$$

are, respectively, the kinetic energy of the time-mean flow and transient eddies. Following Hoskins et al. 1983 and SWB, this may also be written as

$$C(\overline{K}, K') \cong \mathbf{E} \cdot \nabla \overline{u}, \qquad (8)$$

where

$$\mathbf{E} = [(\overline{v'^2} - \overline{u'^2}), -\overline{u'v'}] \qquad (9)$$

is the barotropic ''**E** vector.'' This latter representation is useful for identifying dynamical relationships between transient eddies and the time-mean flow, as will be discussed in more detail later in this section.

The second term in (7), associated with the meridional shear in the mean zonal flow, is identical in form to the barotropic conversion term for zonally symmetric basic states (e.g., Pedlosky 1979; Holton 2004). This term supports eddy growth in regions where eddy phase lines tilt against the shear. In this case, meridional eddy momentum fluxes transfer zonal momentum away from regions where the zonal flow is initially strong (i.e., the jet) thereby smoothing the jet profile (reducing the meridional shear). The first term is nonzero only when there are zonally varying basic states. This term supports eddy growth when zonally elongated eddies ($\overline{u'^2} > \overline{v'^2}$) enter regions where the climatological mean zonal flow is decreasing eastward ($\partial\overline{u}/\partial x < 0$), as is the case in the jet exit regions over the North Pacific and North Atlantic Oceans. Alternatively, barotropic eddy growth is also supported when meridionally elongated eddies enter regions where the mean zonal flow increases eastward, as in the confluent flow region upstream of the time-mean jet streams.

Figure 10 schematically illustrates the mean flow and perturbation relationships favorable for barotropic eddy growth for basic states characterized by diffluence and strong meridional shear, which are commonly observed states over much of the central North Pacific in wintertime. The barotropic conversion term in (8) can be shown to have the simple geometric interpretation that the eddies will gain energy if the mean flow deformation makes them more ''circular,'' that is, increases eddy isotropy (Farrell 1984; Mak and Cai 1989; Cai 1992; Whitaker and Dole 1995; Black and Dole 2000). Conversely, the sense of the conversions will be from the eddies into the mean flow when mean flow deformation makes the eddies more anisotropic. A familiar synoptic

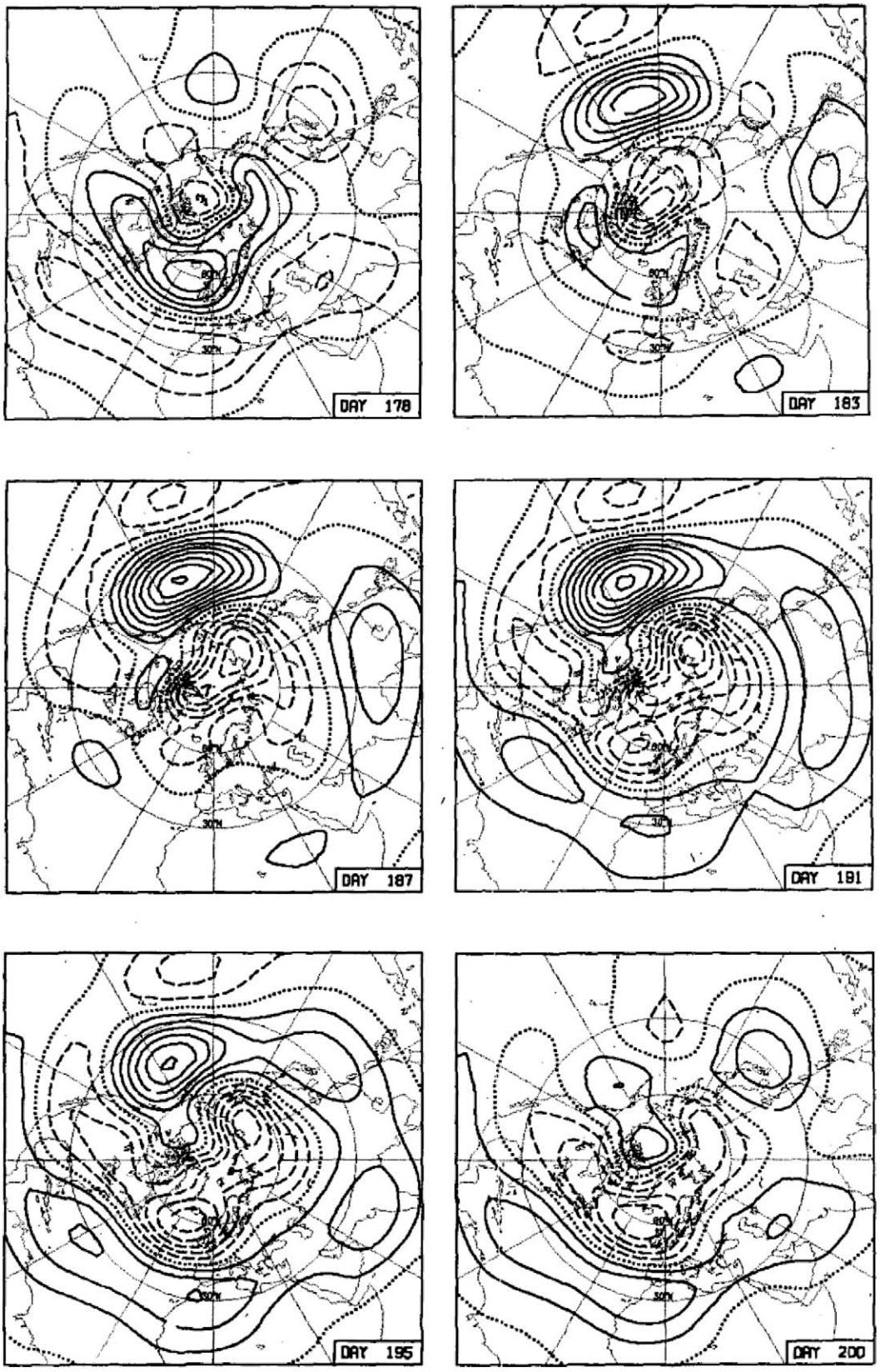

FIG. 9. The streamfunction of the most unstable barotropic mode in a zonal-varying basic state representative of the Northern Hemisphere wintertime time-mean flow, for selected days within its evolution. The contour interval is arbitrary. From Simmons et al. (1983).

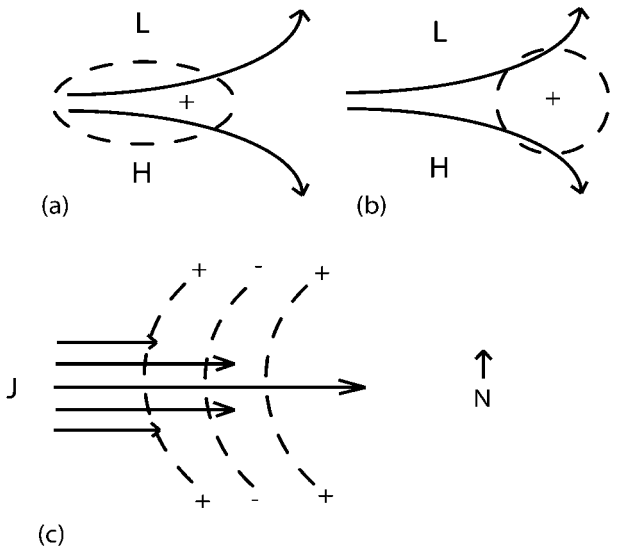

FIG. 10. Schematic illustration of (a) favored structure for barotropic growth for an eddy encountering a diffluent flow downstream of jet maxima, (b) change in eddy structure due to subsequent deformation by large-scale flow, and (c) favored structure for eddy development in a horizontal shear flow. In these figures, the solid lines denote the mean flow streamlines, the dashed lines are the eddy vorticity isopleths, L and H indicate relative minima and maxima in the mean height fields, respectively, and J indicates the mean jet axis.

example is the ''shearing out'' of upper-level short-wave troughs, with scale collapse occurring along one axis (axis of contraction) while stretching occurs along the orthogonal axis (axis of dilatation).

The SWB theory provided a potential explanation for both the observed locations and favored structures of maximum low-frequency variability over the central North Pacific and eastern North Atlantic Oceans (Blackmon et al. 1984; Wallace and Lau 1985; Dole 1986b; Kushnir and Wallace 1989). However, the SWB theory also had potential inadequacies. One was that observational analyses showed strong thermal advection and westward (upshear) vertical tilts in the growing eddy structures over the central North Pacific during PNA development (Dole 1986a; DB90; Black and Dole 1993), suggesting a potentially significant role for baroclinic growth processes. A second issue was the rate of disturbance growth. When realistic damping is included in the SWB model, the barotropic instability mechanism alone appeared inadequate to account for observed growth rates (Borges and Sardeshmukh 1995; Sardeshmukh et al. 1997). Thus, while barotropic instability on a zonally varying basic state could contribute significantly to growth of the PNA and EA patterns, it seemed unlikely to be the sole source. What had emerged from these studies, however, was the central role of zonal variations in the basic state in accounting for both the development and favored locations of observed low-frequency variations.

3) MULTIPLE-EQUILIBRIA AND FLOW REGIMES

A third theory proposed around 1980 was that persistent anomaly patterns are the manifestation of multiple ''quasi-equilibrium'' flow states that could exist even with fixed external forcing. Early studies of the wintertime general circulation (e.g., Rossby et al. 1939; Namias 1947, 1950; Willett 1949) suggested that the midlatitude flow tended to vary between two extreme states, one characterized by a relatively weak stationary waves and a strong westerly flow (high-zonal-index state) and the other by highly amplified stationary waves and weak westerlies (low-zonal-index state). In fact, understanding the causes for high- and low-zonal-index states provided a major motivation for Rossby's seminal paper on planetary waves (Rossby et al. 1939). From our previous discussion on Rossby wave dynamics, it is clear that zonal-mean flow variations have significant implications for wave propagation and energy dispersion. There are several potential causes for such variations, and improving our understanding and ability to model zonal-mean wind changes continues to be an important subject for research (e.g., Weickmann and Sardeshmukh 1994; Feldstein and Lee 1998; Feldstein 2001; Weickmann 2003).

Charney and DeVore (1979) showed that, in a simple nonlinear barotropic model forced by topography, two equilibrium states having features similar to high- and low-zonal-index flows could be produced through wave–mean flow interactions, and suggested that blocking might be a metastable equilibrium associated with the low-index state. In this very simple model, the equilibrium states result from a nonlinear balance among zonal flow driving, topographic forcing, and dissipation. This study was followed by extensions to low-order baroclinic models forced by topography (Charney and Straus 1980; Reinhold and Pierrehumbert 1982). Some early observational analyses found support for this theory in explaining blocking events (Charney et al. 1981); however, others found no convincing evidence (DG83). A host of efforts have since searched for multiple quasi-equilibria, or ''weather regimes,'' in observational data (e.g., Hansen and Sutera 1986, 1988; Molteni et al. 1990; Cheng and Wallace 1993), and the debate has been vigorous on the extent to which recurrent nonlinear regimes have been identified (e.g., Nitsche et al. 1994). While questions continue on whether this theory accounts for specific observed states, the possibility that nonlinear quasi-stationary wave regimes can exist and play a significant role in climate dynamics cannot be discounted. Such a possibility has significant implications for climate predictions as well as for projecting future climate changes due to anthropogenic or natural forcing (Palmer 1998, 1999).

4) FORCING BY SYNOPTIC-SCALE TRANSIENT EDDIES

A fourth potential mechanism for low-frequency variations is systematic forcing by synoptic-scale eddies.

In discussing this mechanism, it is helpful to consider two subquestions: first, what are the effects of the low-frequency flow variations on synoptic-scale eddies, and second, what are the effects of synoptic-scale eddies on the low-frequency flow? The first question is directly related to changes in storm tracks and eddy life cycles that accompany persistent flow anomalies, while the second concerns the role of eddy feedbacks on the development, maintenance, and breakdown of persistent flow anomalies. Although it is conceptually useful to consider the two issues separately, it is also important to recognize that interactions between synoptic-scale eddies and the large-scale flow are nonlinear, and that subtle, indirect effects of the interactions can be quite significant. Consequently, interpreting eddy–mean flow relationships from observational data is especially challenging. This section touches on some of the major advances occurring post-1980, focusing on the behavior of synoptic-scale eddies during blocking events.

(i) Effects of large-scale flow anomalies on synoptic-scale activity

Early synoptic investigations indicated that blocking events are accompanied by major changes in synoptic-scale storm activity (e.g., Berggren et al. 1949; Rex 1950a,b). Other studies described cases where intense synoptic-scale cyclogenesis was followed by the downstream development of large-scale flow anomalies, especially blocking (Sanders and Gyakum 1980; Hansen and Chen 1982; Colucci 1985, 1987; Mullen 1987; Tracton 1990). Several characteristic synoptic features are illustrated in Fig. 11 (from Petterssen 1956). This figure shows daily frontal positions over two 10-day periods prior to and following the establishment of blocking over the eastern Atlantic and western Europe. The 10-day period before blocking formation (Fig. 11a) is characterized by a strong, predominantly zonal upper-level flow over the North Atlantic. Frontal systems during this period propagate mainly eastward along a relatively narrow band across the North Atlantic, with a primary genesis region extending from over the southeastern United States across the western Atlantic. In contrast, following the development of blocking (Fig. 11b), the storm track over the central and eastern Atlantic splits into branches well north and south of its initial latitude. Frontal systems approaching the blocking region from the west appear to elongate meridionally before splitting into the northern or southern branches of the flow. During this period, an area of enhanced cyclogenesis also occurs to the east of Greenland. Prior to blocking development, frequent frontal passages led to heavy precipitation over much of western and central Europe; following blocking development, little or no precipitation was observed over the same region (Petterssen 1956).

The early investigations demonstrated that changes in synoptic-scale eddy activity and low-frequency flow variations are related, but the extent and dynamical interpretation of the relationships remained uncertain. Green (1977), Shutts (1986), Dole (1986a,b), Mullen (1986, 1987), Wallace et al. (1988), Lau (1988), and Nakamura and Wallace (1993) among others, documented the relationships more quantitatively by applying temporal filtering techniques to analyze synoptic eddy behavior during blocking events. Figure 12 (from Mullen 1987) shows a good example of this method for evaluating systematic relationships between the time-mean flow and synoptic-scale eddy activity for a composite of Atlantic blocking cases. Note the qualitative similarities of the ''bandpass'' storm tracks (Fig. 12b) to the earlier synoptic analyses (Fig. 11b), especially the pronounced northward shift over the eastern Atlantic and the indication of a new maximum near southeast Greenland. Nakamura and Wallace (1990) and Neilley (1990) further extended these studies of ''mature phase'' relationships by analyzing changes in synoptic-scale eddy activity through the life cycles of low-frequency circulation anomalies. These studies showed a tendency for enhanced synoptic-scale variance upstream of developing blocking patterns a few days prior to the onset of blocking, consistent with synoptic descriptions of strong upstream synoptic-scale cyclogenesis preceding blocking development.

To first order, the observed differences in eddy activity associated with persistent flow anomalies conform to synoptic experience and simple theory. In general, the storm tracks approximately coincide with the zones of maximum time-mean baroclinicity. Enhanced variability is also preferentially located near and downstream of major long-wave troughs and, conversely, variability is usually suppressed near and immediately east of major long-wave ridges. However, as shown quite strikingly by Nakamura (1992), baroclinicity alone is not the sole factor modulating the strength of synoptic-scale variability. Nakamura found that maximum baroclinic wave activity (as measured by bandpass variance in heights, meridional heat fluxes, and other variables) occurs in autumn and spring over the western and central North Pacific (Fig. 13), with a midwinter suppression in activity at a time when the climatological-mean baroclinicity is strongest. Nakamura showed that this midwinter suppression occurs when the strength of the upper-tropospheric jet exceeds a threshold of $\sim$45 m s^{-1}. He suggested that this midwinter minimum, which is not observed in the Atlantic storm track, might be related to rapid advection of the disturbances through the highly baroclinic region over the western Pacific as well as increased low-level trapping of the waves. Other possible mechanisms, such as seasonal changes in barotropic shearing deformation and condensational heating (Chang 2001) have also been suggested for this interesting within-season variation, which is manifested in interannual (Nakamura et al. 2002) as well as seasonal time scales, and the problem continues to be actively

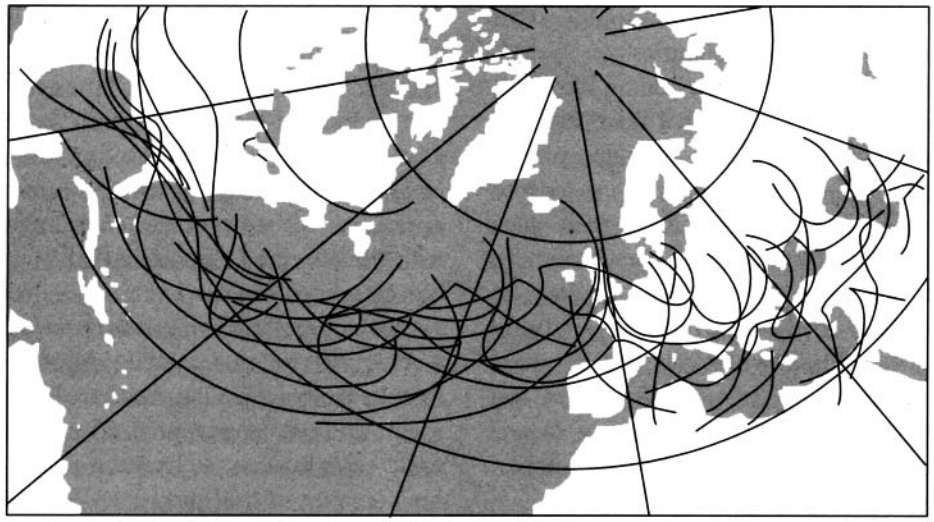

(a)

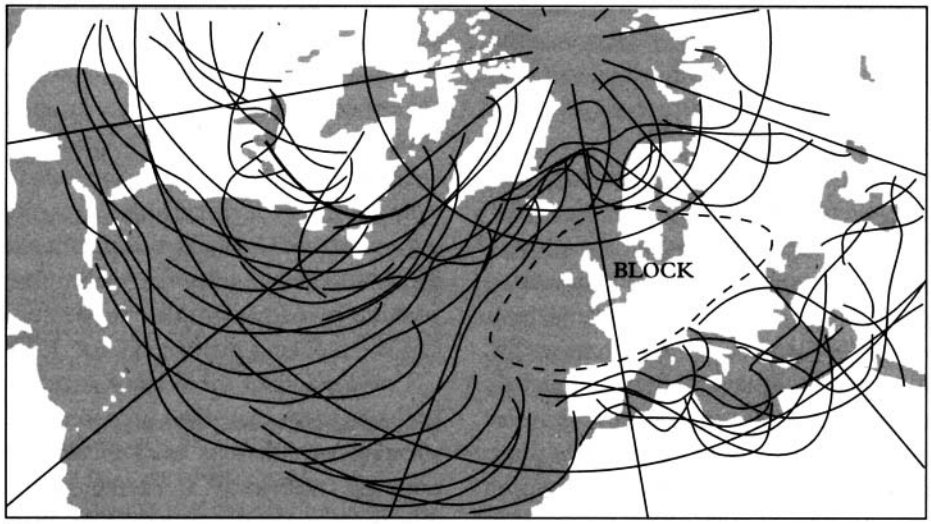

(b)

FIG. 11. Daily frontal positions during two successive 10-day periods (a) preceding the formation and (b) following the development of blocking over the eastern Atlantic and western Europe. From Petterssen (1956).

investigated (Zhang and Held 1999; Chang 2003; Harnik and Chang 2004).

(ii) Advances in dynamical understanding of storm track variations

The progress in describing relationships between low-frequency flow variations and synoptic-scale variability has been accompanied by major advances in our understanding and ability to model storm tracks. For the extratropical wintertime flow, a rough first approximation for preferred storm tracks can be obtained from spatial variations in baroclinicity as shown, for example, by maps of local time-average values of the Eady growth parameter σ (Eady 1949):

$$\sigma = 0.31\frac{f\frac{\partial \overline{u}}{\partial z}}{N}, \tag{10}$$

where N is the buoyancy frequency (Holton 2004). However, rapid development does not always occur in such regions. Through the 1980s and 1990s, horizontal shear (James 1987) and deformation in the basic-state flow (Mak and Cai 1989; Cai and Mak 1990; Lee 1995a,b; Whitaker and Dole 1995; Branstator 1995) became increasingly recognized as playing important roles in organizing storm tracks and determining differences in synoptic-scale storm life cycles (Thorncroft et al. 1993, and their ''type-1'' versus ''type-2'' life cycles).

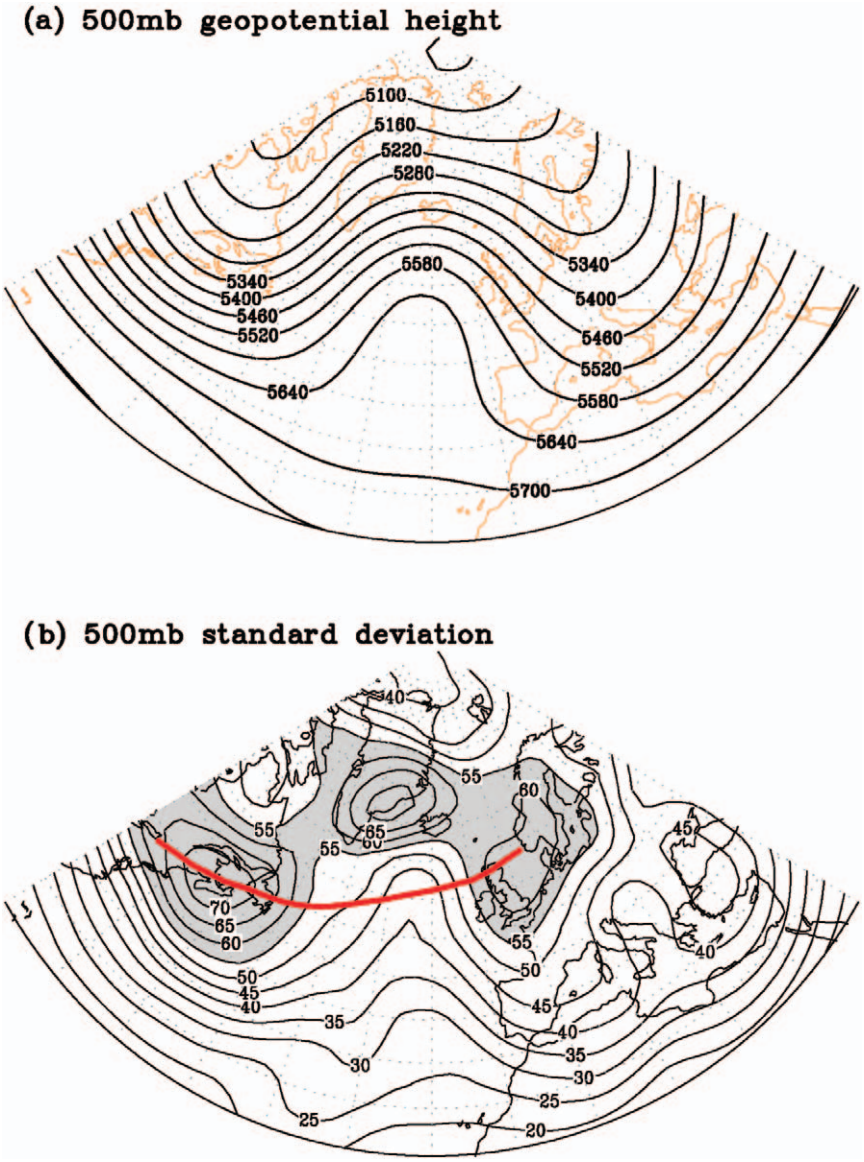

FIG. 12. Distributions of (a) 500-mb composite-mean geopotential height contours and (b) standard deviation of Blackmon's (1976) bandpass-filtered 500-mb geopotential height for observed Atlantic blocking composites. In (b), shading represents values greater than 55 m and the heavy red line represents the axis of the climatological-mean position of the ''storm track.'' From Mullen (1987).

More recent work has reinforced the importance of changes in baroclinicity, horizontal shear and deformation as well as ''seeding'' by upstream disturbances in accounting for storm-track changes (Chang 2001, 2005; Chang and Fu 2002; Orlanski 2005).

Another crucial theoretical advance was to show that significant transient growth of disturbances could occur even if the flow was formally stable, given the presence of favorably configured perturbations in flows that had either vertical or horizontal shear or deformation (Farrell 1982, 1985, 1984; Mak and Cai 1989). This has led to a linear theory of storm tracks in which many of the observed features of Northern Hemisphere synoptic-scale variability can be deduced simply by considering the eddies as stochastically forced disturbances evolving on a baroclinically *stable* basic-state flow (Whitaker and Sardeshmukh 1998; Zhang and Held 1999).

As discussed by Sanders (1988), among others, the evolving vertical structures obtained in theoretical studies by Farrell (Farrell 1984) and others strongly resemble observed cases of ''type-B'' cyclogenesis as described by Petterssen (1955). In this form of development, the vertical structure of disturbances evolves systematically, with an initial upshear vertical tilt between the surface low and upper-level trough that decreases as the disturbance intensifies, until the upper-level

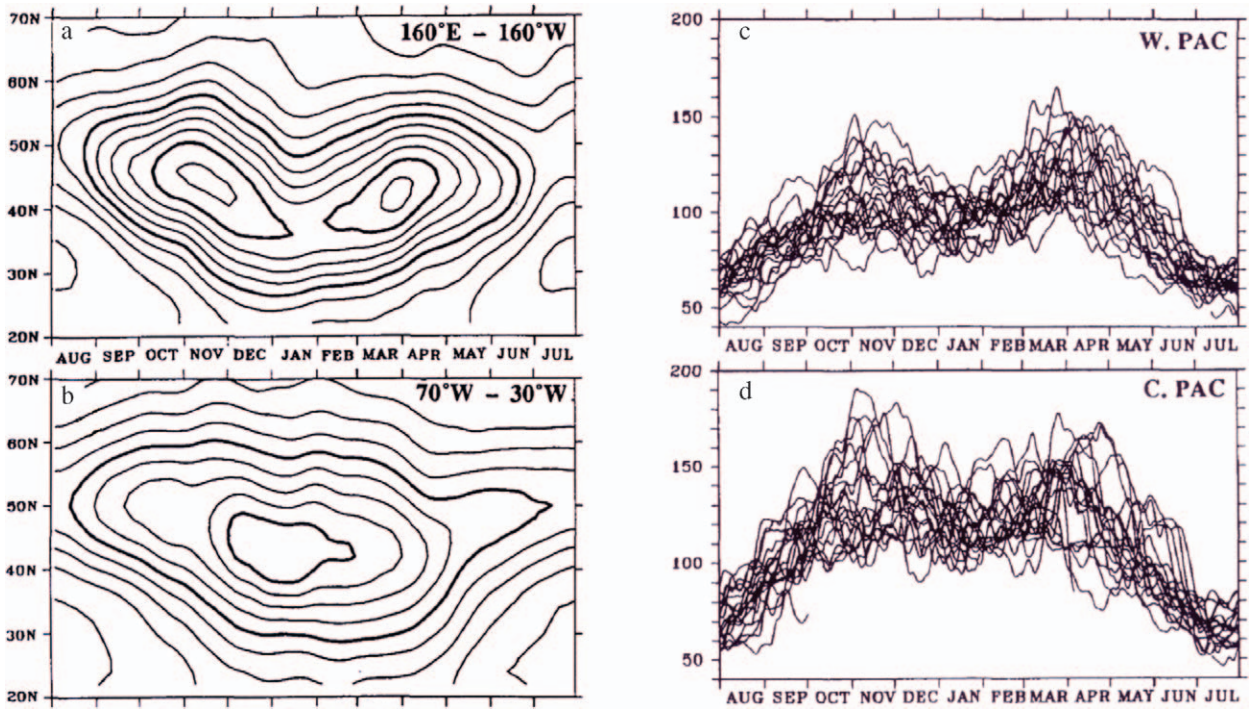

FIG. 13. Latitude–time sections showing the seasonal march of baroclinic wave amplitudes, defined using the temporal filter of Nakamura (1992) in the 250-hPa geopotential heights averaged over the longitude intervals (a) 160°E–160°W and (b) 70°–30°W. Seasonal march of the same fields averaged over (c) the western Pacific (130°–170°E) and (d) central Pacific (160°E–160°W) for individual 12-month periods from August 1965 to July 1984. From Nakamura (1992).

trough becomes approximately in phase with the surface cyclone center. Hoskins et al. (1985, hereafter HMR) provide a simple dynamical interpretation for this type of development in their landmark paper on potential vorticity dynamics. Davis and Emanuel (1991) applied the essential concepts of potential vorticity invertibility discussed in HMR to diagnose the contributions of potential vorticity perturbations at different locations and pressure levels to cyclogenesis. Black and Dole (1993) used a similar method to diagnose sources for the development of cases of strong positive PNA patterns. Their results suggested that nonmodal transient growth involving both barotropic and baroclinic processes likely plays a significant role in these developments (see also Feldstein 2002). Black (1997) subsequently extended these analyses to consider the life cycles of both polarities of the PNA and EA patterns. He found a similar mechanism was responsible for the developments in all types of cases considered. The primary wave source regions were located in the central North Pacific and eastern North Atlantic, respectively, with Rossby wave dispersion from the source regions leading to the establishment of the mature teleconnection patterns.

Beyond these relatively large-scale features, research into storm-track dynamics, most notably by E. Chang and colleagues, shows that synoptic-scale activity is organized into wave packets, which typically disperse energy downstream along baroclinic waveguides at speeds comparable to the strength of the mean flow. Lee and Held (1993) first noted this behavior in simple models of the Southern Hemisphere general circulation, and Chang (1993) showed that this behavior was also prevalent in the Northern Hemisphere. Figure 14, from Chang et al. (2002) illustrates this behavior over a portion of one winter. Individual trough and ridge systems can be seen propagating within the packets at speeds on the order of 10 m s^{-1}. However, these individual disturbances are imbedded within larger wave packets that propagate more rapidly downstream. This is manifested synoptically by a succession of ''downstream developments'' (see also Namias and Clapp 1944). The downstream energy fluxes related to this mechanism extend the storm track from regions of strong baroclinicity to regions less favorable for baroclinic development. Chang et al. (2002) provide an excellent review of storm-track dynamics in which this mechanism is discussed in more detail.

(iii) Effects of synoptic-scale eddies on large-scale flow anomalies

We have seen that low-frequency flow anomalies alter synoptic-scale variability and, hence, can contribute to systematic changes in storm behavior like those inferred from Fig. 1. What about the second question, the effect of synoptic-scale eddies on the low-frequency flow?

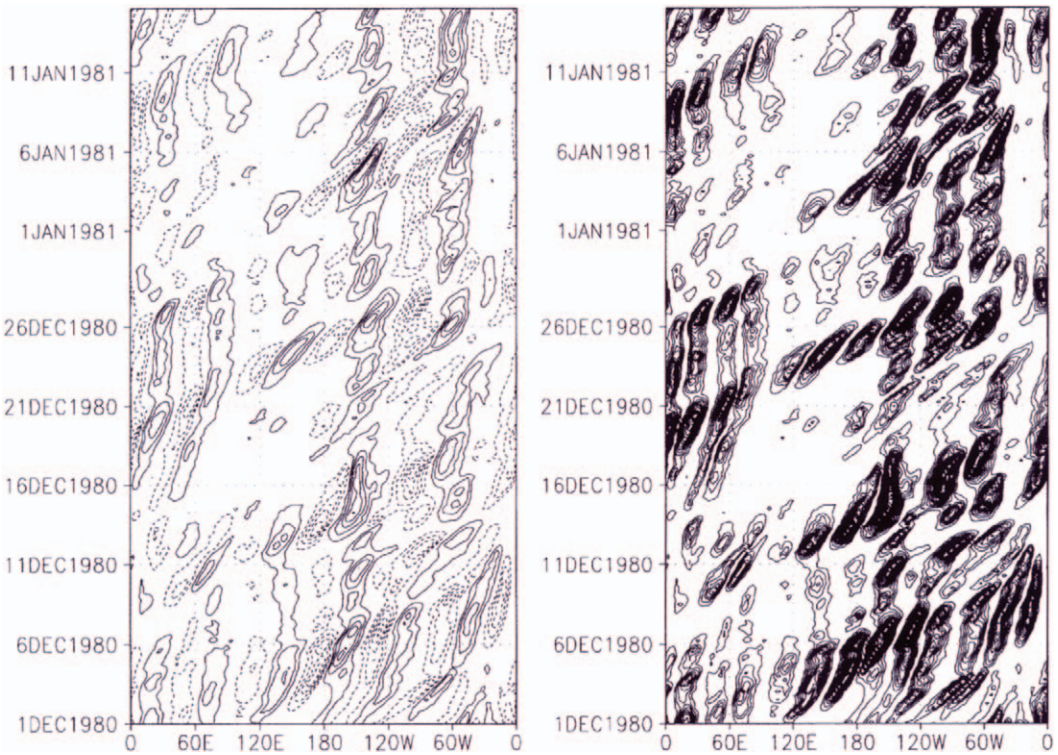

FIG. 14. Hovmöller (longitude–time) diagram of 300-hPa v' and v'^2, unfiltered except for the removal of seasonal mean, for the period 1 Dec 1980 to 14 Jan 1981 (contours 10 m s^{-1} and 100 m s^{-2}). In this figure, v' has been averaged over a 20° latitude band centered on the upper-tropospheric waveguide as defined in Chang and Yu (1999). From Chang et al. (2002).

Here again, there have been substantial advances in understanding. Studies in the late 1970s and early 1980s focused initially on time-mean heat and vorticity budgets during blocking events, in attempts to distinguish relative changes in time-mean and transient eddy forcing (Green 1977; Illari 1984; Shutts 1986; Mullen 1986). To assess the net effects of the eddies, it is necessary to take into account the combined effects of eddy fluxes of vorticity and heat as well as the eddy-induced secondary circulations. The conservation and invertibility principles of potential vorticity dynamics (HMR) play a fundamental role in helping to interpret such relationships.

At the level of quasigeostrophic theory (Holton 2004) the mean flow tendency forced by eddies is due to the convergence of the eddy flux of quasigeostrophic pseudopotential vorticity in the interior of the atmosphere:

$$\frac{\overline{\partial q}}{\partial t} = -\overline{\mathbf{V}} \cdot \boldsymbol{\nabla}\overline{q} - \boldsymbol{\nabla} \cdot (\overline{\mathbf{V}'q'}) + \overline{S}, \qquad (11)$$

where the quasigeostrophic pseudopotential vorticity q is

$$q = \frac{1}{f_0}\boldsymbol{\nabla}\Phi + f + \frac{\partial}{\partial p}\left(\frac{f_0}{N_b}\frac{\partial \Phi}{\partial p}\right) \qquad (12)$$

together with the eddy flux convergence of potential temperature, θ, on the lower boundary (Hoskins 1983):

$$\frac{\overline{\partial \theta}}{\partial t} = \overline{\mathbf{V}} \cdot \boldsymbol{\nabla}\overline{\theta} - \boldsymbol{\nabla} \cdot (\overline{\mathbf{V}'\theta'}) + \overline{H}. \qquad (13)$$

In (11) and (13), the overbars denote any simple averaging process, which here we will take to represent a time mean, with the primes denoting deviations from the mean values. In (11) and (13) $\overline{S}$ and $\overline{H}$ represent time-mean frictional and diabatic forcing terms, respectively. It is worth keeping in mind that, while the eddy forcing appears explicitly only in the eddy flux convergence terms, the eddies can also force the mean flow indirectly by altering the time-mean diabatic and frictional forcing terms (Hoskins 1983).

From (11) and (13), a time-mean ''tendency equation'' for the geopotential height field can be obtained (Lau and Holopainen 1984), which is analogous to the standard quasigeostrophic geopotential tendency equation (Holton 2004), with eddy flux convergence terms for vorticity and temperature replacing the corresponding vorticity advection and thermal advection terms. The eddy contributions to the initial time mean tendency can be written as

$$\left[\frac{1}{f_o}\nabla^2 + f_o\frac{\partial}{\partial p}\left(\frac{1}{N_b}\frac{\partial}{\partial p}\right)\right]\frac{\overline{\partial\Phi}}{\partial t} = D^{\text{HEAT}} + D^{\text{VORT}}, \quad (14)$$

where

$$D^{\text{HEAT}} = f_o\frac{\partial}{\partial p}\left(\frac{\boldsymbol{\nabla}\cdot\overline{V'\theta'}}{N_b}\right) \quad (15)$$

and

$$D^{\text{VORT}} = -\boldsymbol{\nabla}\cdot\overline{V'\zeta'}. \quad (16)$$

Given the eddy forcing terms (15) and (16) together with appropriate boundary conditions for the eddy heat fluxes (Lau and Holopainen 1984), the elliptic equation [(14)] can be solved to give the initial geopotential tendency that would be expected for a specified transient eddy forcing. Lau and Holopainen used this method to determine the initial tendency of the climatological-mean flow due to transient eddies, while Mullen (1987) and Holopainen and Fortelius (1987) applied a similar method to assess the mean-flow tendencies produced by transient eddies during blocking situations. These studies showed that, at least in the vicinity of the blocking patterns, the net upper-level tendency patterns is dominated by the vorticity fluxes [(16)]. Overall, there was net anticyclonic forcing near and upstream of the blocking ridge, tending to reinforce the block and counteracting the tendency for the ridge to be advected eastward by the time-mean flow (Mullen 1987). In a similar analysis of monthly variability, Lau and Nath (1991) found that the initial height tendencies forced by synoptic-scale eddies usually reinforced observed monthly mean upper-level height anomalies. Subsequent studies applying analogous diagnostic approaches indicate that forcing by synoptic-scale eddies can also play a significant role in blocking onset (e.g., Neilley 1990; Nakamura et al. 1997).

An alternative means for assessing wave–mean flow interactions was developed in the 1980s, based on extensions of Eliassen–Palm (EP) flux diagnostics developed for zonal-mean flows to zonally varying time-mean flows (Hoskins et al. 1983; Plumb 1985, 1986; Trenberth 1986). For zonal-mean flows, the EP flux vectors indicate the direction of flux of wave activity, while the EP flux divergence provides a measure of the net eddy forcing of the zonal-mean flow (Andrews and McIntyre 1976; Edmon et al. 1980). Deriving similar relationships for zonally varying time-mean flows requires additional approximations, and hence different formulations have been proposed; see Trenberth (1986) for a discussion of the differences. Here, we will sketch the basic ideas using the formulation of Hoskins et al. (1983).

To illustrate this method, we confine our discussion to the horizontal flux components only, which are then given by the terms in (9). As discussed earlier, the x component of the **E** vectors is related to horizontal shape asymmetries of the disturbances, with positive (eastward) values associated with meridionally elongated eddies, and negative values with zonally elongated eddies. The y component is related to horizontal phase tilts, with positive (northward) values being associated with phase lines that slope westward with increasing latitude (i.e., northwest–southeast-tilted ridges and troughs).

As discussed by Hoskins et al., subject to certain approximations, the contribution to the acceleration of the mean westerly flow by transient eddies is given by

$$\left(\frac{\overline{\partial u}}{\partial t} + \overline{u}\frac{\partial\overline{u}}{\partial x} + \overline{v}\frac{\partial\overline{u}}{\partial y}\right)_{\text{TE}} = \boldsymbol{\nabla}\cdot\mathbf{E}. \quad (17)$$

In particular, where $\boldsymbol{\nabla}\cdot\mathbf{E} > 0$ there is a net eddy forcing that tends to increase the westerly component of the mean flow.

Figure 15 (from Shutts 1986) displays **E** vectors for a case of Atlantic blocking. In this study, **E** vectors were derived from 300-hPa data that had been filtered to retain periods of less than a week (corresponding to synoptic-scale eddies). Well upstream of the blocked region, the **E** vectors are mainly directed eastward, indicating eddies that are primarily meridionally elongated. As the eddies approach the region where the large-scale flow becomes strongly diffluent, the magnitudes of the **E** vectors first increase, and then become very small. The initial increase is the manifestation of baroclinic growth as well as a tendency toward reduction of the eddy zonal wavelengths as disturbances become stretched meridionally in the region of strong large-scale flow deformation. The smaller magnitudes are associated with the very low values of synoptic-scale variability observed in the vicinity of the blocking anticyclone. Shutts interpreted these **E**-vector patterns as the signature of a barotropic ''eddy-straining'' mechanism that reduces the east–west scale of the eddies as they encounter the strongly diffluent flow upstream of the block. The variations in the eddies as they approach the block leads to a $\boldsymbol{\nabla}\cdot\mathbf{E} < 0$ near and just to the south of the anticyclonic vorticity center, implying a tendency to decrease the strength of the mean westerly flow in a region where it is already weak. In addition, there is a latitudinal fanning out of **E** vectors (indicative of ''bowed'' troughs and ridges) in the westerlies well to the south of the anticyclone giving $\boldsymbol{\nabla}\cdot\mathbf{E} > 0$, implying a tendency for the eddies to increase the strength of the mean westerlies in the region where the westerlies are already anomalously strong. An additional region, where $\boldsymbol{\nabla}\cdot\mathbf{E} > 0$, is located in the westerlies to the north of the blocking anticyclone.

Thus, these analyses suggest that the large-scale flow anomalies associated with blocking alter synoptic-scale eddy activity *and* that these changes result in a net positive eddy feedback that reinforces the large-scale flow anomalies. Subsequent studies have made use of similar techniques to document changes in synoptic-scale eddy structures and diagnose eddy feedbacks onto low-frequency anomalies (Neilley 1990; Higgins and Schubert

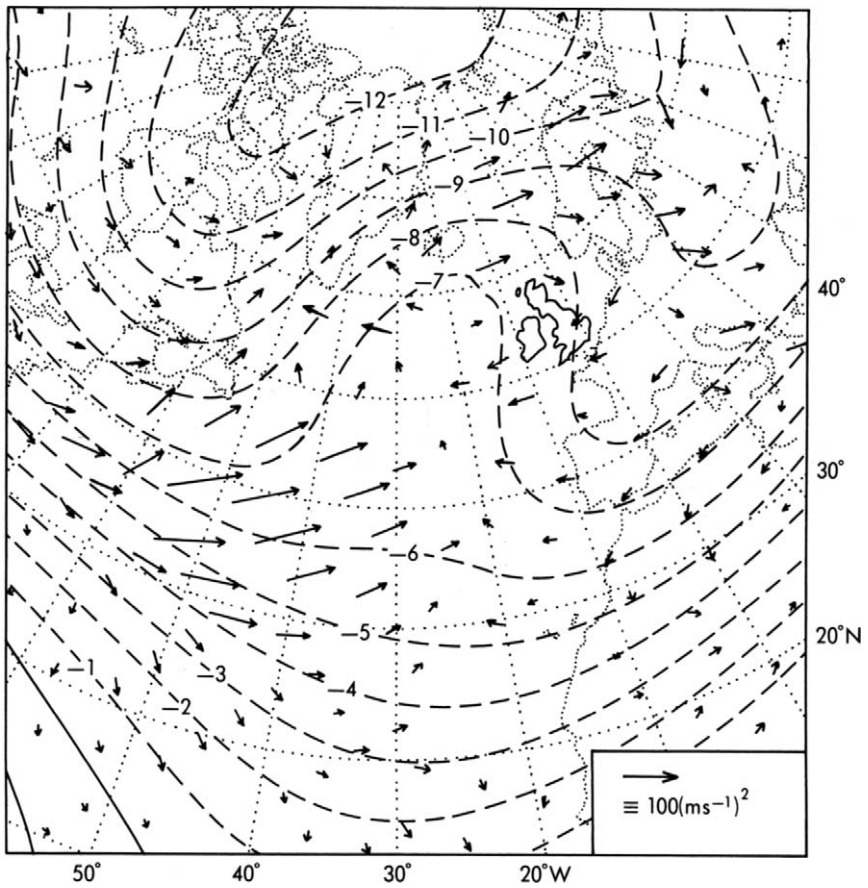

FIG. 15. High-pass-filtered **E** vectors superimposed on the mean streamfunction field for a North Atlantic blocking case for the period 5–22 Feb 1983. From Shutts (1986).

1993, 1994; Nakamura et al. 1997). These studies indicate that positive eddy feedbacks frequently occur in association with both blocking and unusually strong zonal flows. In an interesting diagnostic analysis of an Atlantic blocking case, Hoskins and Sardeshmukh (1987) found that enhanced large-scale diffluence over the western and central Atlantic produced by anomalous tropical heating provided an important catalyst for reorganizing Atlantic synoptic-scale eddy activity, with changes in eddy potential vorticity fluxes then leading to blocking development.

(iv) Additional comments

Aside from the direct effects of the eddy fluxes, synoptic-scale eddies can also exert important indirect effects on the large-scale flow. For example, in midlatitudes, changes in time-mean diabatic heating are related to changes in the storm tracks, primarily through changes in spatial distributions of latent (but also sensible and radiative) heating. The relationships between latent, sensible, and radiative heating distributions and storm tracks are incompletely understood, but certainly are geographically dependent. To the extent that the synoptic-scale eddies influence the mean flow, they also indirectly alter the generation and propagation characteristics of planetary-scale waves.

Interactions of low-frequency flow anomalies with topography can also impact synoptic-scale eddy activity, with variability typically being enhanced on the lee sides of major mountain barriers in regions of stronger-than-normal flow (Hsu and Wallace 1985; Hsu 1987; Dole 1987; Lau 1988). These include secondary maxima to the lee of the U.S. Rockies in the negative PNA cases and to the lee of the Canadian Rockies in the positive PNA cases (Dole 1987), and to the lee of Greenland in the positive EA cases, consistent with Mullen's results (cf. Fig. 12b).

While time-mean budget studies have added significantly to our understanding, their interpretation can be difficult, and in some circumstances they may even obscure important dynamical processes (Held and Hoskins 1985). For example, consider a case in which strong eddy–mean flow interactions occur until the flow approaches a quasi-equilibrium state where the eddy forcing terms becomes very small. Budgets evaluated at this later time may suggest that the role of the eddies is negligible; however, the quasi-equilibrium state may not

be obtainable in the absence of the eddies. Reinhold and Pierrehumbert (1982) found such a behavior in a low-order baroclinic model. In establishing causal mechanisms, careful case studies focusing on the time evolution of events are often most useful; in this regard, Professor Sanders's synoptic case studies provide many clear examples. For large-scale flows in which balance conditions are well met, studies focusing on the time evolution of potential vorticity can be particularly illuminating (HMR; Morgan and Nielsen-Gammon 1998).

Despite the differences in methods, synoptic and diagnostic results are consistent in indicating that, in the development and maintenance of blocking and other persistent flow anomalies, synoptic-scale eddies can and often do play a major reinforcing role. The results paint a rich picture of the interplay between synoptic-scale eddies and the large-scale flow on which they evolve. From an operational standpoint, the results suggest that the failure to adequately simulate the large-scale flow will result in errors in predicting the regions of cyclogenesis and subsequent storm tracks. They also suggest that large-scale flow errors can arise from systematic deficiencies in modeling synoptic-scale disturbances.

c. Tropical connections

We have introduced several potential mechanisms for producing extratropical low-frequency variability, including Rossby waves forced by localized diabatic or topographic sources, large-scale flow instabilities (or nonmodal growth), quasi-equilibrium states representing a nonlinear balance between mean flow and forcing terms, and forcing by anomalous synoptic-scale eddy fluxes. While all of the above mechanisms can occur solely through midlatitude processes, the potential impact of tropical diabatic heating on extratropical low-frequency variability has been and continues to be a major focus for research, especially in studies aimed at improving weather and climate forecasts.

There are several reasons for this emphasis, including 1) the existence of coherent low-frequency variations in organized convection that can act as anomalous Rossby wave sources; 2) the relatively strong extratropical response exhibited in both simple and comprehensive general circulation models to variations in tropical forcing (Simmons 1982; Branstator 1985; Newman and Sardeshmukh 1998; Barsugli and Sardeshmukh 2002); and 3) evidence from predictability studies suggesting that much of the potential predictability of weather and climate beyond 1 week is likely related to tropical heating variations (Winkler et al. 2001; Newman et al. 2003; Compo and Sardeshmukh 2004). This section summarizes advances in our understanding of the role of tropical phenomena in forcing extratropical low-frequency variability over the PNA sector, focusing primarily on ENSO and the Madden–Julian oscillation (MJO).

1) ENSO RELATIONSHIPS

As noted previously, the major El Niño event of 1982/83 was not fully recognized, much less predicted, as it was occurring. This situation would soon change dramatically for several reasons, including: 1) rapidly emerging documentation of systematic relationships between ENSO and tropical and extratropical climate variability (e.g., Horel and Wallace 1981; Rasmusson and Wallace 1983); 2) a developing dynamical basis to interpret the relationships between tropical and midlatitude climate variations (Egger 1977; Hoskins et al. 1977; Opsteegh and Van Den Dool 1980; Hoskins and Karoly 1981; Webster 1981); 3) the ability to reproduce observed relationships in general circulation models (Palmer and Mansfield 1984; Lau 1985; Hoerling and Kumar 2000); 4) the successful prediction of El Niño with a simple coupled tropical ocean–atmosphere model (Cane et al. 1986; Zebiak and Cane 1987); and 5) vastly improved observations and expanded research conducted under the Tropical Ocean and Global Atmosphere (TOGA) program. Extensive reviews of ENSO can be found in Philander (1990), National Research Council (1996), articles within a special issue of the *Journal of Geophysical Research—Oceans* (in 1998) and references therein.

(i) Characteristic features

The essence of the ENSO phenomenon arises from coupling of the atmosphere and ocean over the tropical Pacific (Bjerknes 1969). Changes in tropical heating distributions provide anomalous sources for Rossby waves that can propagate into higher latitudes, leading to global climate impacts (Ropelewski and Halpert 1987, 1989; Kiladis and Diaz 1989; Halpert and Ropelewski 1992; Trenberth et al. 1998). Spectral analyses of atmospheric and oceanic variables related to ENSO show significant variability in periods ranging from 2 to 7 yr (Trenberth and Shea 1987; Ropelewski et al. 1992), and on these time scales, ENSO is the dominant mode of global climate variability.

Within this broad time band, the general character of the ENSO variations is that of an irregular oscillation between two extreme states of the tropical Pacific coupled ocean–atmosphere system. One state is characterized by warmer-than-normal sea surface temperatures over the central and eastern tropical Pacific, with below-normal surface pressures in the same region and above-normal surface pressures over the western tropical Pacific, including Indonesia and Australia. This part of the oscillation is generally termed the ENSO warm phase. The other extreme state, the ENSO cold phase, is characterized by below-normal sea surface temperatures over the central and eastern Pacific together with relatively high surface pressure over this region and lower-than-normal surface pressures over the western tropical Pacific. Because of the very strong coupling between

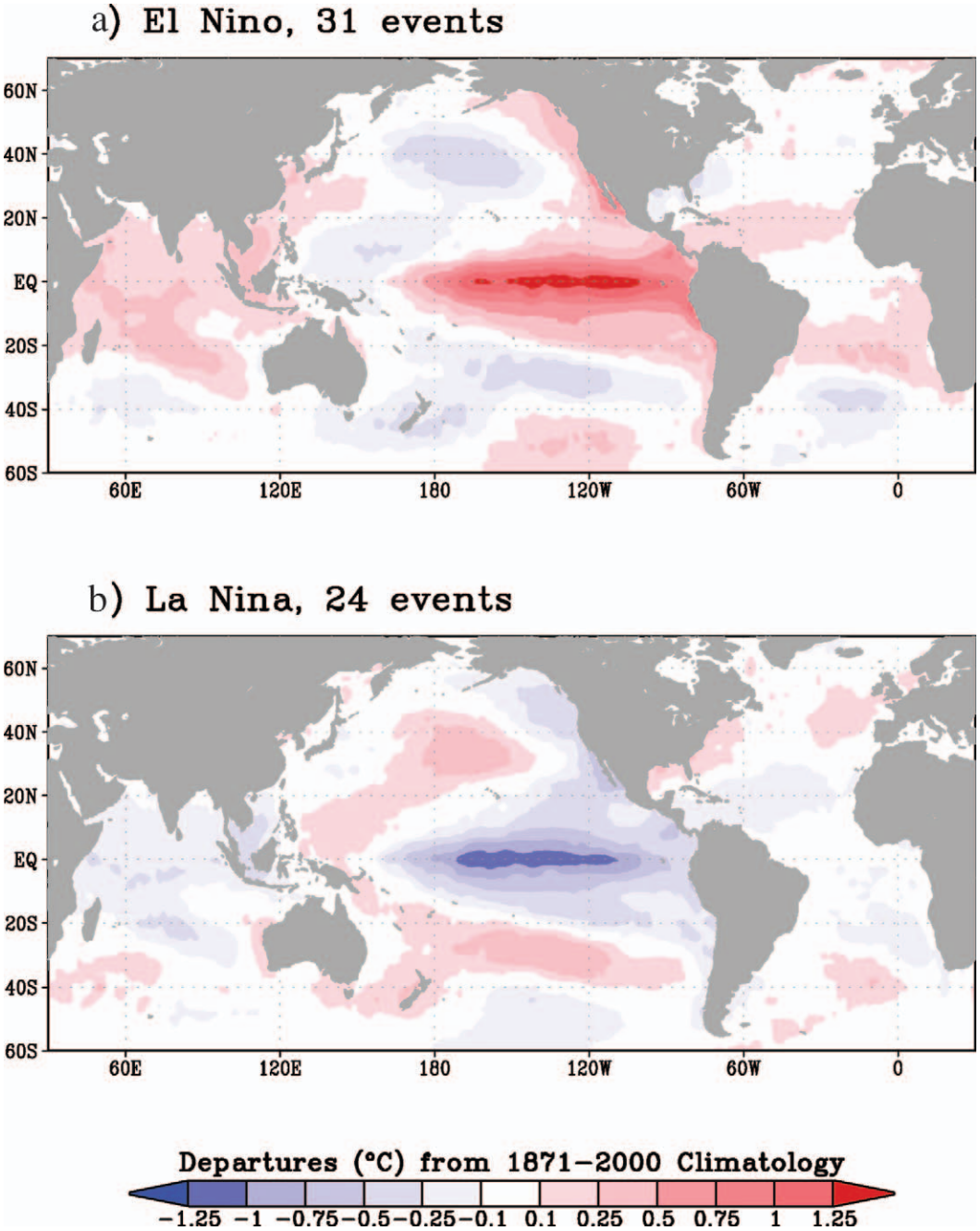

FIG. 16. Composite November–March SST anomalies for (a) El Niño and (b) La Niña. Cases are from the period 1870–2004, extending the cases of Kiladis and Diaz (1989) using the SST index defined in that study.

sea surface temperatures and sea level pressure over these regions, ENSO warm phase conditions are often simply called El Niño, and cold phase conditions La Niña, although strictly these refer only to the ocean component of the system.

Figure 16 shows composite SST analyses for the two phases. Note that in addition to the strong SST variations in the eastern tropical Pacific, there are systematic variations elsewhere. For example, SST anomalies of the same sign as the tropical eastern Pacific anomalies extend to higher latitudes along the west coasts of both North America and South America, same-signed SST anomalies also occur over parts of the Indian and tropical Atlantic Oceans, and anomalies of opposite sign are located in the central North Pacific and subtropical South Pacific Oceans. The coastal anomalies are the result of poleward propagation by oceanic Kelvin waves, which are edge waves that propagate parallel to

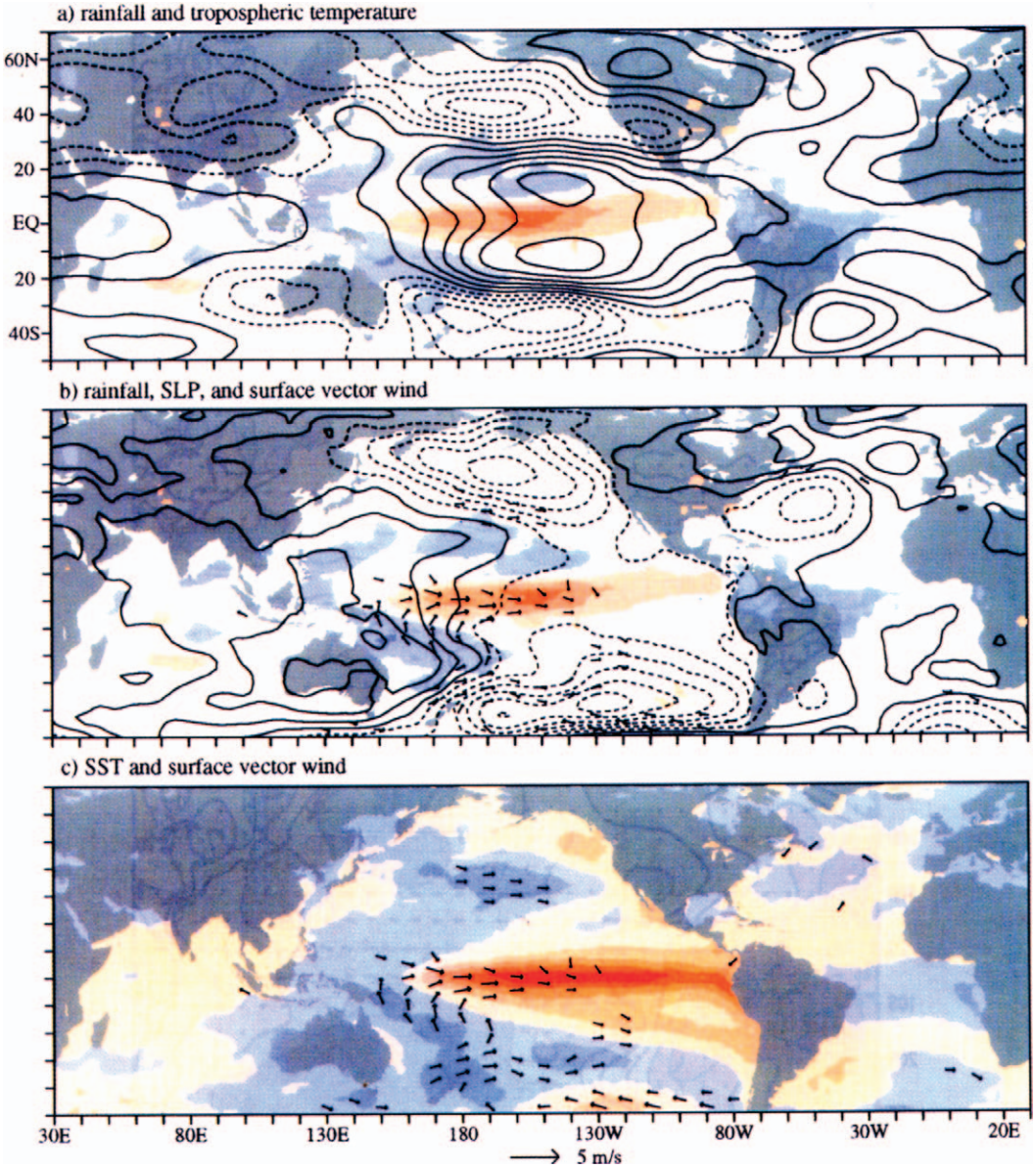

FIG. 17. Composite ENSO surface features. Fields are from NCEP–NCAR reanalyses regressed upon a Pacific cold tongue index defined in Wallace et al. (1998) for the period from January 1985 to December 1993. All regression coefficients are per standard deviation of the cold index. (a) The 1000–200-hPa layer-mean temperature (contour interval 0.1°C; negative contours are dashed) superimposed upon rainfall (anomalies of -1 and -3 cm month^{-1} are shaded blue and greater than 1, 3, 5, and 7 cm month^{-1} are shaded red). (b) SLP (contour interval 0.25 hPa, negative contours are dashed) and surface vector wind superimposed upon rainfall. Only vectors with magnitudes > 0.5 m s^{-1} are plotted. (c) Surface vector wind superimposed upon SST obtained from COADS data. From Wallace et al. (1998), their Fig. 8.

the coastlines with the boundary on the right side in the Northern Hemisphere and on the left side in the Southern Hemisphere (Gill 1982). The anomalies in the North and South Pacific, Atlantic, and Indian Oceans are related to an ''atmospheric bridge'' mechanism, in which tropical Pacific SSTs lead to changes in the global atmospheric circulation, which can then produce changes in SSTs in the underlying oceans (Alexander et al. 2002).

The ''SO'' in ENSO reflects the strong tendency for associated sea level pressures to be antiphase between the eastern and western tropical Pacific, as described by Walker (1924). The Southern Oscillation index (SOI), as measured by mean sea level pressure differences between Tahiti and Darwin, tends to be below normal during El Niño and above normal during La Niña (Trenberth 1976; HW81). Figure 17 shows the characteristic surface features associated with ENSO as obtained from

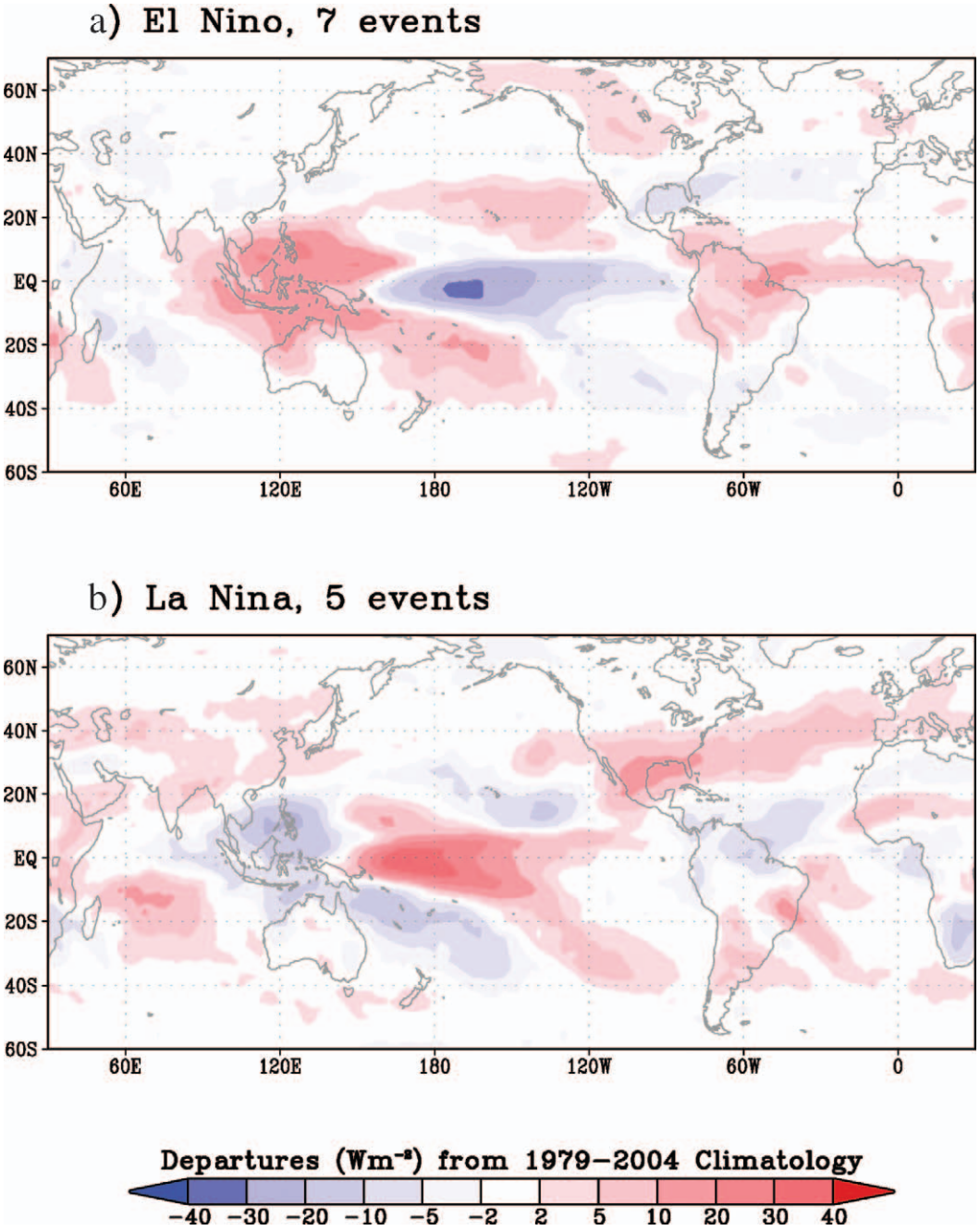

FIG. 18. Composite wintertime OLR anomalies (W m^{-2}) associated with (a) seven El Niño events and (b) five La Niña events over the period from 1979 to 2004.

the National Centers for Environmental Prediction–National Center for Atmospheric Research (NCEP–NCAR) reanalyses. While these features are typical, all events differ in some aspects, and these different ''flavors'' of ENSO (Trenberth 1997a,b; Trenberth and Stepaniak 2001) can have significant implications, especially for seasonal anomalies and climate forecasts in midlatitudes (Kumar and Hoerling 1997; Hoerling and Kumar 1997; Hoerling et al. 1997).

Related changes in tropical rainfall, as inferred from outgoing longwave radiation (OLR), are quite striking, with a tendency for convection to shift toward the region of warmest SSTs (Fig. 18). As discussed previously, the associated upper-level divergence together with advection of mean vorticity by the anomalous divergent flow provide local sources for Rossby waves. Energy dispersion occurs poleward and eastward from the convective source regions, altering the subtropical jets and

extratropical stationary wave patterns. These features can be seen in Fig. 19, which shows respective composite 200-hPa circulation anomalies associated with El Niño and La Niña conditions. During the El Niño events (Fig. 19a) there are flanking anticyclones in the subtropics in both hemispheres located poleward of the regions of maximum anomalous heating, with intensification of the subtropical jets on the poleward sides of the anticyclones. In El Niño winters, the Pacific jet exit region tends to extend well eastward of its normal location, while it remains more confined in the western part of the basin in La Niña years. Figure 20, from Trenberth et al. (1998), provides a schematic illustrating the anticipated upper-level mean flow response to a near-equatorial heat source, as well as expected seasonal-mean storm-track changes, consistent with observed ENSO–storm track relationships (Kok and Opsteegh 1985; Held et al. 1989; Hoerling and Ting 1994).

(ii) Relationships of ENSO to extratropical low-frequency variations

Because of the mismatch in time scales, ENSO is unlikely to be directly responsible for most intraseasonal low-frequency variability. Nevertheless, by modifying the seasonal mean flow and storm tracks, ENSO can effectively load the climate dice by producing conditions that are more (or less) favorable for the development of low-frequency circulation anomalies in a given region. In an early study considering this possibility, Mullen (1989) performed perpetual January experiments with the NCAR general circulation model to assess the responses of Pacific blocking to various tropical and midlatitude sea surface temperature anomalies. His results indicated that the sea surface temperature anomalies did not significantly alter the total blocking frequency over the Pacific, but did affect the preferred locations of blocking formation. He found that ENSO warm phase (El Niño) conditions favored increased blocking along the west coast of North America and suppressed blocking over the mid-Pacific. Conversely, ENSO cold-phase (La Niña) conditions were associated with enhanced mid-Pacific blocking. These basic results were confirmed in later studies (Hoerling and Ting 1994; Renwick and Wallace 1996; Compo et al. 2001). Consistent with the correlations described in HW81, positive PNA patterns are also more likely to occur in the ENSO warm phase, with more negative cases during the ENSO cold phase (Renwick and Wallace 1996; Straus and Shukla 2002).

Studies by Sardeshmukh et al. (2000) and Compo et al. (2001) have examined in more detail the potential influences of El Niño and La Niña on variability across a range of time scales using observational analyses and general circulation model simulations. Sardeshmukh et al. found substantial asymmetries in the remote response to El Niño and La Niña in both time-mean fields and variability. Through analyses of large (180 member) ensembles of general circulation model runs, they were able to detect statistically significant changes in probability distributions for two seasons characterized by El Niño [January–March (JFM) 1987] and La Niña (JFM 1989) conditions. They concluded that the changes in distributions were sufficiently large to substantially alter the risks of extreme climate anomalies.

Compo et al. (2001) examined the responses to ENSO across a range of time scales, including variations at synoptic, intraseasonal, monthly, and seasonal time scales. They found that the responses to ENSO differed sharply depending on the time scale of interest; for example, La Niña events were associated with increased variance of the North Pacific near the Aleutians on intraseasonal and monthly time scales, which they attributed to more frequent blocking activity, while at the same time synoptic-scale variability in this region was suppressed. Three mechanisms were suggested as important in accounting for the observed ENSO-induced changes in extratropical variability. First, asymmetries in the tropical heating anomalies related to El Niño versus La Niña conditions could force some of the observed differences. Second, changes in the extratropical base state due to ENSO could alter the stability and potential for growth of some of the low-frequency modes, for example, related to the PNA pattern. Third, changes in storm tracks could alter the synoptic eddy feedbacks onto low-frequency variations. Sardeshmukh et al. (2000) and Compo et al. (2001) both emphasized the need for large ensembles (order of a few hundred members) to reliably estimate systematic changes in extratropical variability due to El Niño or La Niña conditions.

(iii) Relationships of ENSO to extratropical storm variability

Research within the last several years has provided additional insights on the connections between ENSO and synoptic-scale weather phenomena. Barsugli et al. (1999) applied an innovative approach to evaluate the effects of the 1997/98 El Niño on observed synoptic weather events. In their study, they conducted parallel ensembles of medium-range weather forecasts out to 16 days every day throughout the winter of 1997/98, with the sole difference between ensembles being that one ensemble set used as boundary conditions observed SSTs in both the Tropics and midlatitudes, while the other replaced the tropical SSTs with their climatological-mean values. Because tropical SST anomalies during this winter were largely associated with the strong El Niño event, to first order this approach enabled an assessment of the sensitivity of the forecasts to the presence or absence of El Niño conditions. Barsugli et al. termed the ensemble mean differences between the two sets of forecasts the ''synoptic El Niño signal,'' which is a function of initial date and forecast lead time. They found that, on average, an El Niño signal appeared within the first day of the forecasts in the tropical Pacific.

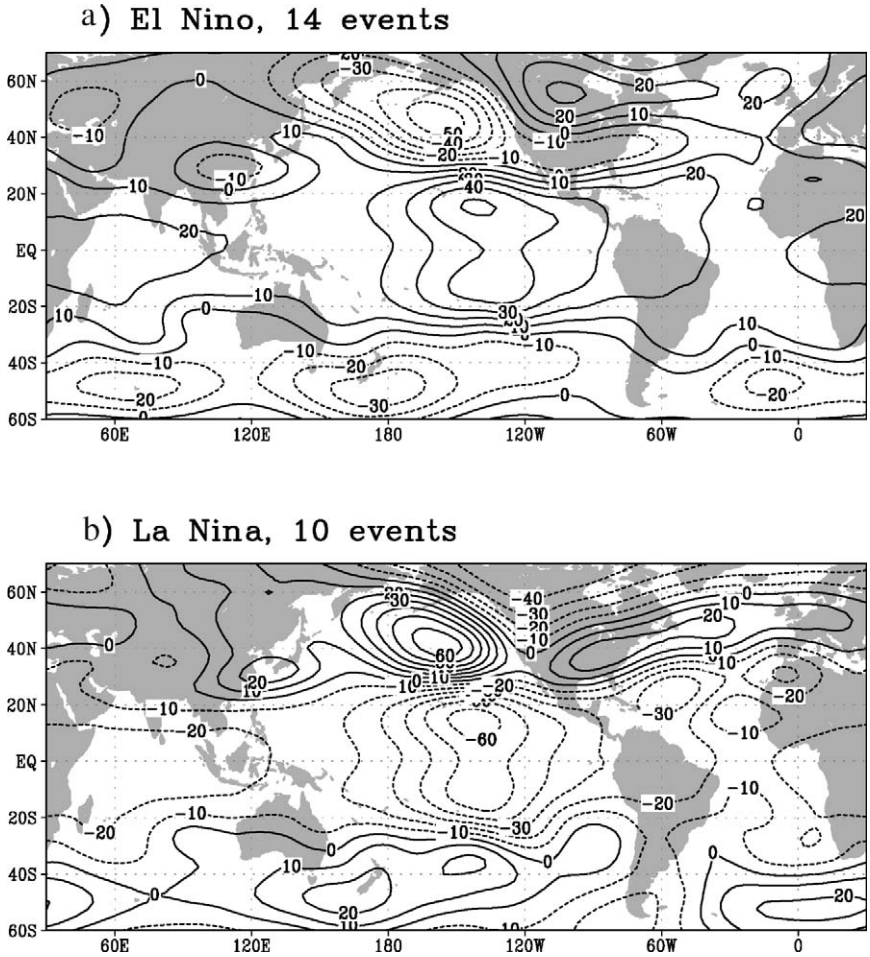

FIG. 19. Composite wintertime 300-hPa height anomalies (m) associated with (a) 14 El Niño and (b) 10 La Niña events over the period from 1950 to 2004, from NCEP–NCAR reanalysis data.

This signal then extended into the extratropics and in some cases substantially altered the midlatitude flow evolution, especially in the second week (days 8–14) of the forecasts.

Interestingly, Barsugli et al. also found that, despite the slow evolution of the SST anomalies, El Niño impacts on the forecasts varied substantially during the course of the season. This suggests that other intraseasonal variations were significantly modulating the effects of the tropical SST anomalies, effectively opening and closing the ''window'' to strong tropical–extratropical interactions. Figure 21 shows one example of a period of significant extratropical El Niño impacts on 8–14-day forecasts. This period marks the onset of heavy rains in California around 1 February 1998. The precipitation forecasts with observed SSTs that include El Niño conditions (Fig. 21a) show a strong, zonally oriented storm track that extends eastward from the central North Pacific to the western United States, with maximum rainfall near the northern California coast. In contrast, the forecasts where tropical SSTs are replaced with their climatological values (Fig. 21b) have a weaker track extending northeastward from the central Pacific to British Columbia, with dry conditions over most of the west coast, including California. The El Niño signal (Fig. 21c) indicates that El Niño forcing contributed substantially to the storm-track changes leading to heavy rainfall in California during this period (Fig. 21d). Barsugli et al. found that for the entire 1997/98 winter season variations in strength of the synoptic El Niño signal broadly coincided with subseasonal rainfall variability over central California, suggesting the importance of tropical–extratropical interactions in modulating rainfall variations for this region and season.

Recent synoptic studies have provided further insights into ENSO impacts on midlatitude storm activity. Shapiro et al. (2001) compared the life cycles of baroclinic storm systems over the North Pacific in two consecutive winters, one characterized by strong El Niño conditions (1997/98) and the other by La Niña conditions (1998/99). The time-mean 250-hPa flow for these two winters is shown in Fig. 22. The contrast in mean flows is clearly evident across the eastern Pacific, with a mean jet axis that extends eastward across Baja California in 1997/

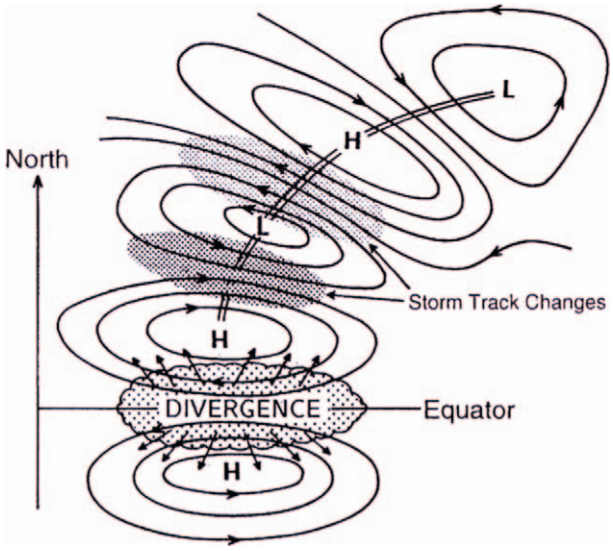

FIG. 20. Schematic of the dominant changes in the upper troposphere, mainly in the Northern Hemisphere, in response to increases in SSTs, enhanced convection, and anomalous upper-tropospheric divergence in the vicinity of the equator (scalloped region). Anomalous outflow into each hemisphere results in subtropical convergence and an anomalous anticyclone pair straddling the equator, as indicated by the streamlines. A wave train of alternating high and low geopotential and streamfunction anomalies results from the quasi-stationary Rossby wave response (linked by the double line). In turn, this typically produces a southward shift in the storm track associated with the subtropical jet stream, leading to enhanced storm-track activity to the south (dark stipple) and diminished activity to the north (light stipple) of the first cyclonic center. Corresponding changes may occur in the Southern Hemisphere. From Trenberth et al. (1998).

98 and is shifted substantially poleward toward the Pacific Northwest in the following year. Shapiro et al. found that the synoptic life cycles and associated eddy fluxes were also quite different in the two winters. Representative examples can be seen in Fig. 23, which shows a pronounced cyclonic roll-up just off the west coast in the region of intense cyclonic shear in the mean zonal flow for an El Niño winter case, while the La Niña winter case shows an example of anticyclonic wave breaking. Shapiro et al.'s results showed that large differences in the mean flows between the El Niño and La Niña winters led to preferential baroclinic life cycles over the North Pacific that closely resembled the life cycle (LC) paradigms LC2 and LC1, respectively, of Thorncroft et al. (1993). Because of the radically differing momentum fluxes between these two life cycles, the results also imply substantial differences in synoptic eddy feedbacks onto the mean flow.

Stepping still further down the scale, recent work shows that El Niño can also impact moisture transports over the eastern Pacific through effects on narrow, concentrated channels termed ''atmospheric rivers'' (Zhu and Newell 1998; Zhu et al. 2000; see also Newell et al. 1992; Iskenderian 1995). Relatively small but systematic differences in wind direction and moisture transports within these atmospheric rivers have been found to vary with respect to ENSO phase, while their interaction with the complex local topography helps determine locations of flooding in El Niño versus non–El Niño years (Ralph et al. 2003, 2004, 2005; Andrews et al. 2004). Figure 24 shows an example of an atmospheric river for a case associated with severe flooding in northern California in February 2004. In addition to systematic effects of ENSO on moisture transports, Persson et al. (2005) found that warm coastal SST anomalies associated with strong El Niño events contribute to enhanced upward sensible and latent heat fluxes that can increase convective available potential energy of air parcels reaching the coast. They conclude that when this destabilized air is forced upward by steep coastal terrain deep convection can be enhanced, with an increased risk of coastal flooding. In a recent study, Bao et al. (2006) document the entrainment of tropical water vapor into atmospheric rivers for extreme West Coast flooding events, and find that the direct linkage to the Tropics is most likely in ENSO-neutral years. These and other effects of climate variations on synoptic, mesoscale, and even microscale processes, represent emerging areas for research on the linkages between weather and climate.

2) THE MADDEN–JULIAN OSCILLATION

The previous results indicate that ENSO can alter the probability of occurrence of certain intraseasonal phenomena within a season and region, as well as change the likelihood of extreme weather events. ENSO itself, however, cannot determine the precise timing of such events. Beyond ENSO, a rich diversity of intraseasonal tropical phenomena exist that also modulate large-scale convection and flow fields, and hence can act as potential wave sources for exciting extratropical variability (Kiladis and Weickmann 1997). Of these, the dominant intraseasonal mode has a spectral peak in the range of approximately 40–50 days (Madden and Julian 1971, 1972), and is now generally known as the MJO. This section briefly summarizes the major features of the MJO, with emphasis on potential linkages to extratropical low-frequency variability and storm behavior. More extensive reviews of the MJO can be found in Madden and Julian (1994) and Zhang (2005).

(i) Tropical features

A remarkable aspect of tropical convection is its tendency to organize on scales much larger than that of individual convective elements. This is clearly evident in climatological-mean conditions, as well as on seasonal-to-interannual time scales in association with ENSO. For both climatological-mean and ENSO conditions, this organization is determined largely by ocean boundary conditions, with enhanced convection typically occurring near the region of warmest waters, which shift eastward from the western tropical Pacific toward

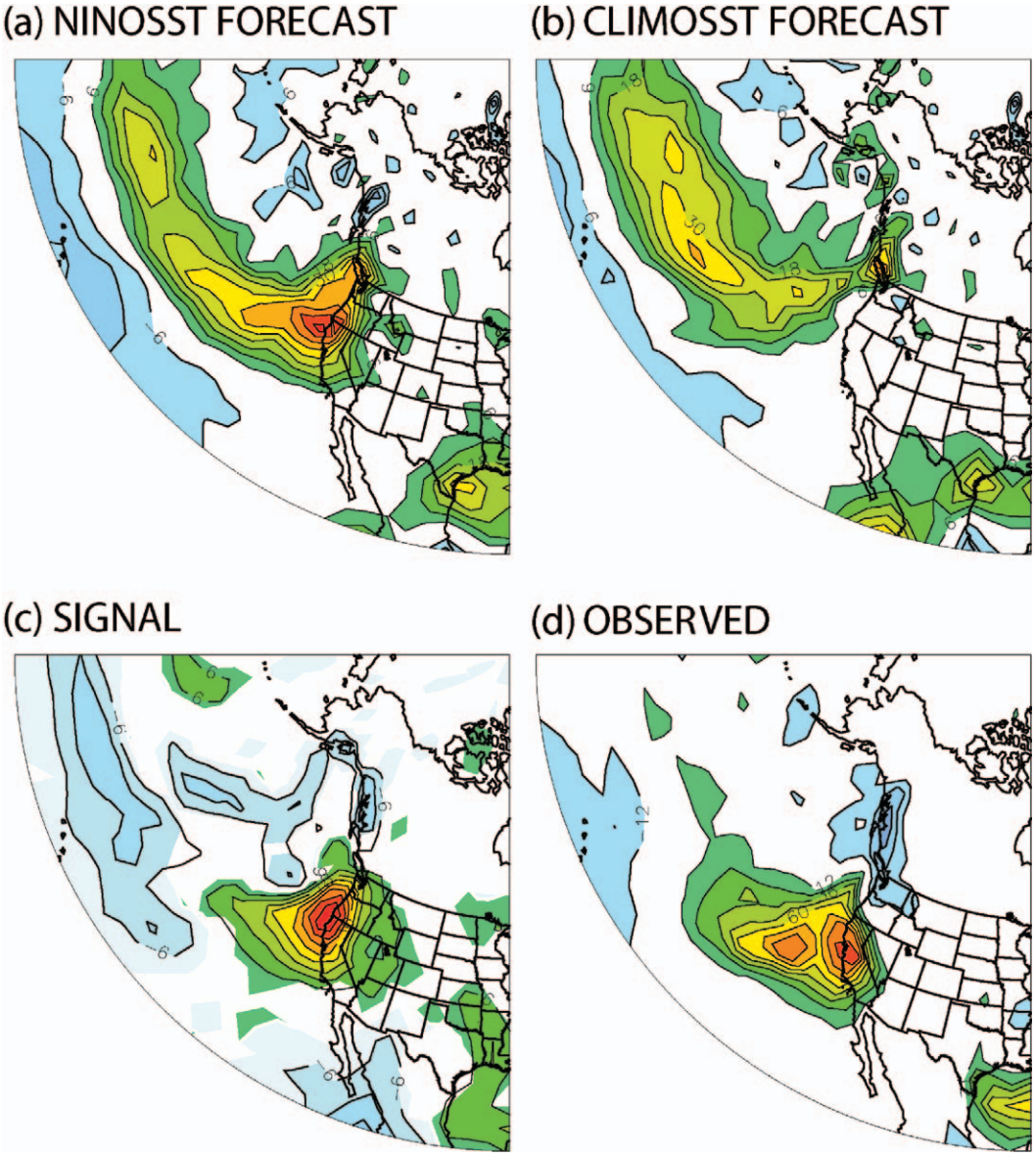

FIG. 21. The 8–14-day mean forecasts of accumulated precipitation anomaly initialized on 24 Jan 1998 and verifying the first week of February 1998 (the ''California rain'' case): (a) NiñoSST forecast, (b) CLIMOSST forecast, (c) synoptic El Niño signal, and (d) the observed precipitation (estimated from the NCEP–NCAR reanalysis). From Barsugli et al. (1999).

the east-central tropical Pacific during El Niño years. Because of the relatively slow evolution of the SSTs, the associated convective heating anomalies remain nearly stationary on subseasonal time scales.

In contrast, organized convection associated with the MJO does not remain geographically fixed, but rather propagates slowly eastward with time from the tropical Indian Ocean to the west-central Pacific, with an average zonal speed of ~5 m s^{-1} (Weickmann et al. 1985; Knutson and Weickmann 1987; Hendon and Salby 1994). This speed in not constant, but varies for different events and stages of the MJO life cycles. While the direction of propagation is primarily zonal, meridional propagation is also often apparent in certain regions, for example, across south Asia and the far western Pacific (Lau and Chan 1985), and toward northern Australia. During the Asian summer monsoon, impacts of the MJO often propagate northward into India and modulate rainfall between ''active'' and ''break'' periods, with effects that may be predictable 15–30 days in advance (Webster and Hoyos 2004).

Figure 25 illustrates the major modes of large-scale tropical convective organization as inferred from OLR anomalies for two winters, one (1996/97) marked by

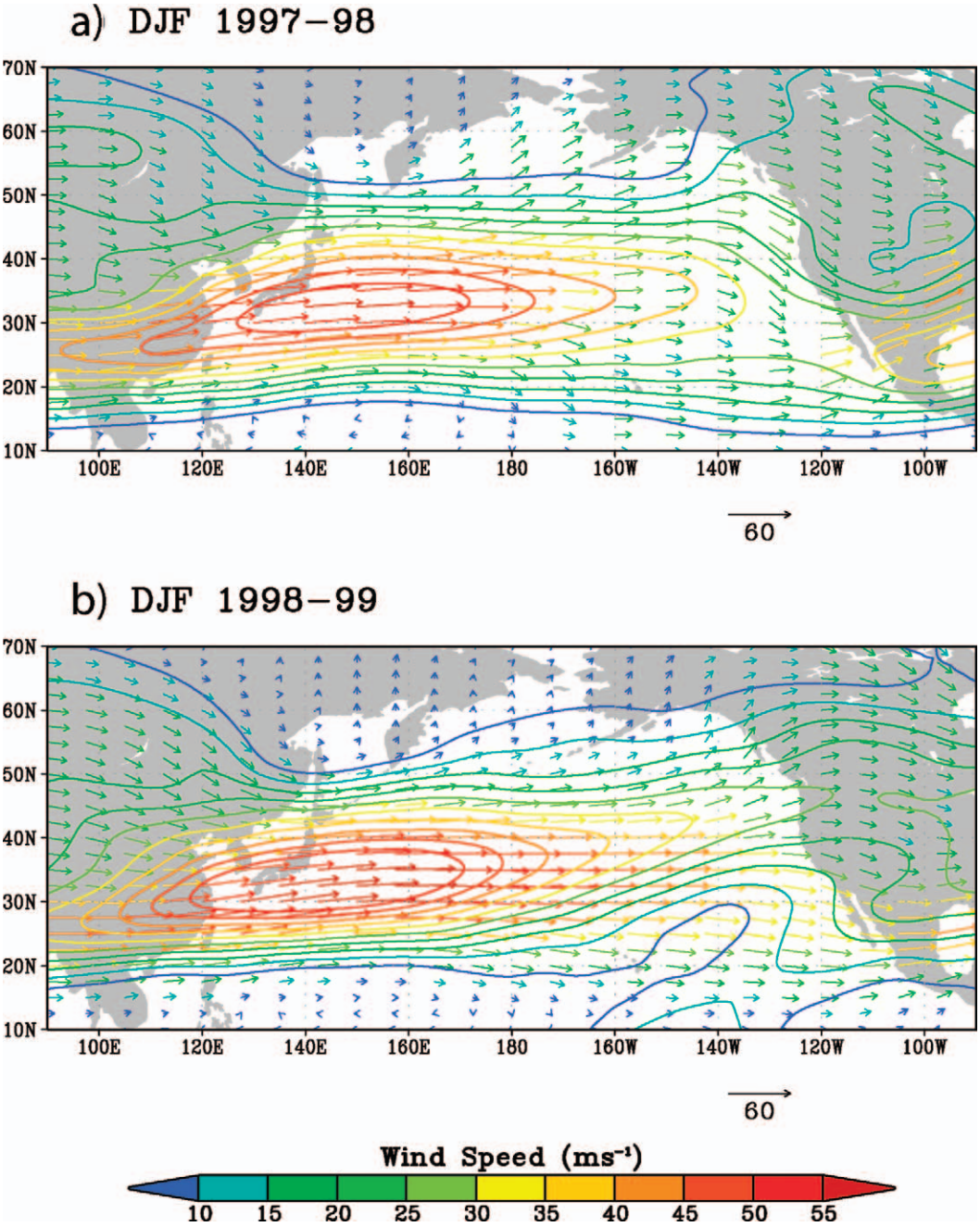

FIG. 22. The 300-hPa time-mean vector winds and wind speeds (m s^{-1}, contours) for winters (a) 1997/98 and (b) 1998/99.

strong MJO activity and relatively weak quasi-stationary (ENSO) forcing, and the other (1997/98) by a strong El Niño event during which MJO activity was nearly absent. In 1996/97, two strong and another two weaker MJO events are evident (Fig. 25a). These events show a tendency for organized convection to develop over the Indian Ocean around 60°E, and propagate slowly eastward until decaying near the date line. While a rough periodicity is evident, this phenomenon occurs over a relatively broad intraseasonal time band of 30–60 days. The events also exhibit notable differences from case to case, much as found for ENSO. In contrast, during 1997/98 (Fig. 25b), there is much less evidence of the slow eastward propagation of convection that could be related to the MJO. Rather, the predominant convective patterns remain quasi-stationary, with a broad maximum in enhanced convection centered east of the date line near the region of warmest SST anomalies (not shown)

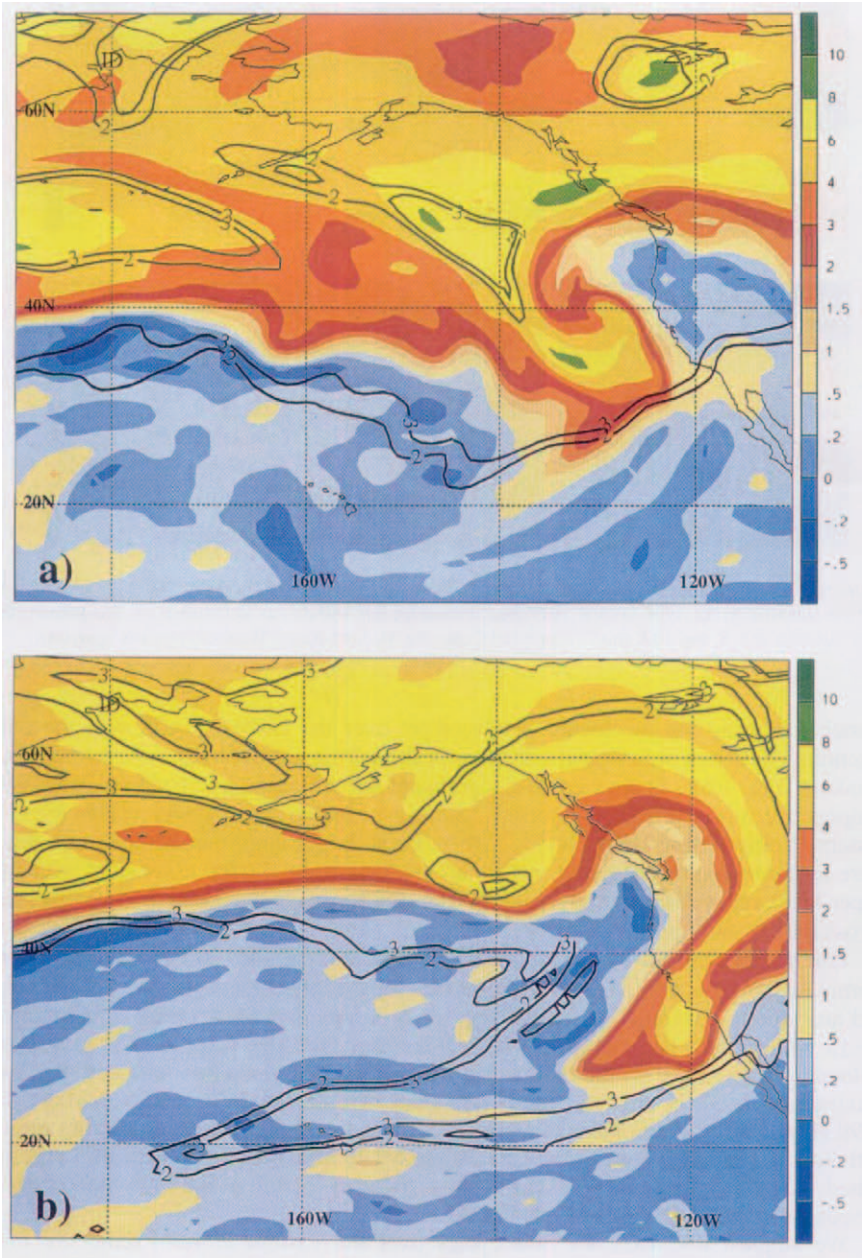

FIG. 23. Potential vorticity at three isentropic levels for (a) 1200 UTC 6 Feb 1998 (El Niño) and (b) 1200 UTC 5 Feb 1999 (La Niña). The 300-K isentropic potential vorticity [IPV; green lines, 2 and 3 potential vorticity units (PVUs)]; 320-K IPV (color shading, PVU, as in color bar); and 340-K PV (black lines, 2 and 3 PVUs) (derived from ECMWF analyses). From Shapiro et al. (2001).

and suppressed convection over much of western tropical Pacific.

In addition to ENSO and MJO, other modes of organized tropical convection are also evident in both winters, including westward-propagating features that are associated with equatorial Rossby waves, and very rapid eastward-propagating features that are a manifestation of equatorial Kelvin waves (Wheeler and Kiladis 1999; Wheeler et al. 2000; Wheeler and Weickmann 2001). (These modes of variability are now monitored routinely for their potential value for medium and extended range predictions, with real-time analyses available online at http://www.cdc.noaa.gov/map/clim/olr_modes/.)

While all the above modes contribute to tropical convective organization, they do not fully account for the overall temporal variations seen in Fig. 25, which are much richer and more complex. Hence composites or schematics should be interpreted as providing only roughly expected relationships. In addition, MJO activity exhibits substantial interannual variability (Hendon

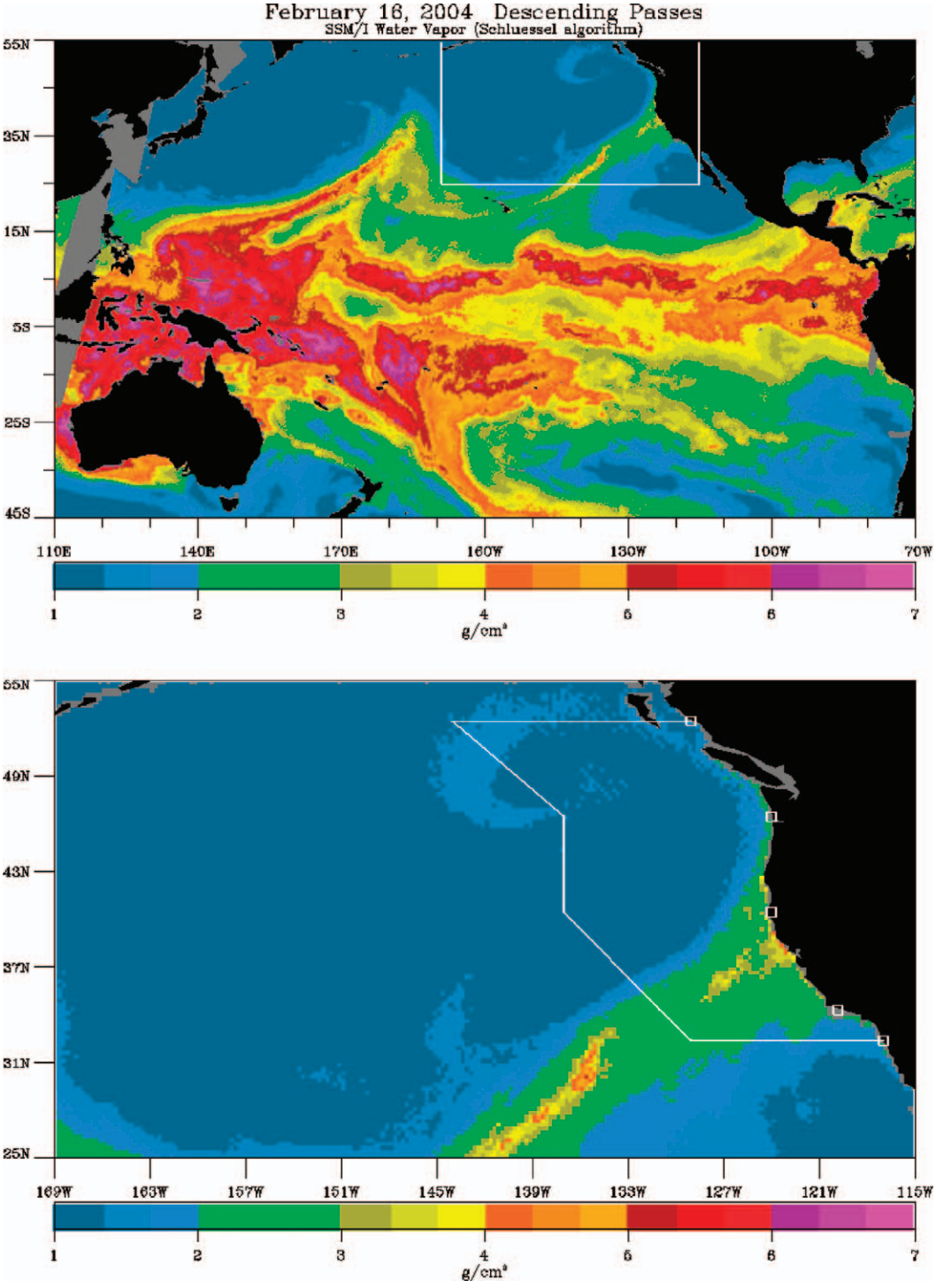

FIG. 24. Composite image of vertically integrated water vapor (cm) taken by the Special Sensor Microwave Imager (SSM/I) on 16 Feb 2004. The top image shows the large-scale connection within the Tropics, with the white box indicating the area of the zoomed-in image for the bottom figure, which shows finer-scale structure within this atmospheric river. This case was associated with severe flooding along the Russian River in northern California. From Bao et al. (2006).

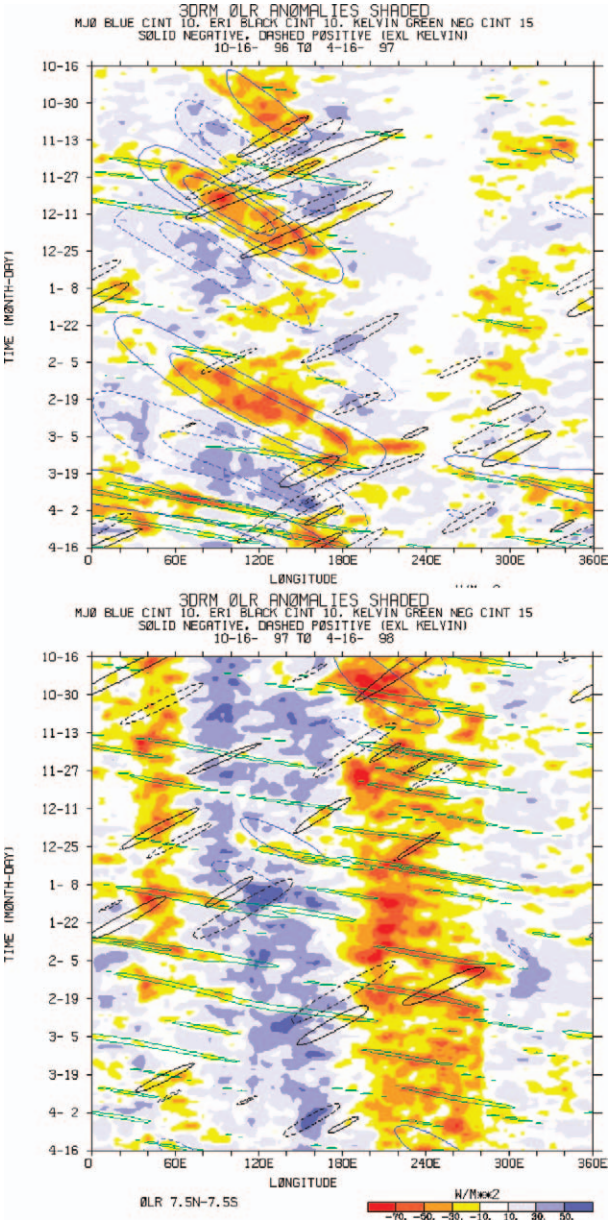

FIG. 25. Hovmöller plot (time–longitude section) of OLR anomalies averaged between 7.5°N and 7.5°S, where the contours illustrate space–time filtered coherent tropical convection modes for (top) 16 Oct 1996–16 Apr 1997 and (bottom) 16 Oct 1997–16 Apr 1998. The blue contours represent the MJO (solid blue for enhanced convective phase, dashed blue for suppressed phase). The green contours are for Kelvin waves and the brown contours for equatorial Rossby wave mode 1. See Wheeler and Kiladis (1999) for additional details. The red shading shows negative OLR anomalies (positive convection anomalies), and the blue shading shows positive OLR anomalies (suppressed convection).

et al. 1999), although in most seasons and years some level of MJO activity is present. Winters with high levels of MJO activity are frequently associated with warmer-than-normal waters over the western Pacific the preceding autumn season (Bergman et al. 2001), consistent with the idea that an expanded warm pool favors strong MJO activity (Wang and Li 1994). This empirical relationship may provide some guidance on anticipated levels of MJO activity for a given winter.

Figure 26, from Madden and Julian (1972), illustrates some of the principal tropical synoptic features related to the MJO. Typical zonal scales, as determined by the distance between maxima and minima in OLR anomalies, are roughly 10 000–20 000 km. Thus, this phenomenon represents a planetary-scale mode of convective organization. More detailed analyses show that within this large-scale structure organized smaller-scale convective features are embedded that include both eastward- and westward-propagating components (Nakazawa 1988). Convection tends to develop preferentially on the eastern side of the large-scale complex and dissipate on the western side, contributing to the slow eastward propagation.

In the Tropics, large-scale diabatic heating anomalies are approximately balanced by adiabatic cooling (Hoskins and Karoly 1981), with regions of active convection characterized by mean ascending motions, low-level convergence, and upper-level divergence. The descending branches of the circulations associated with organized convection occur far from the convectively active regions as part of the tropical atmospheric response to localized heating (Gill 1980; Salby et al. 1994). Anomalies in velocity potential χ (Holton 2004) whose gradients are directly related to the divergent wind component, provide an alternate, very useful means for monitoring the divergent flows associated with tropical convection. Figure 27 shows one example of such analyses, as obtained for the 200-hPa level, in which the tendency for systematic eastward propagation can be seen with periods of roughly 30–50 days.

(ii) Relationships of the MJO to extratropical circulation patterns

Studies beginning in the early 1980s extended previous research by considering relationships between the MJO and extratropical circulation patterns (Weickmann 1983; Weickmann et al. 1985; Knutson and Weickmann 1987; Kiladis and Weickmann 1992a). A schematic (Fig. 28) from Weickmann et al. (1985) illustrates typical upper-level circulation features observed during the phase of the MJO when the convection is centered over Indonesia. Note the twin flanking anticyclones poleward of the maximum convection, similar to what is usually observed with El Niño events, and broadly resembling solutions that were obtained by Gill (1980) in a two-layer dynamical model forced by localized heating on the equator. To the east of the heating there is strong westerly outflow along the equator, again similar to the Gill solutions. In addition, cyclonic circulations extend into higher latitudes. As the convection propagates eastward, midlatitude flows vary between contracted and extended subtropical jets, which can impact midlatitude

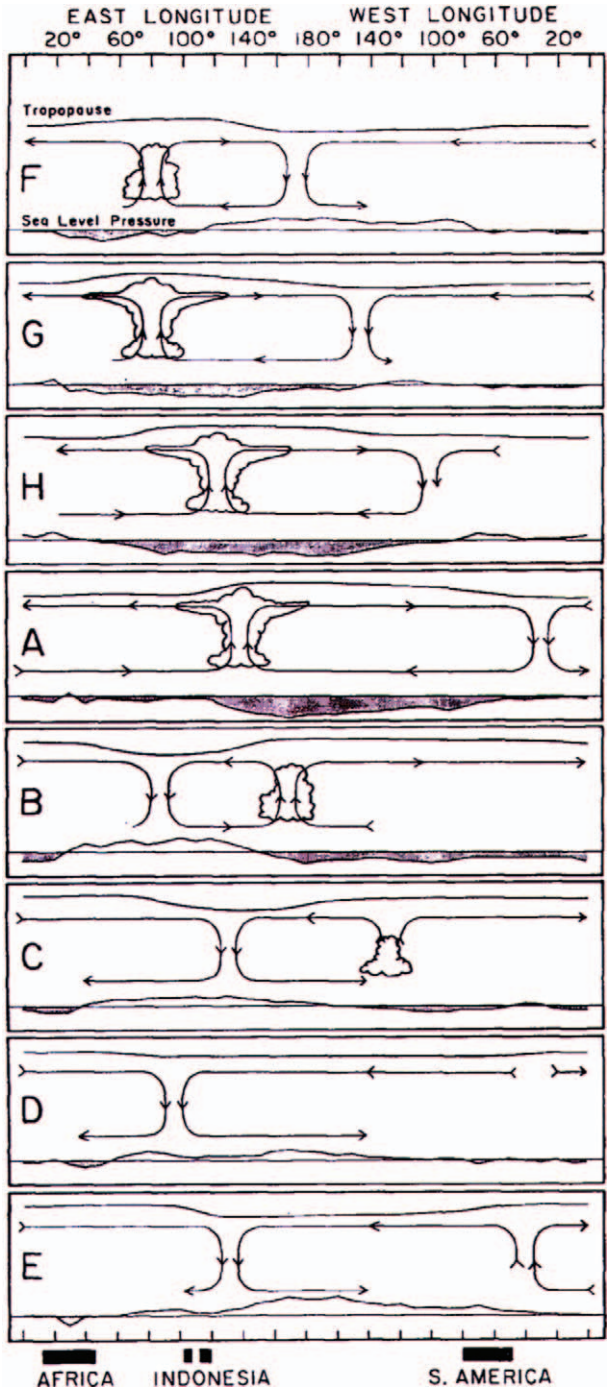

FIG. 26. Schematic of the time–space (zonal plane) variations of the disturbance associated with the 40–50-day oscillation. Dates are indicated symbolically by the letters at the left of each chart and correspond to dates associated with the oscillation in station pressure at Canton, as described in Madden and Julian (1972). Regions of enhanced large-scale convection are indicated schematically by the cumulus and cumulonimbus clouds. The relative tropopause height is indicated at the top of each chart. From Madden and Julian (1972).

weather conditions. Within the Tropics, low-level circulations are approximately antiphase with the upper-level circulations, with low-level inflow into the region of maximum convection. In contrast, at higher latitudes, the low- and upper-level circulations are more nearly in phase, with the upper-level circulation usually substantially stronger.

Subsequent work has refined descriptions of the MJO and evaluated potential connections to extratropical weather systems. Higgins and Mo (1997) found that persistent circulation anomalies over the North Pacific were often preceded by convective anomalies over the tropical western Pacific 1–2 weeks earlier (see also the modeling study by Higgins and Schubert 1996). Several studies have shown that unusually wet conditions in California and the southwest, with drier conditions in the Pacific Northwest are associated with enhanced tropical convection over the central equatorial Pacific (Mo and Higgins 1998a,b; Mo 1999; Jones et al. 2000; Higgins et al. 2000; Whitaker and Weickmann 2001).

Whitaker and Weickmann (2001) developed a statistical prediction model using tropical OLR anomalies as a predictor, first removing the ENSO signal in order to focus on the predictive implications of subseasonal tropical convective variations. They found potential predictability for U.S. west coast precipitation at lead times out to 2 weeks that was connected to subseasonal variations in convection over the central tropical Pacific. Figure 29, adapted from Whitaker and Weickmann, shows a pattern of tropical convective anomalies that is associated 2 weeks later with a doubling of the probability of heavy (upper quintile) rainfall in southern California. The changes in precipitation probabilities on weekly time scales due to the subseasonal variations are roughly comparable to those that would be obtained from an ENSO signal alone (Whitaker and Weickmann 2001). These results suggest that the subseasonal variations in tropical convection can either strongly reinforce or nearly cancel the expected ENSO response.

(iii) Additional comments

While the previous discussion has emphasized the role of the Tropics in forcing extratropical low-frequency variability, it is important to keep in mind that interactions occur in both directions. Wave propagation from higher toward lower latitudes can initiate new convection and produce changes in the tropical wind field (Webster and Holton 1982; Arkin and Webster 1985; Kiladis and Weickmann 1992b; Kiladis 1998). Such changes may initiate new sources for Rossby waves as well as alter the basic state through which the waves propagate.

In addition, surface westerly wind anomalies associated with the MJO can force ocean Kelvin waves that transport warm water eastward from the western Pacific to eastern Pacific. As these waves reach the west coast of South America, they reduce near-coastal upwelling,

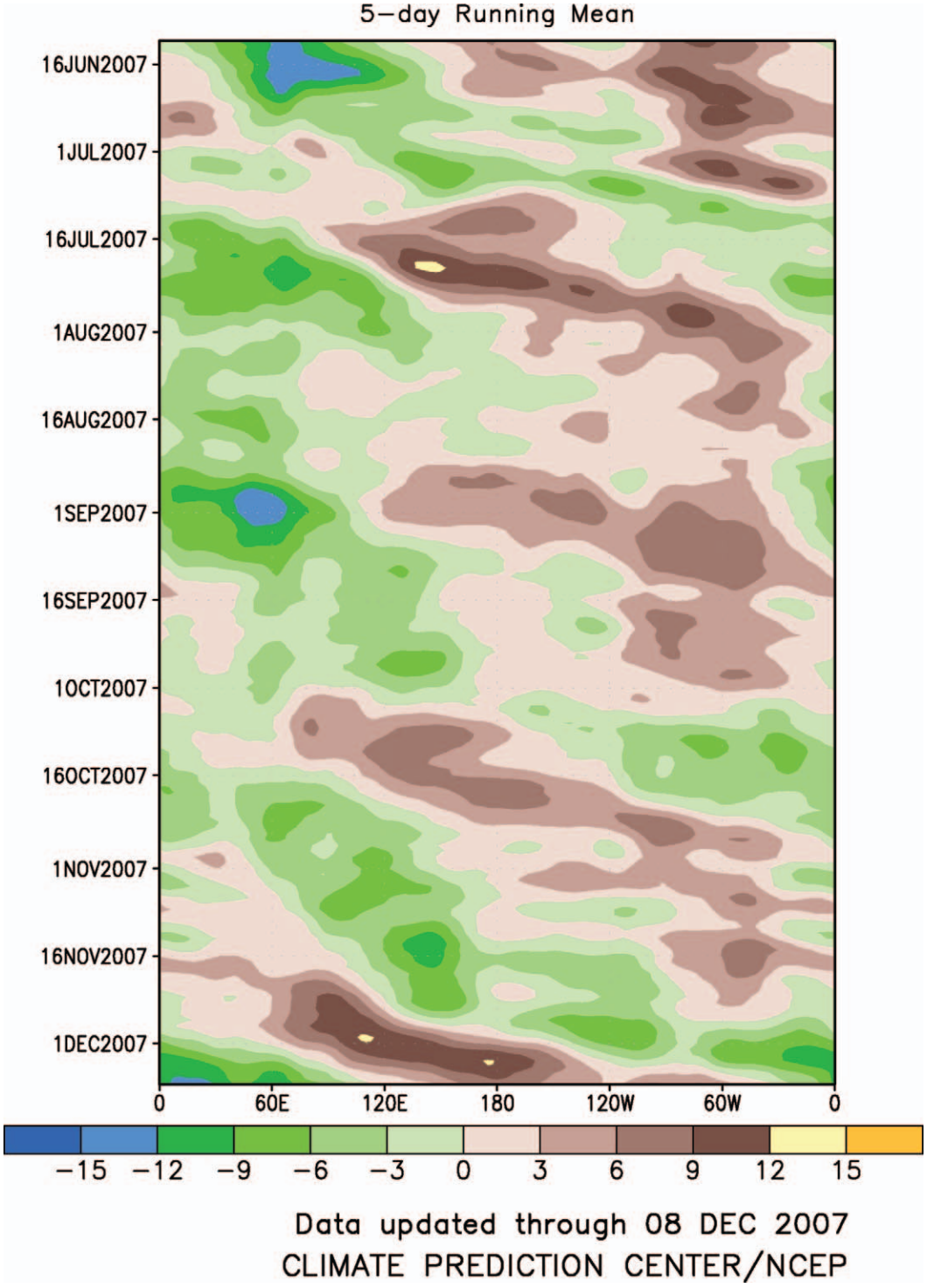

FIG. 27. Time–longitude plot of 200-hPa velocity potential anomalies averaged between 5°N and 5°S. The period is for six months ending 8 Jan 2006. Green colors signify large-scale 200-hPa divergence, while brown colors signify large-scale 200-hPa convergence.

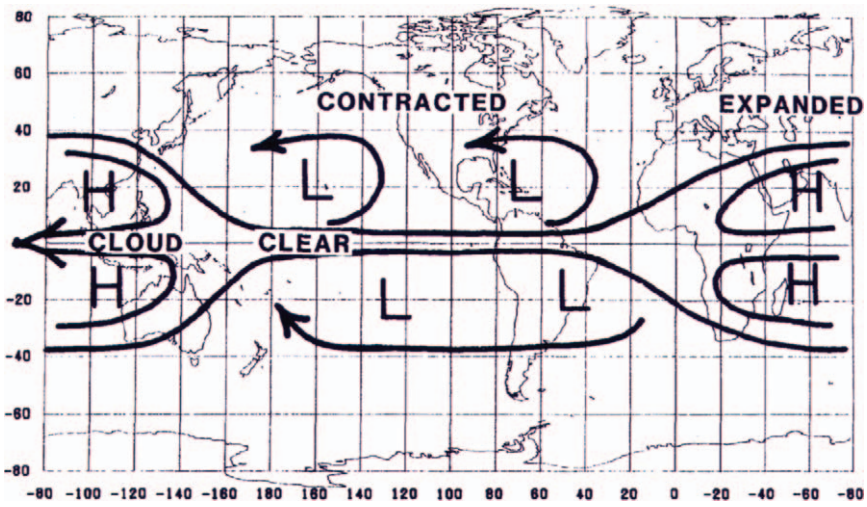

FIG. 28. Schematic of the relationship between OLR and 250-mb circulation for the MJO at a time when convection is at a maximum over Indonesia. From Weickmann et al. (1985).

which can result in rapid SST increases in this region. Several studies suggest that through such atmosphere–ocean interactions MJO events can significantly influence the onset and breakdown, and perhaps also the intensity, of ENSO events (Kessler and Kleeman 2000; Zhang and Gottschalck 2002; McPhaden 2004). Perhaps the biggest lesson emerging from studies in this area is the fundamental importance of coupling between the Tropics and high latitudes, and between the atmosphere and ocean, both of which occur on time scales that are sufficiently short to have implications for the predictability of extratropical low-frequency variability.

d. Other phenomena and processes affecting extratropical low-frequency variability

The previous sections have outlined some key phenomena and processes linking weather and climate variability. We describe here a few other systematic behaviors, most of which have been identified within the past decade. Interestingly, while most research has emphasized the effects of tropical ocean–atmosphere interactions on extratropical low-frequency variability, recent research suggests that additional sources of low-frequency variability, and also extended-range predictability, may be obtained from a very different direction; in particular, circulation variations in the stratosphere and at high latitudes.

Several studies have provided substantial evidence that dynamical coupling between the stratosphere and troposphere can provide an additional source of predictability on time scales from a week to a few months in advance. This is possible in part because the stratospheric circulation varies on relatively long time scales compared with typical tropospheric synoptic-scale disturbances, and thus provides a potential source of memory in the system, just as with the slow tropical atmosphere and ocean variations previously discussed. The difference in characteristic time scales between the stratosphere and troposphere is closely related to the vertical propagation characteristics of Rossby waves (Charney and Drazin 1961). Rapid changes in potential vorticity gradients that occur near the tropopause act as a kind of dynamical low-pass filter that prevents higher-frequency synoptic-scale waves from propagating significantly into the stratosphere (Charney and Drazin 1961; Held 1983). Rossby waves that propagate upward into the stratosphere are characterized by large spatial scales (predominantly zonal wavenumbers 1–3), and are largely forced by topography and quasi-stationary diabatic sources.

The question then becomes to what extent changes in the stratospheric circulation influence tropospheric variability. Recent studies indicate that, at least in some instances, the effects can be substantial. Baldwin and Dunkerton (1999, 2001) found a statistically significant tendency for wind anomalies in the wintertime polar vortex to ''propagate'' downward from the midstratosphere to the tropopause, with effects extending down to the surface pressure and wind fields. Their results indicated that the midstratospheric polar vortex anomalies lead those in the troposphere by 1–2 weeks. Using potential vorticity inversion techniques described earlier, Black (2002) showed that the tropospheric circulation anomalies are related to the balanced flow response to potential vorticity anomalies just above the tropopause. At the surface, the resulting circulation anomalies strongly resemble the Arctic Oscillation (AO) described by Thompson and Wallace (1998, 2000). The AO is characterized by variations in the strength of the tropospheric polar vortex and zonal flow along ~55°N, with zonal wind anomalies of the opposite sign near 35°N, which tend to be somewhat more prominent in the Atlantic than in the Pacific sector (Fig. 30). Because

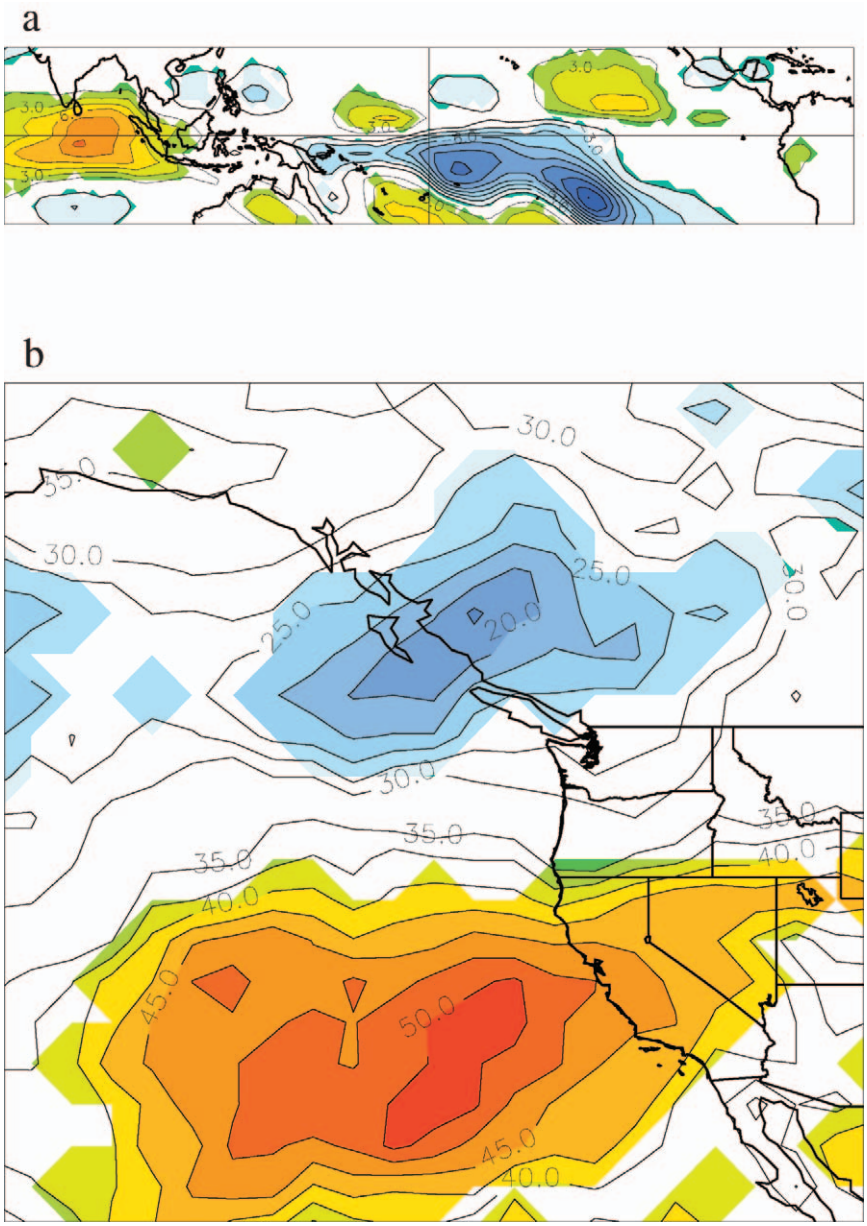

FIG. 29. (a) OLR regressed on leading canonical predictor variable at lag 7 days; map is scaled for one standard deviation of the canonical predictor variable. (b) Probability of precipitation being in the upper tercile given that the leading canonical predictor variable 2 weeks prior is in the upper quintile. Adapted from Whitaker and Weickmann (2001).

of the relatively weaker correlation over the North Pacific, there has been considerable debate on whether the AO and the NAO should be considered as dynamically distinct phenomena (Ambaum et al. 2001; Wallace and Thompson 2002b), and the term ''AO–NAO pattern'' is sometimes used in the literature.

Thompson et al. (2002) and Baldwin et al. (2003a,b) examined, in more detail, the lag relationships between stratospheric and tropospheric flow variations at high latitudes in the wintertime Northern Hemisphere. Both studies concluded that statistically significant skill exists on time scales of a few weeks to months in predicting persistent anomalies in the tropospheric polar circulation from prior knowledge of the stratospheric conditions. Thompson et al. showed that these variations were related to the phase of the QBO and the upper-level manifestation of the AO, the Northern Annular Mode (NAM), which is a quasi-symmetric circulation pattern characterized by variations in the strength of the polar vortex (Wallace and Thompson 2002a).

One phase of the NAM is characterized by an intense, confined tropospheric polar vortex with strong potential

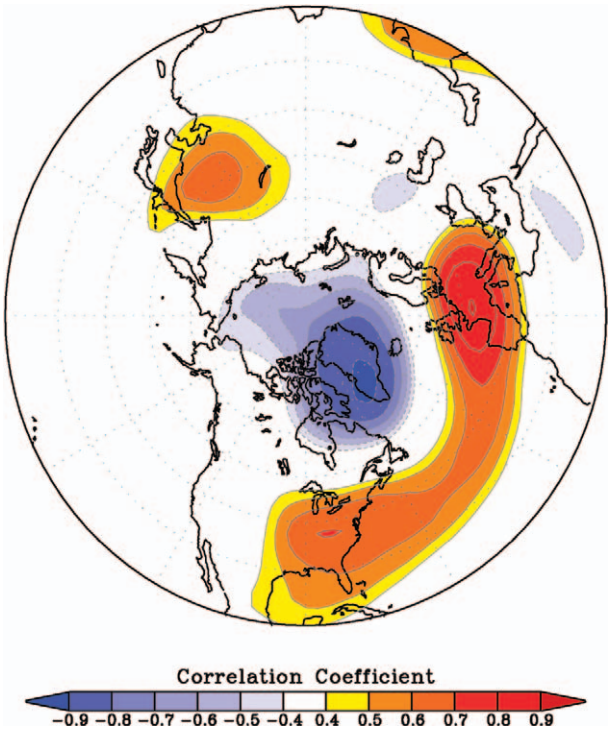

FIG. 30. Correlation of the 500-hPa wintertime (DJF) geopotential heights with the AO index from the NOAA/Climate Prediction Center for the years 1950–2004.

vorticity anomalies along its outer edge, while the other is manifested by a weakened polar vortex with reduced meridional potential vorticity gradients. Because strong positive vorticity gradients increase the horizontal stability of the vortex and inhibit meridional mixing (Charney 1973), surface polar air masses interior to the strong vortex can become extremely cold due to sustained radiative heat losses. Higher vortex stability reduces the likelihood that the cold air will be displaced southward into the midlatitudes. Conversely, a weakened polar vortex allows more mixing and meridional excursions of polar air into midlatitudes. In empirical studies, Thompson et al. (2002) and Thompson and Wallace (2001) found such relationships between changes in the AO and NAM and the subsequent probability of extreme cold-air outbreaks into midlatitudes, with effects persisting out to approximately 2 months. In addition to altering the frequency and extent of cold-air outbreaks, Thompson and Wallace also identified significant impacts on midlatitude storm behavior and high-latitude blocking. However, current understanding of the physical mechanisms associated with the above statistical relationships remains limited.

With the exception of the MJO, most of the modes of low-frequency variability that we have discussed so far are quasi-stationary. Such quasi-stationary features contribute substantially to low-frequency variability at any given geographical location, and frequently produce prolonged anomalies in local and regional weather conditions. However, beyond the MJO there is evidence for other propagating low-frequency phenomena. Branstator (1987) described an example of a long-lived westward-propagating high-latitude mode reminiscent of some early synoptic descriptions of high-latitude blocking anticyclones, which frequently migrate westward (retrogress) when the centers are displaced well north of the main latitudes of the westerlies (Namias 1947; Rex 1950a,b).

More recently, Branstator (2002) showed that the focusing and trapping effects of the time-mean jet stream act as a waveguide that connects variability around the hemisphere. This behavior is manifested synoptically by chains of perturbations that extend along the jet axis and have maximum amplitudes in the upper troposphere (Fig. 31). Branstator's results suggest that extended wave trains are most efficiently excited by forcing in the vicinity of the jets near Southeast Asia and the east coast of North America. In comparison to the teleconnection patterns identified by WG81 and others, characteristic zonal wavelengths are significantly shorter, and hence rapid downstream dispersion can occur along the jet axis at speeds comparable to the local jet strength [cf. Eqs. (4) and (5)]. This mode of evolution appears well established, but potential predictive implications remain to be determined.

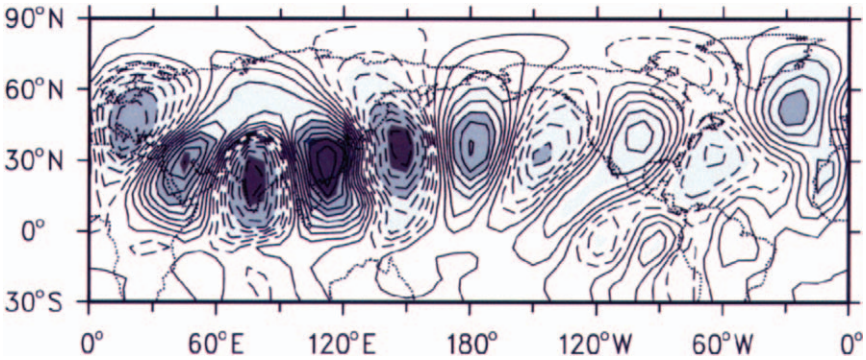

FIG. 31. One-point correlations with a base point at 28.9°N, 112.5°E for internal variability in the winter mean DJF 300-hPa nondivergent meridional winds obtained from the NCAR CCM3. From Branstator (2002).

e. Summary

We began this section by considering the problem of whether early studies on blocking could be placed within a more general and systematic framework. Since 1980, our recognition of phenomena and physical processes contributing to extratropical low-frequency variability has advanced considerably. It is vital to recognize that the typical low-frequency patterns that we have described (e.g., teleconnections) are not fixed physical entities, but rather reflect composites of many individual events, each of which will vary in some aspects. The characteristic patterns we described are useful to the extent that they reveal certain dominant or frequently recurrent physical and dynamical processes that operate on these time scales.

Several potential mechanisms were discussed for producing low-frequency flow variations, including Rossby wave dispersion from localized topographic or diabatic sources; large-scale instabilities and initial value growth; quasi-equilibrium states that represent an approximate balance between forcing, advection, and dissipation; and anomalous eddy forcing associated with changes in synoptic-scale storm activity. It is likely that all of these processes contribute to the total observed spectrum of intraseasonal low-frequency variations, with their relative importance varying from case to case. The specific mechanisms help us understand when and where large low-frequency phenomena will most frequently occur, and what would be the expected flow structures.

For example, consideration of the growth mechanisms suggests why persistent anomalies are more prevalent in the jet exit regions downstream from maxima in synoptic-scale eddy activity, and less favored well upstream of the jet maxima, where barotropic mechanisms would support growth of meridionally elongated eddies [which are associated with rapid eastward energy dispersion; cf. (8)], where the disturbances have yet to enter regions favorable for strong baroclinic growth, and where synoptic-scale feedbacks are generally weaker. To the degree that these processes depend on the mean flow structure and localized sources, they will vary from event to event and year to year as in conjunction with changes in the basic flow and forcing.

Even with steady forcing anomalies, anomalous low-frequency variability will be produced because the climatological-mean flow changes through the year (Newman and Sardeshmukh 1998; Frederisken and Branstator 2005). Changes in responses to a given forcing may be particularly rapid at times of the year when the mean flow itself changes rapidly, as over the central and eastern North Pacific in spring, when a rapid transition occurs from a single- to a double-jet structure. Both the MJO and ENSO also produce systematic changes in the zonal-mean zonal wind fields that tend to propagate slowly poleward from the Tropics into higher latitudes (Black et al. 1996; Kumar and Hoerling 2003). These poleward jet shifts appear to be related to synoptic eddy feedbacks and the response of the meridional circulation to anomalous tropical convection (Weickmann et al. 1997; Feldstein 1998). To the extent that the zonal wind changes are predictable, they may provide another potential source of predictability for extratropical stationary waves.

We then turned our attention to the question of how changes in synoptic-scale variability are related to the low-frequency flow variations. This question is central for two reasons. First, synoptic-scale disturbances are primarily responsible for the midlatitude weather that we seek to predict, especially wintertime precipitation. Hence, understanding the relationships between low-frequency variability, storm tracks, and the evolution of synoptic-scale disturbances is fundamental to the problem of advancing extended range weather predictions. Second, eddy fluxes associated with the synoptic-scale disturbances can force changes in the low-frequency flow, especially in regions of eddy growth and decay. Such interactions appear particularly important in certain classes of events, of which blocking patterns represent one important example.

During blocking events low potential vorticity air is advected far poleward and high potential vorticity air is advected far equatorward of normal. This often leads to breaking Rossby waves, manifested by the formation of closed centers of low potential vorticity (associated with the blocking anticyclone) located far poleward of the subtropical source regions, and closed centers of high potential vorticity (synoptically manifested as cutoff lows) at unusually low latitudes. Such signatures of Rossby wave breaking on upper-level isentropic or constant potential vorticity surfaces have been proposed as a dynamical criterion for defining blocking (Pelly and Hoskins 2003). Observational analyses indicate that blocking occurs preferentially downstream of maxima in synoptic-scale eddy activity in regions where the climatological-mean flow is diffluent. Theoretical analyses of eddy–mean flow interactions (Hoskins 1983; Haines and Marshall 1987) show that regions in which eddy activity decreases eastward will be accompanied by net equatorward fluxes of high potential vorticity (poleward fluxes of low potential vorticity). In regions favorable for blocking, such fluxes tend to weaken the midlatitude westerlies where the mean flow itself is already relatively weak. Thus, theoretical, synoptic and diagnostic analyses are consistent in indicating the likely importance of both the mean flow structure and synoptic-scale eddy feedbacks in the development and maintenance of blocking.

While low-frequency variability can be produced solely through midlatitude processes, tropical heating and flow variations appear to be especially important in determining the potential predictability of the extratropical circulation. Tropical phenomena most likely to enhance predictability are characterized by relatively long time scales, of which we emphasized ENSO and

the MJO. However, just as for the teleconnection patterns, it is the dynamical processes that are in fact crucial. Therefore, tropical heating and flow variations other than ENSO and MJO may also excite significant low-frequency variability in the extratropics (Simmons 1982; Barsugli and Sardeshmukh 2002). In addition to tropical–extratropical interactions, there is growing evidence that variability in the stratosphere influences the evolution of the tropospheric circulation, especially at high latitudes.

In summary, over the past 25 years there have been major advances in our ability to describe and understand mechanisms for low-frequency variability. However, compared with synoptic-scale variability, our detailed knowledge of the phenomena and mechanisms connecting short-term weather with longer-term climate variations is still relatively limited, and abundant opportunities remain for future progress in this area.

4. Advances in forecast skill and analyses of potential predictability

Since 1980, skill in short-range model predictions had increased substantially. By measures for which long-term records are available, such as 500-hPa height root-mean-square errors and anomaly correlations (which, as Professor Sanders would be quick to remind us, are not the same as weather) the rate of increase in numerical weather prediction (NWP) model skill over this period has been roughly 1 day per decade (Kalnay et al. 1998; Simmons and Hollingsworth 2002). So, for example, current NWP forecasts of the 500-hPa heights at lead times between 5 and 6 days are roughly as skillful as were 3-day forecasts in 1980.

At first sight, this would still seem to leave prospects for forecast skill beyond a week just out of reach. However, recent research supports the view that skillful forecasts can be made into the second week of the forecast (‘‘week 2’’), using a combination of model-based and statistical techniques. Further, some predictability studies suggest that forecast skill of weekly-average conditions beyond week 2 is feasible in many regions. Here, we briefly summarize a few of these recent studies on forecast skill and potential predictability.

a. Advances in forecast skill

Of the many steps that have contributed to forecast improvements over the last few decades, one in particular must be highlighted: the introduction of *ensemble prediction methods.* Ensemble predictions were first implemented operationally at both NCEP and ECMWF in December 1992, and subsequently at other major centers (Tracton and Kalnay 1993; Molteni et al. 1996; Houtekamer et al. 1996). The initial practical motivation for introducing ensemble methods was to advance skill in medium-range weather forecasts. This innovation reflected a fundamental change in forecast strategy for the

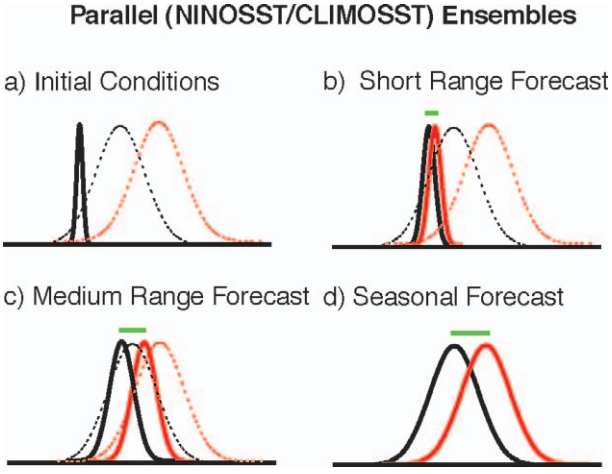

FIG. 32. Schematic probability distribution functions for (a) model initialization, (b) short-term weather forecasts, (c) medium-range weather forecasts, and (d) long-range or seasonal forecasts. The red curve represents the NiñoSST ensemble and the black curves the CLIMOSST ensemble. In (a)–(c) the dotted lines reproduce the long-term or seasonal forecast PDFs from (d). For further details, see text. From Barsugli et al. (1999).

operational centers from a deterministic approach in which numerical weather predictions were derived from a single run of a ‘‘best’’ model, to a more probabilistic approach in which forecasts were derived from an ensemble of model runs obtained from slightly different (perturbed) initial conditions. In order for the ensemble runs to be completed within operational time constraints, this required a trade-off, generally that the individual ensemble members be run at substantially lower spatial resolution, and perhaps also with less sophisticated physical parameterizations, than the single best model.

Ensemble prediction methods are potentially useful at all time scales, but for medium- and extended-range predictions they become crucial, because any single model run can be quite unrepresentative of the distribution of possible outcomes. Figure 32, from Barsugli et al. 1999, illustrates the basic concepts. Even at the analysis time (Fig. 32a), some uncertainty is present due to inevitable observational (and model) limitations. However, the spread in this initial probability distribution function (PDF) is far smaller than that of either climatological-mean PDFs or those associated with anomalous forcing, such as associated with El Niño, as in this illustration. Perturbations to the initial conditions are derived from within the space of possible initial states through a variety of methods (for a recent review, see Buizza et al. 2005). For short-range forecasts (Fig. 32b), the forecast PDF evolves away from the initial state and broadens slightly, but still remains much narrower than, and quite distinct from, either the climatological or El Niño distributions. Thus, these short-range forecasts appear ‘‘almost deterministic.’’ At these ranges, the forecasts are fundamentally initial value

problems, with proper specification of initial conditions being crucial to forecast skill.

Beyond some lead time, which will depend on flow predictability, forecast variable, and user need, the range of possible outcomes becomes so large that the forecasts must be considered probabilistic. At the time shown in Fig. 32c, the forecast PDF is still strongly affected by initial conditions, but has begun to evolve toward the El Niño PDF, suggesting that within this time range boundary conditions have also begun to substantially influence the forecasts. This is the medium-range forecast problem. Finally, the seasonal forecast (Fig. 32d) shows a PDF whose width is comparable to that of the climatological distribution. Forecast skill in this time range is determined predominantly by the ability to project the response of the atmosphere to the anomalous boundary conditions, in this example associated with El Niño. Note that even though the shift in seasonal means is relatively small compared to the overall spread of the climatological distribution, indicative of a modest signal-to-noise ratio (consistent with most midlatitude responses to ENSO), large changes can occur in relative probabilities at the tails of the distributions (i.e., in the extreme events that can have important practical and forecast implications).

Ensemble prediction methods have contributed substantially to increases in weather and climate forecast skill (Kalnay et al. 1998; Kalnay 2003). Despite the advantages of such methods, systematic model errors and insufficient spread of the model forecasts have limited the utility of distributions derived directly from model output (Hamill et al. 2004a,b). These shortcomings are related to the use of a single model in deriving all ensemble members. In this case, only initial condition errors are being sampled, without accounting for other sources of uncertainties (e.g., in the physical parameterizations of the model).

One proposed approach to addressing this issue is by constructing ''superensembles,'' which are weighted averages of ensemble forecasts derived from multiple models (Krishnamurti et al. 2003; Hagedorn et al. 2005; Doblas Reyes et al. 2005) that each differ in their representations of model physics (and perhaps also resolution). This method has shown the ability to substantially increase some measures of forecast skill, and is likely to see increasing use in operational practice. On a very grand scale, the Climateprediction.net (CPDN) Project (Allen 1999; Allen and Stainforth 2002; Stainforth et al. 2002; Piani et al. 2005) is constructing very large superensembles of climate predictions for the twenty-first century. In the CPDN, the Hadley Centre unified climate model (HadSM3) that includes a simplified, thermodynamic representation of the ocean (i.e., a slab ocean model). This model is integrated over a wide range of physical parameter values and initial conditions using a distributed computing strategy, with the model runs being performed on numerous home and other remote computers for which volunteers have donated computing time for the experiments. This strategy has enabled the CPDN project to produce multithousand member ensembles of climate projections, with nearly 150 000 runs and over 10 000 000 model years completed as of early 2006 (for details, see online at http://www.climateprediction.net/index.php). The results of this fascinating project are beginning to be analyzed (e.g., Piani et al. 2005). It is interesting to contemplate whether such distributed computing efforts could be applied to a broader range of weather and climate prediction problems; for example, in forecasting extreme events such as hurricanes, in which current ensemble sizes may be insufficient for adequately estimating probability distributions.

Beyond multimodel ensembles, another promising method toward incorporating effects of model uncertainties is through the use of stochastic parameterizations. In this method, statistical representations of the uncertainties in modeling physical processes are introduced directly into the parameterization schemes (Buizza et al. 1999; Palmer et al. 2005a,b). More recently, an alternative approach, ''ensemble reforecasting,'' has been introduced that shows considerable promise for improving forecast skill (Hamill et al. 2004a,b, 2006). In essence, the ensemble reforecast (ER) method applies a long (multiyear) set of ''reforecasts'' together with model output statistics (MOS) methods to statistically adjust forecast distributions obtained directly from the ensemble forecasts. The use of long training periods enables greatly improved estimates of model systematic errors in both the mean and shape of the distributions. To demonstrate this approach, Hamill et al. (2004a,b) generated a 15-member ensemble of 15-day forecast for every day over a 23-yr period from 1979 to 2001, using a 1998 version of the NCEP medium-range forecast model. Forecasts were evaluated by multiple techniques, including comparisons with 6–10- and 8–14-day operational forecasts of temperatures and precipitation over the continental United States for the winters of 2001 and 2002.

Figure 33 shows a comparison of the ER and operational forecast skill for 6–10-day temperature and precipitation forecasts for the two winters. In this reliability diagram (Wilks 2006), points that lie along the diagonal indicate ''reliable forecasts''; that is, forecasts whose probabilities accurately reflect the likelihood that an event will actually occur (e.g., for all events when the forecast precipitation probability is 60%, precipitation occurs 60% of the time). The spread in the distributions provides a measure of forecast ''resolution'' with, for example, forecasts remaining clustered close to climatological probabilities having low resolution. Probabilistic forecast skill is evaluated through a rank probability skill score (RPSS), which provides a measure of the ''distance'' between the forecast probabilities and the outcome (Epstein 1969; Murphy 1971). Here, the RPSS would have a value of 0 for climatological probability forecasts and 1 for perfect forecasts, the latter

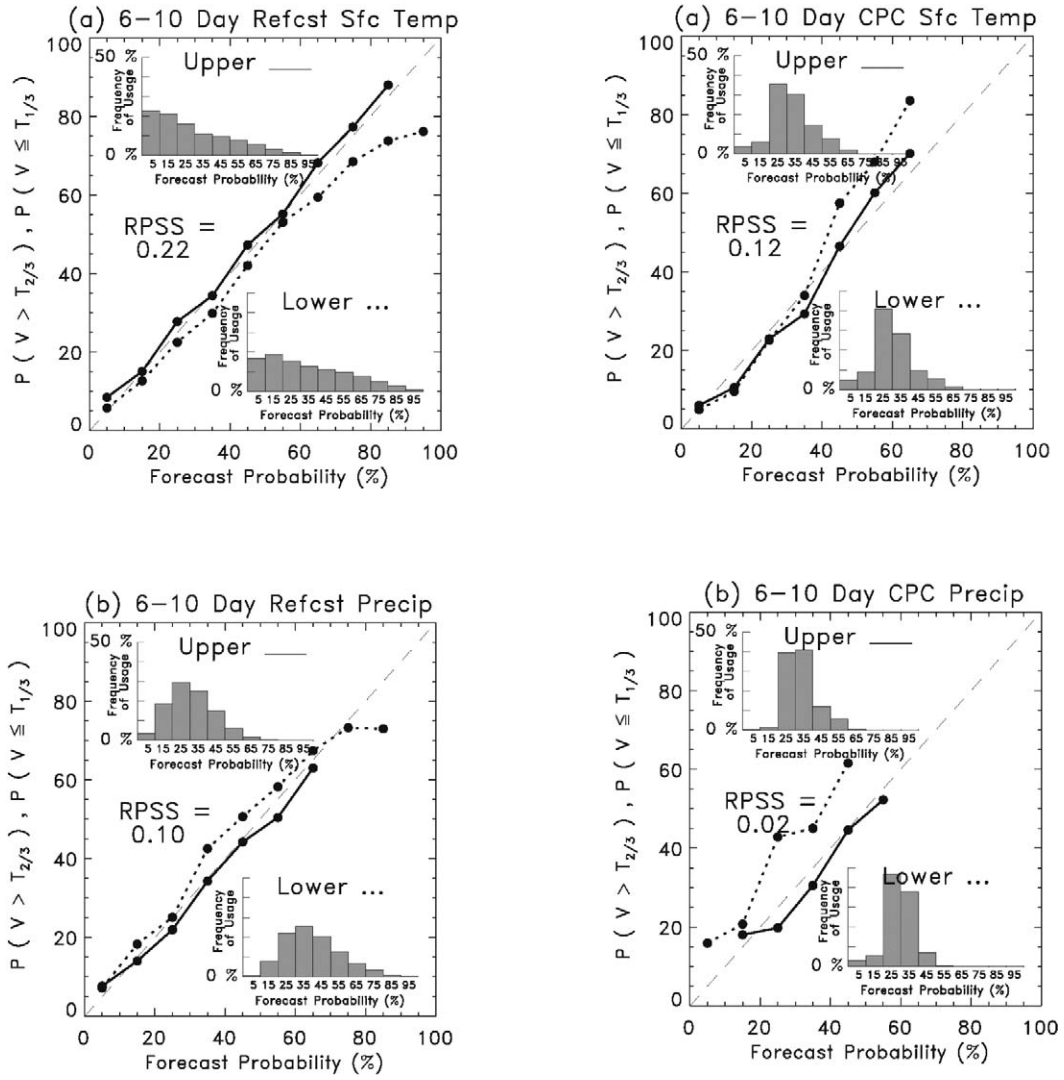

FIG. 33. Reliability diagrams for days 6–10 tercile temperature and precipitation forecasts obtained from (left) the ensemble reforecast method and from (right) NOAA/Climate Prediction Center official forecasts. Forecast skill was evaluated at 484 U.S. stations for a subset of 100 days from the 2001/02 winter. The dotted line denotes lower tercile probability forecasts; the solid line denoted upper tercile forecast probability forecasts. The closeness of the forecast probabilities to the diagonal dashed line provides a measure of forecast reliability; that is, how well forecast and observed probabilities agree. The inset histograms indicate the frequencies with which extreme tercile probability forecasts were made, thus providing a measure of the sharpness of the forecasts. The inset RPSS value indicates the ranked probability skill score. From Hamill et al. (2004b).

requiring that the observed outcome always be predicted with 100% confidence. Comparisons show that the ER forecasts are significantly more skillful than the operational forecasts as measured by the RPSS, due both to increased reliability and resolution. Further analyses indicate that for these years the 8–14-day ER forecasts were also more skillful than the 6–10-day operational forecasts (Hamill et al. 2004a,b), suggesting an improvement in effective forecast lead time of 2–4 days.

Interestingly, Sanders (1979) study also used the RPSS to evaluate skill in 1–4-day probabilistic temperature and precipitation forecasts. While several factors, including differences in temperature and precipitation categories and forecast periods, preclude a precise comparison between studies, a very rough assessment of relative skill is still possible. Such a comparison suggests that probabilistic skill of 6–10-day forecasts of temperature and precipitation in winter using ER is now at roughly the same level as the corresponding cool season (autumn and spring semester at MIT) 3-day temperature and precipitation forecasts evaluated by Sanders for the period 1968–78, while skill in the 8–14-day temperature forecasts from ER is comparable to the average skill of the 4-day temperature forecasts in Sanders's study. While the skill values at these lead times might be considered marginal, they do suggest that the

frontiers of forecast skill have been pushed outward from roughly a 4-day lead time prior to 1980 into the second forecast week today.

b. Potential predictability

If forecast skill has been pushed out into the second week, are we now reaching a point where prospects for additional progress are limited; that is, are we approaching the limits of potential predictability? The seminal studies of Lorenz (1963, 1965, 1969a,b) showed that because of the chaotic nature of atmospheric dynamics, even very small errors in initial conditions inevitably grow until all forecast skill is lost. Estimates by Lorenz, since reinforced in later studies, suggest that on average this *deterministic* predictability limit is reached within a few weeks. Indeed, given the lack of trends in forecast skill in Sanders (1979) study, one might have wondered even at that time whether some sort of predictability limit was already being approached.

However, as Lorenz also clearly recognized, there are different types of prediction problems, and hence also of potential predictability. In addition, as in any theory, the theoretical predictability limits deduced by Lorenz and others are founded on certain assumptions that, when violated, provide opportunities to extend the range of forecasts. One possibility is the existence of phenomena whose intrinsic time scales are much longer than a few weeks. We have previously discussed examples of such phenomena, which include ENSO, QBO, and the MJO. There is clear evidence that such slow variations can lead to *probabilistic* forecast skill at lead times beyond a few weeks. This can occur even if details of the evolution cannot be predicted on these time ranges, as expected from the results of Lorenz and others. Therefore, in considering potential predictability, it is vital to distinguish between deterministic predictability limits and the potential for improved probabilistic forecasts. It is the latter that are at the heart of medium- and extended-range forecasting. Here, we will briefly summarize a few studies suggesting that there remains room for progress in this area.

In a recent study, Newman et al. (2003) examined the potential predictability of weekly-averaged Northern Hemisphere circulation anomalies in winter and summer months. Newman et al. employed the method of linear inverse modeling (LIM), which uses contemporaneous and lagged statistics derived from observations to construct a linear, stable, and stochastically forced model that best approximates the dynamics of the full nonlinear system. This technique has shown great value in understanding and predicting the evolution of tropical sea surface temperatures (Penland and Magorian 1993; Penland and Sardeshmukh 1995; Penland and Matrosova 1998), and despite its great simplicity, is competitive with fully coupled models in forecasting SST anomalies one to four seasons in advance.

In the Newman et al. study, the LIM predictors were derived from 250- and 750-hPa streamfunction fields and vertically integrated diabatic heating fields obtained as iterative solutions of the ''chi problem'' (Sardeshmukh 1993; Winkler et al. 2001). Newman et al. compared the skill of the 2- and 3-week forecasts obtained from the LIM with the skill of medium-range forecasts obtained directly from the NCEP Medium-Range Forecast (MRF) model. The LIM results showed evidence of skill in upper-level streamfunction fields out to at least the third week (week 3) over much of the Northern Hemisphere in winter. The LIM and MRF forecasts had roughly comparable skill in week 2, with the LIM method perhaps slightly superior by week 3. Diagnostic analyses with the LIM indicated that much of the predictability beyond the first week could be attributed to anomalies in tropical heating, which were poorly forecast in the MRF but more successfully predicted with LIM. Newman et al. suggested that weekly averages of upper-level streamfunction were potentially predictable from 2–3 weeks in advance over large portions of the Northern Hemisphere (Fig. 34), with the greatest source of potential predictability coming from the tropical heating fields. Other factors that may increase potential predictability, such as stratospheric flow variations, were not considered in this study.

If tropical variations are important, how well do models do, for example, in predicting anomalies associated with the MJO? There is considerable evidence that models are deficient in representing the MJO, as well as other modes related to tropical convection, and that this may be an important factor limiting extended-range predictability (Jones et al. 2000, 2004; Waliser et al. 1999, 2003). In an illuminating study, Hendon et al. (2000) examined medium-range forecast errors associated with the MJO. Figure 35 shows one example of their results, for 850-hPa zonal wind anomalies, where the analyses are conducted relative to phases of the MJO cycle as identified through a principal components analysis. As expected, the observed zonal wind anomalies propagate slowly eastward. However, the forecast wind anomalies instead propagate westward or remain quasi-stationary, and show a pronounced tendency to weaken with increasing forecast lead time. Similar errors are evident in Hendon et al's analyses of the tropical diabatic heating forecasts (not shown here). Such errors in tropical heating and flow fields can propagate into midlatitudes within a few days (Cai et al. 1996) leading to systematic model errors that may compromise any potential predictability that might be gained from the MJO. While more recent models have improved simulations of the MJO, there are still fundamental deficiencies across a large range of models (Lin et al. 2006). This general problem of improving model simulations and predictions of tropical heating and flow fields constitutes a primary target for future progress in advancing model prediction skill.

The above studies have emphasized forecasts and po-

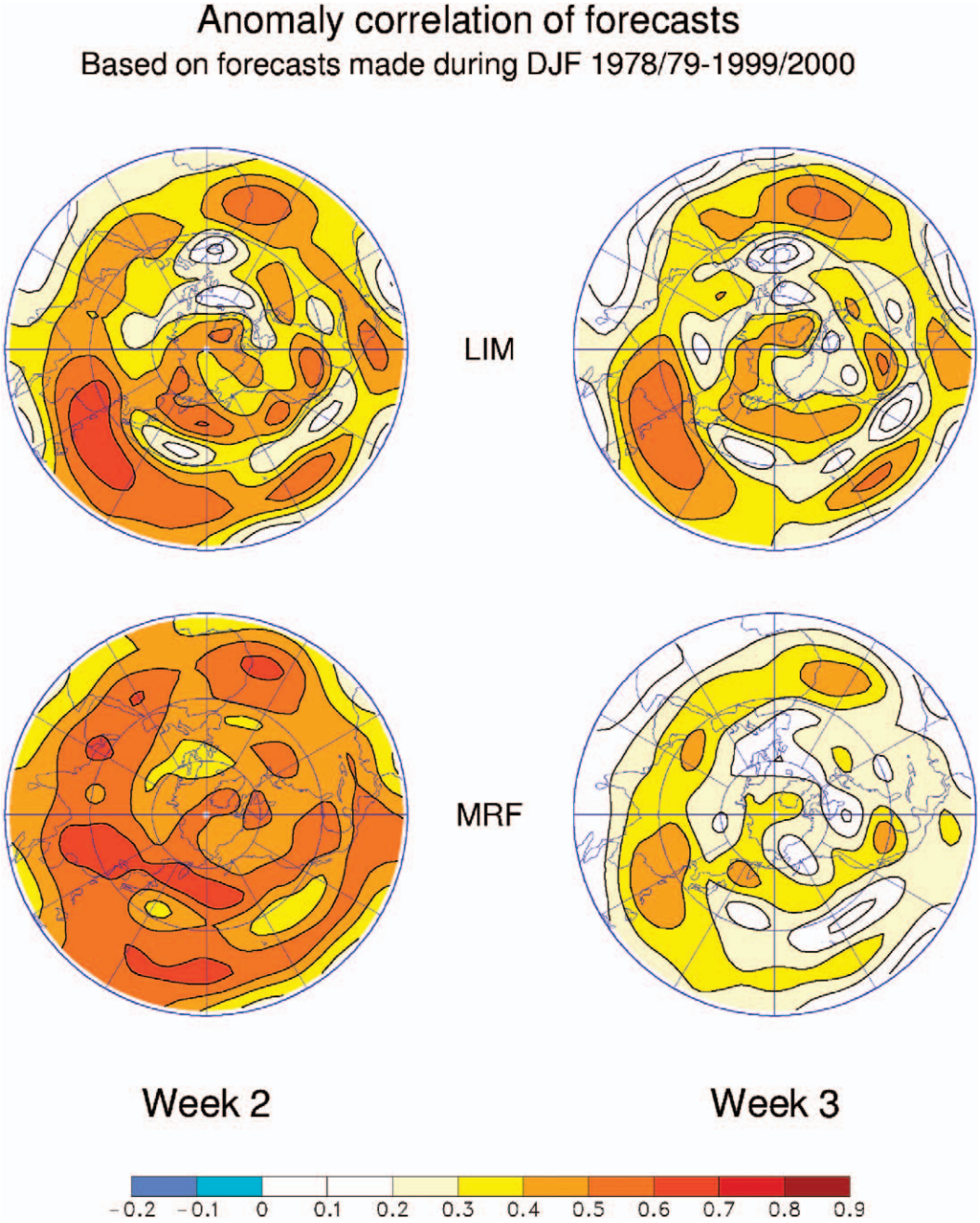

FIG. 34. Comparison of local anomaly correlations of 250-hPa streamfunction wintertime forecasts for the LIM with a 1998 version of the NCEP MRF model: (top) LIM and (bottom) MRF98. The contour interval is 0.1 with negative and zero contours indicated by blue shading and dashed lines. Shading of positive values starts at 0.2; redder shading denotes larger values of correlation, with the reddest shading indicating values above 0.6. From Newman et al. (2003).

tential predictability extending from weather time scales out. There are also vigorous efforts to determine to what extent climate variations influence the statistics of weather variability (Gershunov and Barnett 1998; Gershunov 1998; Gershunov and Cayan 2003; Cayan et al. 1999). To date, most research in this area has been empirical, but new efforts are emerging to employ ensemble modeling techniques to estimate changes in the probability distributions of weather events. In one recent example, Schubert et al. (2005) applied this approach to estimate the potential impact of ENSO on the probability of extreme winter storms developing along the U.S. Gulf and East Coasts (Schubert et al. 2005), and found significant differences in storm probabilities for El Niño versus La Niña winters. This approach is likely to provide new avenues for forecast progress, and will

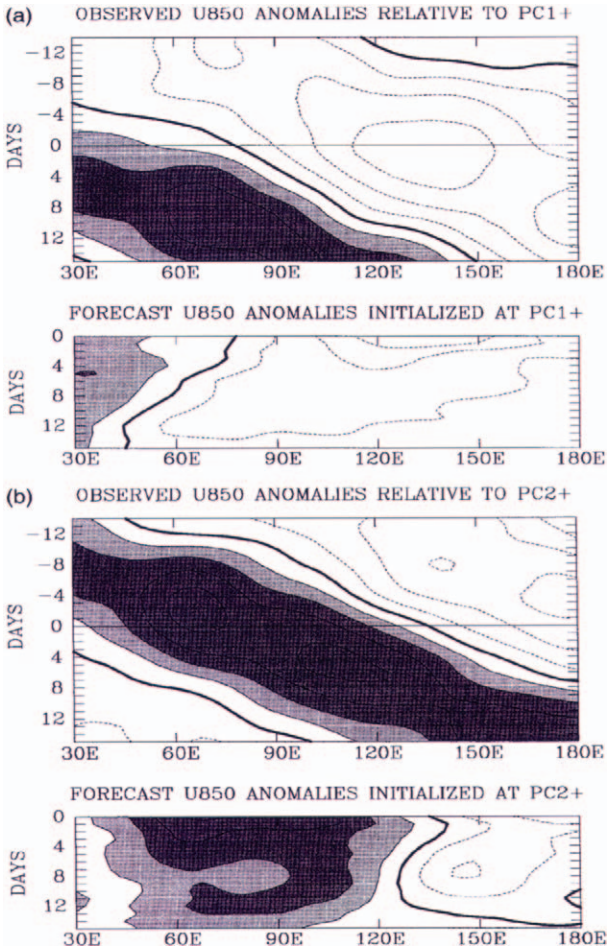

FIG. 35. Composite anomalies (annual cycle removed) of 850-hPa zonal wind relative to (a) maximum PC1+ and (b) maximum PC2+, where PC1+ and PC2+ are principal component patterns representing different phases of the MJO. Anomalies are averaged over latitudes from 5°N to 15°S. (top) The observed anomalies from time −14 to +14 days, where day 0 is the maximum for the principal component. (bottom) The forecast anomalies (mean model error and annual cycle removed) for forecasts initialized at day 0. From Hendon et al. (2000).

also further our understanding of the links between weather and climate phenomena.

5. Future directions

The previous sections have highlighted advances in our understanding and capabilities to predict phenomena at the interface between weather and climate. While progress has been impressive, the research also illuminates areas where significant future gains are possible. Over the next decade, it is likely that improving understanding and capabilities to predict the links between weather and climate will serve as increasingly vital components of an overall research strategy in the earth system science.

In this regard, emerging thrusts in international and national research priorities suggest that over time, artificial distinctions will be removed between weather and climate, as we begin to achieve a more unified understanding of phenomena and processes across time scales. Over the next decade, the World Meteorological Organization (WMO) World Weather Research Program (WWRP) is proposing a major international research and development program called The Observations, Research, and Prediction Experiment (THORPEX) to accelerate improvements in forecasts of high-impact weather on time scales from 1 day to 2 weeks (THORPEX 2004). During this same period, the WMO World Climate Research Program (WCRP) is proposing the Coordinated Observation and Prediction of the Earth System (COPES) Program to address the seamless prediction problem on time scales from weeks to centuries in advance (COPES 2005). Within the United States, the Climate Change Science Program (CCSP) 10-yr strategic plan (CCSP 2003) identifies as a key research question the relationships between climate variations and change and extreme events, such as droughts, floods, wildfires, heat waves, and hurricanes. Achieving the objectives of these programs will require a more unified approach than in the past to understanding the connections between weather and climate. Such an approach is entirely in keeping with the growing demand from the public and decision makers for a seamless suite of weather and climate forecasts that span time scales from very short range forecasts to decadal to centennial climate change projections.

As in the past, it will be fruitful to continue attacking problems on weather–climate linkages from both the weather side out and climate side in. Results from both approaches indicate that a key common issue will be to improve the modeling of tropical convection. Predictability studies described previously suggest that beyond about 10 days, tropical heating variations provide a primary source for potential predictability. By the second week in forecasts, even very simple models that incorporate improved predictions of tropical heating are competitive with operational prediction models, because of major deficiencies in the latter models in predicting the tropical heating fields. Improved observations and simulations of the stratospheric circulation and links to tropospheric weather provide another possible source for extended-range predictability.

Given the chaotic nature of the weather–climate system, probabilistic forecasts will always be at the heart of forecasts at and beyond the medium range. Advances in ensemble prediction techniques as well as data assimilation methods will be central to improving probabilistic estimates. As discussed previously, accurate probabilistic estimates of extreme events will require large ensemble sizes, as well as improved methods for estimating probability distributions from the ensembles. Novel prediction approaches and new applications of ensemble forecasts, including multimodel and reforecast methods, provide significant potential for improving

forecast skill, as well for identifying the strengths and limitations of present-generation numerical weather prediction models.

Beyond these steps, there are abundant opportunities for advances through more detailed analyses and improved modeling of the various mechanisms that contribute to low-frequency variability. While several mechanisms were discussed, others not covered in this overview also need thorough consideration. Some examples include influence of land surface properties, including soil moisture, snow, vegetation, and topography; other modes of climate variability beyond those discussed in this review; and the role of tropical ocean variability outside the Pacific. For the latter, emerging evidence suggests the Indian Ocean may hold particular importance (e.g., Hoerling and Kumar 2003).

In considering future research directions, it is useful to recall the three general questions for understanding the links between weather and climate raised at the start of this overview. The first question was how climate variations and change can affect weather phenomena. A central issue in addressing this question will be to determine how probability distribution functions of various weather phenomena, and especially extreme events, are altered by climate variations and change. The study by Schubert et al. (2005) cited earlier provides one recent example of a modeling approach toward addressing this question for the case of wintertime storms along the U.S. Gulf and East Coasts. Advances in ensemble modeling techniques will be fundamental in making further progress in this area. A second important requirement will be to improve methods for modeling or downscaling climate predictions to the scales required for extreme weather events. A third challenge will be to improve our understanding of the mechanisms by which climate variations and change lead to systematic changes in weather events, and the regional and local implications of such connections. To achieve this objective will require improved scientific understanding of the mechanisms by which natural climate variations such as ENSO, AO–NAO, QBO, polar, and stratospheric–tropospheric interactions influence weather phenomena, especially storm-track changes, and determination of the full predictive implications for surface weather conditions.

New lines of research are emerging from questions on how aerosols, trace constituent species, dust transports, and other variables of the climate system influence weather variations. Of vital societal importance is how storm behavior, including changes in storm tracks and intensities, may change in response to anthropogenic forcing. While most current model projections indicate relatively greater warming at higher latitudes, implying a decrease in midlatitude baroclinicity, effects of changes in moisture and planetary wave patterns remain as major sources of uncertainty for projecting future changes in storm tracks and intensities.

Near-term research thrusts related to the second question, how weather phenomena affect climate variations and change, will likely focus on tropical–extratropical interactions, especially the role of tropical convection, boundary layer processes, and ocean–atmosphere–land interactions. Addressing this question will require significant efforts to better understand the hydrological cycle and coupling between short time-scale and climate processes.

The third question, identifying key phenomena and processes that bridge the time scales between weather and climate, will likely also have a major focus on improving the observations, analysis, and modeling of links between tropical and midlatitude phenomena, especially intraseasonal phenomena such as the Madden–Julian oscillation. Variations in the hydrological cycle and ocean–atmosphere interactions at these intermediate time scales are high near-term research priorities. As noted earlier, compared to our knowledge of synoptic-scale storm systems, our detailed understanding of the phenomena and mechanisms connecting short-term weather with longer-term climate variations still remains relatively limited. Attempts to create ''synoptic–dynamic models'' to aid in interpreting and forecasting features within the medium- to extended-range forecasts are just being developed (Weickmann and Berry 2007), and there is ample room for more work in this area. In this regard, studies cited previously by Shapiro et al. (2001) and Ralph and colleagues suggest new directions for research linking weather and climate phenomena.

Traditionally, different scientific communities have focused on ''weather prediction'' and ''climate prediction.'' To make progress over the next decade, we will need to move past this dichotomy and build stronger links between these two communities. We will also need to develop more scientists who are fluent in both weather and climate problems and in the associated methodological approaches. And we will certainly always need scientists like Fred Sanders to make the fundamental connections between observations and analysis of phenomena, dynamical understanding, and the science of weather and climate forecasting.

Acknowledgments. My understanding on this subject has benefited from many years of conversations and interactions with my colleagues at the former NOAA–CIRES Climate Diagnostics Center, now part of the NOAA/Earth System Research Laboratory. I am grateful to Dr. Klaus Weickmann and Professor Lance Bosart for carefully reviewing earlier drafts of this paper and providing many useful suggestions, and to Mr. Jon Eischeid for his extraordinary help in preparing the figures. I also thank Drs. Jeffery Whitaker, Thomas Hamill, and Marty Ralph for their helpful comments and suggestions, and Drs. Robert Black and Steve Mullen for their very thoughtful reviews, which led to substantial improvements in this paper. And, of course, my great thanks to Professor Fred Sanders, whose incisive approaches to problems and enthusiasm for understanding

atmospheric phenomena profoundly influenced my thinking, surely the objective as well as the mark of a great teacher.

REFERENCES

Alexander, M. A., I. Blade, M. Newman, J. R. Lanzante, N. C. Lau, and J. D. Scott, 2002: The atmospheric bridge: The influence of ENSO teleconnections on air–sea interaction over the global oceans. *J. Climate,* **15,** 2205–2231.

Allen, M. R., 1999: Do it yourself climate prediction. *Nature,* **401,** 642.

——, and D. A. Stainforth, 2002: Towards objective probabalistic climate forecasting. *Nature,* **419,** 228.

Ambaum, M. H. P., B. J. Hoskins, and D. B. Stephenson, 2001: Arctic Oscillation or North Atlantic Oscillation? *J. Climate,* **14,** 3495–3507.

Andrews, D. G., and M. E. McIntyre, 1976: Planetary waves in horizontal and vertical shear: The generalized Eliassen–Palm relation and the mean zonal acceleration. *J. Atmos. Sci.,* **33,** 2031–2048.

Andrews, E. D., R. C. Antweiler, P. J. Neiman, and F. M. Ralph, 2004: Influence of ENSO on flood frequency along the California coast. *J. Climate,* **17,** 337–348.

Arkin, P. A., and P. J. Webster, 1985: Annual and interannual variability of tropical-extratropical interaction: An empirical study. *Mon. Wea. Rev.,* **113,** 1510–1523.

Baldwin, M. P., and T. J. Dunkerton, 1999: Propagation of the Arctic Oscillation from the stratosphere to the troposphere. *J. Geophys. Res.,* **104D,** 30 937–30 946.

——, and ——, 2001: Stratospheric harbingers of anomalous weather regimes. *Science,* **294,** 581–584.

——, D. B. Stephenson, D. W. J. Thompson, T. J. Dunkerton, A. J. Charlton, and A. O'Neill, 2003a: Stratospheric memory and skill of extended-range weather forecasts. *Science,* **301,** 636–640.

——, D. W. J. Thompson, E. F. Shuckburgh, W. A. Norton, and N. P. Gillett, 2003b: Weather from the stratosphere? *Science,* **301,** 317.

Bao, J. W., S. A. Michelson, P. J. Neiman, F. M. Ralph, and J. M. Wilczak, 2006: Interpretation of enhanced integrated water vapor bands associated with extratropical cyclones: Their formation and connection to tropical moisture. *Mon. Wea. Rev.,* **134,** 1063–1080.

Barnston, A. G., and R. E. Livezey, 1987: Classification, seasonality, and persistence of low-frequency atmospheric circulation patterns. *Mon. Wea. Rev.,* **115,** 1083–1126.

Barsugli, J. J., and P. D. Sardeshmukh, 2002: Global atmospheric sensitivity to tropical SST anomalies throughout the Indo-Pacific basin. *J. Climate,* **15,** 3427–3442.

——, J. S. Whitaker, A. F. Loughe, P. D. Sardeshmukh, and Z. Toth, 1999: The effect of the 1997/98 El Niño on individual large-scale weather events. *Bull. Amer. Meteor. Soc.,* **80,** 1399–1411.

——, S. I. Shin, and P. D. Sardeshmukh, 2005: Tropical climate regimes and global climate sensitivity in a simple setting. *J. Atmos. Sci.,* **62,** 1226–1240.

Berggren, R., B. Bolin, and C. G. Rossby, 1949: An aerological study of zonal motion, its perturbation and breakdown. *Tellus,* **1,** 14–37.

Bergman, J. W., H. H. Hendon, and K. M. Weickmann, 2001: Intraseasonal air–sea interactions at the onset of El Niño. *J. Climate,* **14,** 1702–1719.

Bjerknes, J., 1969: Atmospheric teleconnections from the equatorial Pacific. *Mon. Wea. Rev.,* **97,** 163–172.

Black, R. X., 1997: Deducing anomalous wave source regions during the life cycles of persistent flow anomalies. *J. Atmos. Sci.,* **54,** 895–907.

——, 2002: Stratospheric forcing of surface climate in the Arctic oscillation. *J. Climate,* **15,** 268–277.

——, and R. M. Dole, 1993: The dynamics of large-scale cyclogenesis over the North Pacific Ocean. *J. Atmos. Sci.,* **50,** 421–442.

——, and ——, 2000: Storm tracks and barotropic deformation in climate models. *J. Climate,* **13,** 2712–2728.

——, and B. A. McDaniel, 2004: Diagnostic case studies of the northern annular mode. *J. Climate,* **17,** 3990–4004.

——, D. A. Salstein, and R. D. Rosen, 1996: Interannual modes of variability in atmospheric angular momentum. *J. Climate,* **9,** 2834–2849.

Blackmon, M. L., 1976: Climatological spectral study of 500 mb geopotential height of the Northern Hemisphere. *J. Atmos. Sci.,* **33,** 1607–1623.

——, J. M. Wallace, N. C. Lau, and S. L. Mullen, 1977: Observational study of Northern Hemisphere wintertime circulation. *J. Atmos. Sci.,* **34,** 1040–1053.

——, R. A. Madden, J. M. Wallace, and D. S. Gutzler, 1979: Geographical variations in the vertical structure of geopotential height fluctuations. *J. Atmos. Sci.,* **36,** 2450–2466.

——, Y. H. Lee, and J. M. Wallace, 1984: Horizontal structure of 500-mb height fluctuations with long, intermediate, and short-time scales. *J. Atmos. Sci.,* **41,** 961–979.

Borges, M. D., and P. D. Sardeshmukh, 1995: Barotropic Rossby wave dynamics of zonally varying upper-level flows during northern Winter. *J. Atmos. Sci.,* **52,** 3779–3796.

Bove, M. C., J. J. O'Brien, J. B. Eisner, C. W. Landsea, and X. Niu, 1998: Effect of El Niño on U.S. landfalling hurricanes, revisited. *Bull. Amer. Meteor. Soc.,* **79,** 2477–2482.

Branstator, G., 1985: Analysis of general circulation model sea surface temperature anomaly simulations using a linear model. Part I: Forced solutions. *J. Atmos. Sci.,* **42,** 2225–2241.

——, 1987: A striking example of the atmospheres leading traveling pattern. *J. Atmos. Sci.,* **44,** 2310–2323.

——, 1995: Organization of storm track anomalies by recurring low-frequency circulation anomalies. *J. Atmos. Sci.,* **52,** 207–226.

——, 2002: Circumglobal teleconnections, the jet stream waveguide, and the North Atlantic oscillation. *J. Climate,* **15,** 1893–1910.

Buizza, R., M. Miller, and T. N. Palmer, 1999: Stochastic representation of model uncertainties in the ECMWF Ensemble Prediction System. *Quart. J. Roy. Meteor. Soc.,* **125,** 2887–2908.

——, P. L. Houtekamer, Z. Toth, G. Pellerin, M. Z. Wei, and Y. J. Zhu, 2005: A comparison of the ECMWF, MSC, and NCEP global ensemble prediction systems. *Mon. Wea. Rev.,* **133,** 1076–1097.

Cai, M., 1992: A physical interpretation for the stability property of a localized disturbance in a deformation flow. *J. Atmos. Sci.,* **49,** 2177–2182.

——, and M. Mak, 1990: On the basic dynamics of regional cyclogenesis. *J. Atmos. Sci.,* **47,** 1417–1442.

——, J. S. Whitaker, R. M. Dole, and K. L. Paine, 1996: Dynamics of systematic errors in the NMC medium range forecast model. *Mon. Wea. Rev.,* **124,** 265–276.

Cane, M. A., S. E. Zebiak, and S. C. Dolan, 1986: Experimental forecasts of El Niño. *Nature,* **321,** 827–832.

Cayan, D. R., K. T. Redmond, and L. G. Riddle, 1999: ENSO and hydrologic extremes in the western United States. *J. Climate,* **12,** 2881–2893.

CCSP, 2003: Strategic plan for the U.S. Climate Change Science Program. Climate Change Science Program and the Subcommittee on Global Change Research Rep., Climate Change Program Office, Washington, DC, 202 pp.

Chang, E. K. M., 1993: Downstream development of baroclinic waves as inferred from regression-analysis. *J. Atmos. Sci.,* **50,** 2038–2053.

——, 2001: The structure of baroclinic wave packets. *J. Atmos. Sci.,* **58,** 1694–1713.

——, 2003: Midwinter suppression of the Pacific storm track activity as seen in aircraft observations. *J. Atmos. Sci.,* **60,** 1345–1358.

——, 2005: The impact of wave packets propagating across Asia on Pacific cyclone development. *Mon. Wea. Rev.,* **133,** 1998–2015.

——, and D. B. Yu, 1999: Characteristics of wave packets in the

upper troposphere. Part I: Northern Hemisphere winter. *J. Atmos. Sci.,* **56,** 1708–1728.
——, and Y. F. Fu, 2002: Interdecadal variations in Northern Hemisphere winter storm track intensity. *J. Climate,* **15,** 642–658.
——, S. Y. Lee, and K. L. Swanson, 2002: Storm track dynamics. *J. Climate,* **15,** 2163–2183.
Charney, J. G., 1947: The dynamics of long waves in a baroclinic westerly current. *J. Meteor.,* **4,** 136–162.
——, 1973: Planetary fluid dynamics. *Dynamic Meteorology,* P. Morel, Ed., Reidel, 97–352.
——, and P. G. Drazin, 1961: Propagation of planetary-scale disturbances from the lower to the upper atmosphere. *J. Geophys. Res.,* **66,** 83–109.
——, and J. G. DeVore, 1979: Multiple flow equilibria in the atmosphere and blocking. *J. Atmos. Sci.,* **36,** 1205–1216.
——, and D. M. Straus, 1980: Form-drag instability, multiple equilibria, and propagating planetary waves in baroclinic, orographically forced, planetary wave systems. *J. Atmos. Sci.,* **37,** 1157–1176.
——, J. Shukla, and K. C. Mo, 1981: Comparison of a barotropic blocking theory with observation. *J. Atmos. Sci.,* **38,** 762–779.
Cheng, X., and J. M. Wallace, 1993: Cluster analysis of the Northern Hemisphere wintertime 500-hPa height field: Spatial patterns. *J. Atmos. Sci.,* **50,** 2674–2696.
Colucci, S. J., 1985: Explosive cyclogenesis and large-scale circulation changes: Implications for atmospheric blocking. *J. Atmos. Sci.,* **42,** 2701–2717.
——, 1987: Comparative diagnosis of blocking versus nonblocking planetary-scale circulation changes during synoptic-scale cyclogenesis. *J. Atmos. Sci.,* **44,** 124–139.
Compo, G. P., and P. D. Sardeshmukh, 2004: Storm track predictability on seasonal and decadal scales. *J. Climate,* **17,** 3701–3720.
——,——, and C. Penland, 2001: Changes of subseasonal variability associated with El Niño. *J. Climate,* **14,** 3356–3374.
COPES, 2005: The World Climate Research Programme Strategic Framework 2005–2015: Coordinated Observation and Prediction of the Earth System (COPES). WCRP-123, WMO/TDF-1291, World Meteorological Organization, Geneva, Switzerland, 65 pp.
Davis, C. A., and K. A. Emanuel, 1991: Potential vorticity diagnostics of cyclogenesis. *Mon. Wea. Rev.,* **119,** 1929–1953.
Dickson, R. R., and J. Namias, 1976: North American influences on circulation and climate of the North Atlantic sector. *Mon. Wea. Rev.,* **104,** 1255–1265.
Doblas-Reyes, F. J., R. Hagedorn, and T. N. Palmer, 2005: The rationale behind the success of multi-model ensembles in seasonal forecasting. II. Calibration and combination. *Tellus,* **57A,** 234–252.
Dole, R. M., 1982: Persistent anomalies of the extratropical Northern Hemisphere wintertime circulation. Ph.D. thesis, Massachusetts Institute of Technology, 226 pp.
——, 1983: Persistent anomalies of the extratropical Northern Hemisphere wintertime circulation. *Large-Scale Dynamical Processes in the Atmosphere,* B. J. Hoskins and R. P. Pearce, Eds., Academic Press, 95–110.
——, 1986a: The life cycles of persistent anomalies and blocking over the North Pacific. *Advances in Geophysics,* Vol. 29, Academic Press, 31–69.
——, 1986b: Persistent anomalies of the extratropical Northern Hemisphere wintertime circulation: Structure. *Mon. Wea. Rev.,* **114,** 178–207.
——, 1987: Persistent large-scale flow anomalies. Part II: Relationships to variations in synoptic-scale eddy activity and cyclogenesis. *The Nature and Prediction of Extratropical Weather Systems,* Vol. II, European Centre for Medium-Range Weather Forecasts, 73–122.
——, 1989: Life cycles of persistent anomalies. Part I: Evolution of 500 mb height fields. *Mon. Wea. Rev.,* **117,** 177–211.
——, and N. D. Gordon, 1983: Persistent anomalies of the extratropical Northern Hemisphere wintertime circulation: Geographical distribution and regional persistence characteristics. *Mon. Wea. Rev.,* **111,** 1567–1586.
——, and R. X. Black, 1990: Life cycles of persistent anomalies. Part II: The development of persistent negative height anomalies over the North Pacific Ocean. *Mon. Wea. Rev.,* **118,** 824–846.
Eady, E. T., 1949: Long waves and cyclone waves. *Tellus,* **1,** 33–52.
Edmon, H. J., B. J. Hoskins, and M. E. McIntyre, 1980: Eliassen–Palm cross-sections for the troposphere. *J. Atmos. Sci.,* **37,** 2600–2616.
Egger, J., 1977: On the linear theory of the atmospheric response to sea surface temperature anomalies. *J. Atmos. Sci.,* **34,** 603–614.
Eliasen, E., and B. Machenhauer, 1965: A study of the fluctuations of the atmospheric planetary flow patterns represented by spherical harmonics. *Tellus,* **17,** 220–238.
Elliott, R. D., and T. B. Smith, 1949: A study of the effects of large blocking highs on the general circulation of the Northern Hemisphere westerlies. *J. Meteor.,* **6,** 67–85.
Emanuel, K. A., 2001: The contribution of tropical cyclones to the oceans' meridional heat transport. *J. Geophys. Res.,* **106,** 14 777–14 781.
——, 2002: A simple model of multiple climate regimes. *J. Geophys. Res.,* **107,** 4077, doi: 10.1029/2001JD001002.
Epstein, E. S., 1969: A scoring system for probability forecasts of ranked categories. *J. Appl. Meteor.,* **8,** 985–987.
Farrell, B., 1982: The initial growth of disturbances in a baroclinic flow. *J. Atmos. Sci.,* **39,** 1663–1686.
——, 1984: Modal and non-modal baroclinic waves. *J. Atmos. Sci.,* **41,** 668–673.
——, 1985: Transient growth of damped baroclinic waves. *J. Atmos. Sci.,* **42,** 2718–2727.
Feldstein, S. B., 1998: An observational study of the intraseasonal poleward propagation of zonal mean flow anomalies. *J. Atmos. Sci.,* **55,** 2516–2529.
——, 2000: The timescale, power spectra, and climate noise properties of teleconnection patterns. *J. Climate,* **13,** 4430–4440.
——, 2001: Friction torque dynamics associated with intraseasonal length-of-day variability. *J. Atmos. Sci.,* **58,** 2942–2953.
——, 2002: Fundamental mechanisms of the growth and decay of the PNA teleconnection pattern. *Quart. J. Roy. Meteor. Soc.,* **128,** 775–796.
——, and S. Lee, 1998: Is the atmospheric zonal index driven by an eddy feedback? *J. Atmos. Sci.,* **55,** 3077–3086.
Frederiksen, J. S., 1983: A unified three-dimensional instability theory of the onset of blocking and cyclogenesis. Part II: Teleconnection patterns. *J. Atmos. Sci.,* **40,** 2593–2609.
——, and G. Branstator, 2005: Seasonal variability of teleconnection patterns. *J. Atmos. Sci.,* **62,** 1346–1365.
Gershunov, A., 1998: ENSO influence on intraseasonal extreme rainfall and temperature frequencies in the contiguous United States: Implications for long-range predictability. *J. Climate,* **11,** 3192–3203.
——, and T. P. Barnett, 1998: ENSO influence on intraseasonal extreme rainfall and temperature frequencies in the contiguous United States: Observations and model results. *J. Climate,* **11,** 1575–1586.
——, and D. R. Cayan, 2003: Heavy daily precipitation frequency over the contiguous United States: Sources of climatic variability and seasonal predictability. *J. Climate,* **16,** 2752–2765.
Gill, A. E., 1980: Some simple solutions for heat-induced tropical circulation. *Quart. J. Roy. Meteor. Soc.,* **106,** 447–462.
——, 1982: *Atmosphere–Ocean Dynamics.* Academic Press, 662 pp.
Gilman, D. L., 1985: Long-range forecasting—The present and the future. *Bull. Amer. Meteor. Soc.,* **66,** 159–164.
Gray, W. M., 1984a: Atlantic seasonal hurricane frequency. Part I: El Niño and 30 mb quasi-biennial oscillation influences. *Mon. Wea. Rev.,* **112,** 1649–1668.
——, 1984b: Atlantic seasonal hurricane frequency. Part II: Forecasting its variability. *Mon. Wea. Rev.,* **112,** 1669–1683.
Green, J. S. A., 1977: The weather during July 1976: Some dynamical considerations of the drought. *Weather,* **32,** 120–128.

Grose, W. L., and B. J. Hoskins, 1979: Influence of orography on large-scale atmospheric flow. *J. Atmos. Sci.,* **36,** 223–234.
Hagedorn, R., F. J. Doblas-Reyes, and T. N. Palmer, 2005: The rationale behind the success of multi-model ensembles in seasonal forecasting. I. Basic concept. *Tellus,* **57A,** 219–233.
Haines, K., and J. Marshall, 1987: Eddy-forced coherent structures as a prototype of atmospheric blocking. *Quart. J. Roy. Meteor. Soc.,* **113,** 681–704.
Halpert, M. S., and C. F. Ropelewski, 1992: Surface temperature patterns associated with the Southern Oscillation. *J. Climate,* **5,** 577–593.
Hamill, T. M., J. S. Whitaker, and X. Wei, 2004a: Medium-range ensemble ''re-forecasting.'' *Bull. Amer. Meteor. Soc.,* **85,** 507–508.
——, ——, and ——, 2004b: Ensemble reforecasting: Improving medium-range forecast skill using retrospective forecasts. *Mon. Wea. Rev.,* **132,** 1434–1447.
——, ——, and S. L. Mullen, 2006: Reforecasts: An important dataset for improving weather predictions. *Bull. Amer. Meteor. Soc.,* **87,** 33–46.
Hansen, A. R., and T.-C. Chen, 1982: A spectral energetics analysis of atmospheric blocking. *Mon. Wea. Rev.,* **110,** 1146–1165.
——, and A. Sutera, 1986: On the probability density distribution of planetary-scale atmospheric wave amplitude. *J. Atmos. Sci.,* **43,** 3250–3265.
——, and ——, 1988: Planetary wave amplitude bimodality in the Southern Hemisphere. *J. Atmos. Sci.,* **45,** 3771–3783.
Harnik, N., and E. K. M. Chang, 2004: The effects of variations in jet width on the growth of baroclinic waves: Implications for midwinter Pacific storm track variability. *J. Atmos. Sci.,* **61,** 23–40.
Held, I. M., 1983: Stationary and quasi-stationary eddies in the extratropical troposphere: Theory. *Large-scale Dynamical Processes in the Atmosphere,* B. J. Hoskins and R. P. Pearce, Eds., Academic Press, 127–168.
——, and B. J. Hoskins, 1985: Large-scale eddies and the general-circulation of the troposphere. *Advances in Geophysics,* Vol. 28, Academic Press, 3–31.
——, S. W. Lyons, and S. Nigam, 1989: Transients and the extratropical response to El Niño. *J. Atmos. Sci.,* **46,** 163–174.
Hendon, H. H., and M. L. Salby, 1994: The life-cycle of the Madden–Julian Oscillation. *J. Atmos. Sci.,* **51,** 2225–2237.
——, C. Zhang, and J. D. Glick, 1999: Interannual variation of the Madden–Julian Oscillation during austral summer. *J. Climate,* **12,** 2538–2550.
——, B. Liebmann, M. Newman, J. D. Glick, and J. E. Schemm, 2000: Medium-range forecast errors associated with active episodes of the Madden–Julian Oscillation. *Mon. Wea. Rev.,* **128,** 69–86.
Higgins, R. W., and S. D. Schubert, 1993: Low-frequency synoptic-eddy activity in the Pacific storm track. *J. Atmos. Sci.,* **50,** 1672–1690.
——, and ——, 1994: Simulated life-cycles of persistent anticyclonic anomalies over the North Pacific—Role of synoptic-scale eddies. *J. Atmos. Sci.,* **51,** 3238–3260.
——, and ——, 1996: Simulations of persistent North Pacific circulation anomalies and interhemispheric teleconnections. *J. Atmos. Sci.,* **53,** 188–207.
——, and K. C. Mo, 1997: Persistent North Pacific circulation anomalies and the tropical intraseasonal oscillation. *J. Climate,* **10,** 223–244.
——, J. K. E. Schemm, W. Shi, and A. Leetmaa, 2000: Extreme precipitation events in the western United States related to tropical forcing. *J. Climate,* **13,** 793–820.
Hoerling, M. P., and M. Ting, 1994: Organization of extratropical transients during El Niño. *J. Climate,* **7,** 745–766.
——, and A. Kumar, 1997: Origins of extreme climate states during the 1982–83 ENSO winter. *J. Climate,* **10,** 2859–2870.
——, and ——, 2000: Understanding and predicting extratropical teleconnections related to ENSO. *El Niño and the Southern Oscillation: Multiscacle Variability and Global and Regional Impacts,* H. F. Diaz and V. Markgraf, Eds., Cambridge University Press, 57–88.
——, and ——, 2003: The perfect ocean for drought. *Science,* **299,** 691–694.
——, ——, and M. Zhong, 1997: El Niño, La Niña, and the nonlinearity of their teleconnections. *J. Climate,* **10,** 1769–1786.
Holopainen, E., and C. Fortelius, 1987: High-frequency transient eddies and blocking. *J. Atmos. Sci.,* **44,** 1632–1645.
Holton, J. R., 2004. *An Introduction to Dynamic Meteorology.* Elsevier Academic Press, 535 pp.
Horel, J. D., and J. M. Wallace, 1981: Planetary-scale atmospheric phenomena associated with the Southern Oscillation. *Mon. Wea. Rev.,* **109,** 813–829.
Hoskins, B. J., 1983: Dynamical processes in the atmosphere and the use of models. *Quart. J. Roy. Meteor. Soc.,* **109,** 1–21.
——, and D. J. Karoly, 1981: The steady linear response of a spherical atmosphere to thermal and orographic forcing. *J. Atmos. Sci.,* **38,** 1179–1196.
——, and P. D. Sardeshmukh, 1987: A diagnostic study of the dynamics of the Northern-Hemisphere winter of 1985–86. *Quart. J. Roy. Meteor. Soc.,* **113,** 759–778.
——, and T. Ambrizzi, 1993: Rossby-wave propagation on a realistic longitudinally varying flow. *J. Atmos. Sci.,* **50,** 1661–1671.
——, A. J. Simmons, and D. G. Andrews, 1977: Energy dispersion in a barotropic atmosphere. *Quart. J. Roy. Meteor. Soc.,* **103,** 553–567.
——, I. N. James, and G. H. White, 1983: The shape, propagation and mean-flow interaction of large-scale weather systems. *J. Atmos. Sci.,* **40,** 1595–1612.
——, M. E. McIntyre, and A. W. Robertson, 1985: On the use and significance of isentropic potential vorticity maps. *Quart. J. Roy. Meteor. Soc.,* **111,** 877–946.
Houtekamer, P. L., L. Lefaivre, J. Derome, H. Ritchie, and H. L. Mitchell, 1996: A system simulation approach to ensemble prediction. *Mon. Wea. Rev.,* **124,** 1225–1242.
Hsu, H. H., 1987: Propagation of low-level circulation features in the vicinity of mountain-ranges. *Mon. Wea. Rev.,* **115,** 1864–1892.
——, and J. M. Wallace, 1985: Vertical structure of wintertime teleconnection patterns. *J. Atmos. Sci.,* **42,** 1693–1710.
Illari, L., 1984: A diagnostic study of the potential vorticity in a warm blocking anticyclone. *J. Atmos. Sci.,* **41,** 3518–3526.
Iskenderian, H., 1995: A 10-year climatology of Northern Hemisphere tropical cloud plumes and their composite flow patterns. *J. Climate,* **8,** 1630–1637.
James, I., 1987: Suppression of baroclinic instability in horizontally sheared flows. *J. Atmos. Sci.,* **44,** 3710–3720.
Jones, C., D. E. Waliser, J. K. E. Schemm, and W. K. M. Lau, 2000: Prediction skill of the Madden and Julian Oscillation in dynamical extended range forecasts. *Climate Dyn.,* **16,** 273–289.
——, ——, K. M. Lau, and W. Stern, 2004: The Madden–Julian oscillation and its impact on Northern Hemisphere weather predictability. *Mon. Wea. Rev.,* **132,** 1462–1471.
Kalnay, E., 2003: *Atmospheric Modeling, Data Assimilation, and Predictability.* Cambridge University Press, 341 pp.
——, S. J. Lord, and R. D. McPherson, 1998: Maturity of operational numerical weather prediction: Medium range. *Bull. Amer. Meteor. Soc.,* **79,** 2753–2769.
Kessler, W. S., and R. Kleeman, 2000: Rectification of the Madden–Julian oscillation into the ENSO cycle. *J. Climate,* **13,** 3560–3575.
Kiladis, G. N., 1998: Observations of Rossby waves linked to convection over the eastern tropical Pacific. *J. Atmos. Sci.,* **55,** 321–339.
——, and H. F. Diaz, 1989: Global climatic anomalies associated with extremes in the Southern Oscillation. *J. Climate,* **2,** 1069–1090.
——, and K. M. Weickmann, 1992a: Circulation anomalies associated

with tropical convection during northern winter. *Mon. Wea. Rev.,* **120,** 1900–1923.
——, and ——, 1992b: Extratropical forcing of tropical Pacific convection during northern winter. *Mon. Wea. Rev.,* **120,** 1924–1938.
——, and ——, 1997: Horizontal structure and seasonality of large-scale circulations associated with submonthly tropical convection. *Mon. Wea. Rev.,* **125,** 1997–2013.
Klein, W. H., 1952: Some empirical characteristics of long waves on monthly mean charts. *Mon. Wea. Rev.,* **80,** 203–219.
Klotzbach, P. J., and W. M. Gray, 2003: Forecasting September Atlantic basin tropical cyclone activity. *Wea. Forecasting,* **18,** 1109–1128.
——, and ——, 2004: Updated 6–11-month prediction of Atlantic basin seasonal hurricane activity. *Wea. Forecasting,* **19,** 917–934.
Knutson, T. R., and K. M. Weickmann, 1987: 30–60 day atmospheric oscillations—Composite life-cycles of convection and circulation anomalies. *Mon. Wea. Rev.,* **115,** 1407–1436.
Kok, C. J., and J. D. Opsteegh, 1985: Possible causes of anomalies in seasonal mean circulation patterns during the 1982–83 El Niño event. *J. Atmos. Sci.,* **42,** 677–694.
Krishnamurti, T. N., and Coauthors, 2003: Improved skill for the anomaly correlation of geopotential heights at 500 hPa. *Mon. Wea. Rev.,* **131,** 1082–1102.
Kumar, A., and M. P. Hoerling, 1997: Interpretation and implications of the observed inter-El Niño variability. *J. Climate,* **10,** 83–91.
——, and ——, 2003: The nature and causes for the delayed atmospheric response to El Niño. *J. Climate,* **16,** 1391–1403.
Kushnir, Y., and J. M. Wallace, 1989: Low-frequency variability in the Northern Hemisphere winter: Geographical distribution, structure and time-scale dependence. *J. Atmos. Sci.,* **46,** 3122–3142.
Lau, K. M., and P. H. Chan, 1985: Aspects of the 40–50 day oscillation during the Northern winter as inferred from outgoing longwave radiation. *Mon. Wea. Rev.,* **113,** 1889–1909.
Lau, N. C., 1978: Three-dimensional structure of observed transient eddy statistics of Northern Hemisphere wintertime circulation. *J. Atmos. Sci.,* **35,** 1900–1923.
——, 1979: Structure and energetics of transient disturbances in the Northern Hemisphere wintertime circulation. *J. Atmos. Sci.,* **36,** 982–995.
——, 1985: Modeling the seasonal dependence of the atmospheric response to observed El Niños in 1972–76. *Mon. Wea. Rev.,* **113,** 1970–1996.
——, 1988: Variability of the observed midlatitude storm tracks in relation to low-frequency changes in the circulation pattern. *J. Atmos. Sci.,* **45,** 2718–2743.
——, and J. M. Wallace, 1979: Distribution of horizontal transports by transient eddies in the Northern Hemisphere wintertime circulation. *J. Atmos. Sci.,* **36,** 1844–1861.
——, and E. O. Holopainen, 1984: Transient eddy forcing of the time-mean flow as identified by geopotential tendencies. *J. Atmos. Sci.,* **41,** 313–328.
——, and M. J. Nath, 1991: Variability of the baroclinic and barotropic transient eddy forcing associated with monthly changes in the midlatitude storm tracks. *J. Atmos. Sci.,* **48,** 2589–2613.
Lee, S., 1995a: Linear modes and storm tracks in a two-level primitive equation model. *J. Atmos. Sci.,* **52,** 1841–1862.
——, 1995b: Localized storm tracks in the absence of local instability. *J. Atmos. Sci.,* **52,** 977–989.
——, and I. M. Held, 1993: Baroclinic wave-packets in models and observations. *J. Atmos. Sci.,* **50,** 1413–1428.
Lin, J. L., and Coauthors, 2006: Tropical intraseasonal variability in 14 IPCC AR4 climate models. Part I: Convective signals. *J. Climate,* **19,** 2665–2690.
Lorenz, E. N., 1963: Deterministic nonperiodic flow. *J. Atmos. Sci.,* **20,** 130–141.
——, 1965: A study of the predictability of a 28-variable atmospheric model. *Tellus,* **17,** 321–333.
——, 1968a: The predictability of a flow which possesses many scales of motion. *Tellus,* **21,** 289–307.
——, 1969b: Atmospheric predictability as revealed by naturally occurring analogues. *J. Atmos. Sci.,* **26,** 636–646.
Madden, R. A., and P. R. Julian, 1971: Detection of a 40–50 day oscillation in the zonal wind in the tropical Pacific. *J. Atmos. Sci.,* **28,** 702–708.
——, and ——, 1972: Description of global-scale circulation cells in the Tropics with a 40–50 day period. *J. Atmos. Sci.,* **29,** 1109–1123.
——, and ——, 1994: Observations of the 40–50-day tropical oscillation—A review. *Mon. Wea. Rev.,* **122,** 814–837.
Mak, M., and M. Cai, 1989: Local barotropic instability. *J. Atmos. Sci.,* **46,** 3289–3311.
McPhaden, M. J., 2004: Evolution of the 2002/03 El Niño. *Bull. Amer. Meteor. Soc.,* **85,** 677–695.
McWilliams, J. C., 1980: An application of equivalent modons to atmospheric blocking. *Dyn. Atmos. Oceans,* **5,** 43–66.
Mo, K. C., 1999: Alternating wet and dry episodes over California and intraseasonal oscillations. *Mon. Wea. Rev.,* **127,** 2759–2776.
——, and R. E. Livezey, 1986: Tropical–extratropical geopotential height teleconnections during the Northern Hemisphere winter. *Mon. Wea. Rev.,* **114,** 2488–2515.
——, and R. W. Higgins, 1998a: Tropical convection and precipitation regimes in the western United States. *J. Climate,* **11,** 2404–2423.
——, and ——, 1998b: Tropical influences on California precipitation. *J. Climate,* **11,** 412–430.
Molteni, F., S. Tibaldi, and T. N. Palmer, 1990: Regimes in the wintertime circulation over northern extratropics. 1. Observational evidence. *Quart. J. Roy. Meteor. Soc.,* **116,** 31–67.
——, R. Buizza, T. N. Palmer, and T. Petroliagis, 1996: The ECMWF ensemble prediction system: Methodology and validation. *Quart. J. Roy. Meteor. Soc.,* **122,** 73–119.
Morgan, M. C., and J. W. Nielsen-Gammon, 1998: Using tropopause maps to diagnose midlatitude weather systems. *Mon. Wea. Rev.,* **126,** 2555–2579.
Mullen, S. L., 1986: The local balances of vorticity and heat for blocking anticyclones in a spectral general-circulation model. *J. Atmos. Sci.,* **43,** 1406–1441.
——, 1987: Transient eddy forcing of blocking flows. *J. Atmos. Sci.,* **44,** 3–22.
——, 1989: Model experiments on the impact of Pacific sea surface temperature anomalies on blocking frequency. *J. Climate,* **2,** 997–1013.
Murphy, A. H., 1971: A note on the ranked probability score. *J. Appl. Meteor.,* **10,** 155–156.
Nakamura, H., 1992: Midwinter suppression of baroclinic wave activity in the Pacific. *J. Atmos. Sci.,* **49,** 1629–1642.
——, and J. M. Wallace, 1990: Observed changes in baroclinic wave activity during the life-cycles of low-frequency circulation anomalies. *J. Atmos. Sci.,* **47,** 1100–1116.
——, and ——, 1993: Synoptic behavior of baroclinic eddies during the blocking onset. *Mon. Wea. Rev.,* **121,** 1892–1903.
——, M. Nakamura, and J. L. Anderson, 1997: The role of high- and low-frequency dynamics in blocking formation. *Mon. Wea. Rev.,* **125,** 2074–2093.
——, T. Izumi, and T. Sampe, 2002: Interanual and decadal modulations recently observed in the Pacific storm track activity and East Asian winter monsoon. *J. Climate,* **15,** 1855–1874.
Nakazawa, T., 1988: Tropical super clusters within intraseasonal variations over the western Pacific. *J. Meteor. Soc. Japan,* **66,** 823–839.
Namias, J., 1947: Physical nature of some fluctuations in the speed of the zonal circulation. *J. Meteor.,* **4,** 125–133.
——, 1950: The index cycle and its role in the general circulation. *J. Meteor.,* **7,** 130–139.
——, and P. F. Clapp, 1944: Studies of the motion and development of long waves in the westerlies. *J. Meteor.,* **1,** 57–77.
National Research Council, 1996: *Learning to Predict Climate Variations Associated with El Niño and the Southern Oscillation:*

Accomplishments and Legacies of the TOGA Program. National Academy Press, 171 pp.

Neilley, P. P., 1990: Interaction between synoptic-scale eddies and the large-scale flow during the life cycles of persistent flow anomalies. Ph.D. disseration, Massachusetts Institute of Technology, 272 pp. [Available from Department of Earth Atmospheric and Planetary Sciences, Massachusetts Institue of Technology, Cambridge, MA 02139.]

Newell, R. E., N. E. Newell, Y. Zhu, and C. Scott, 1992: Tropospheric rivers—A pilot study. *Geophys. Res. Lett.,* **19,** 2401–2404.

Newman, M., and P. D. Sardeshmukh, 1998: The impact of the annual cycle on the North Pacific–North American response to remote low-frequency forcing. *J. Atmos. Sci.,* **55,** 1336–1353.

——, ——, C. R. Winkler, and J. S. Whitaker, 2003: A study of subseasonal predictability. *Mon. Wea. Rev.,* **131,** 1715–1732.

Nitsche, G., J. M. Wallace, and C. Kooperberg, 1994: Is there evidence of multiple equilibria in planetary wave amplitude statistics. *J. Atmos. Sci.,* **51,** 314–322.

Opsteegh, J. D., and H. M. Van Den Dool, 1980: Seasonal differences in the stationary response of a linearized primitive equation model: Prospects for long-range weather forecasting? *J. Atmos. Sci.,* **37,** 2169–2185.

Orlanski, I., 2005: A new look at the Pacific storm track variability: Sensitivity to tropical SSTs and to upstream seeding. *J. Atmos. Sci.,* **62,** 1367–1390.

Owens, B. F., and C. W. Landsea, 2003: Assessing the skill of operational Atlantic seasonal tropical cyclone forecasts. *Wea. Forecasting,* **18,** 45–54.

Palmen, E., and C. W. Newton, 1969: *Atmospheric Circulation Systems.* Academic Press, 603 pp.

Palmer, T. N., 1998: Nonlinear dynamics and climate change: Rossby's legacy. *Bull. Amer. Meteor. Soc.,* **79,** 1411–1423.

——, 1999: A nonlinear dynamical perspective on climate prediction. *J. Climate,* **12,** 575–591.

——, and D. A. Mansfield, 1984: Response of two atmospheric general circulation models to sea-surface temperatures in the tropical East and West Pacific. *Nature,* **310,** 483–485.

——, F. J. Doblas-Reyes, R. Hagedorn, and A. Weisheimer, 2005a: Probabilistic prediction of climate using multi-model ensembles: From basics to applications. *Philos. Trans. Roy. Soc.,* **360,** 1991–1998.

——, G. J. Shutts, R. Hagedorn, F. J. Doblas-Reyes, T. Jung, and M. Leutbecher, 2005b: Representing model uncertainty in weather and climate prediction. *Annu. Rev. Earth Planet. Sci.,* **33,** 163–193.

Pedlosky, J., 1979: *Geophysical Fluid Dynamics.* Springer-Verlag, 624 pp.

Pelly, J. L., and B. J. Hoskins, 2003: A new perspective on blocking. *J. Atmos. Sci.,* **60,** 743–755.

Penland, C., and T. Magorian, 1993: Prediction of Niño-3 sea surface temperatures using linear inverse modeling. *J. Climate,* **6,** 1067–1076.

——, and P. D. Sardeshmukh, 1995: The optimal growth of tropical sea surface temperature anomalies. *J. Climate,* **8,** 1999–2024.

——, and L. Matrosova, 1998: Prediction of tropical Atlantic sea surface temperatures using linear inverse modeling. *J. Climate,* **11,** 483–496.

Persson, P. O. G., P. J. Neiman, B. Walter, J. W. Bao, and F. M. Ralph, 2005: Contributions from California coastal-zone surface fluxes to heavy coastal precipitation: A CALJET case study during the strong El Niño of 1998. *Mon. Wea. Rev.,* **133,** 1175–1198.

Petterssen, S., 1955: A general survey of some factors influencing development at sea level. *J. Meteor.,* **12,** 36–42.

——, 1956: *Weather Forecasting and Analysis.* Vol. 1, McGraw-Hill, 428 pp.

Philander, S. G., 1990: *El Niño, La Niña, and the Southern Oscillation.* Academic Press, 293 pp.

Piani, C., D. J. Frame, D. A. Stainforth, and M. R. Allen, 2005: Constraints on climate change from a multi-thousand member ensemble of simulations. *Geophys. Res. Lett.,* **32,** L23825, doi: 10.1029/2005GL024452.

Platzman, G. W., 1968: The Rossby wave. *Quart. J. Roy. Meteor. Soc.,* **94,** 225–248.

Plumb, R. A., 1985: On the three-dimensional propagation of stationary waves. *J. Atmos. Sci.,* **42,** 217–229.

——, 1986: Three-dimensional propagation of transient quasi-geostrophic eddies and its relationship with the eddy forcing of the time-mean flow. *J. Atmos. Sci.,* **43,** 1657–1678.

Ralph, F. M., P. J. Neiman, D. E. Kingsmill, P. O. G. Persson, A. B. White, E. T. Strem, E. D. Andrews, and R. C. Antweiler, 2003: The impact of a prominent rain shadow on flooding in California's Santa Cruz Mountains: A CALJET case study and sensitivity to the ENSO cycle. *J. Hydrometeor.,* **4,** 1243–1264.

——,——, and G. A. Wick, 2004: Satellite and CALJET aircraft observations of atmospheric rivers over the eastern North Pacific Ocean during the winter of 1997/98. *Mon. Wea. Rev.,* **132,** 1721–1745.

——, ——, and R. Rotunno, 2005: Dropsonde observations in low-level jets over the northeastern Pacific Ocean from CALJET-1998 and PACJET-2001: Mean vertical profile and atmospheric river characteristics. *Mon. Wea. Rev.,* **133,** 889–910.

Rasmusson, E. M., and J. M. Wallace, 1983: Meteorological aspects of the El Niño–Southern Oscillation. *Science,* **222,** 1195–1202.

Reinhold, B. B., and R. T. Pierrehumbert, 1982: Dynamics of weather regimes: Quasi-stationary waves and blocking. *Mon. Wea. Rev.,* **110,** 1105–1145.

Renwick, J. A., and J. M. Wallace, 1996: Relationships between North Pacific wintertime blocking, El Niño, and the PNA pattern. *Mon. Wea. Rev.,* **124,** 2071–2076.

Rex, D., 1950a: Blocking action in the middle troposphere and its effects on regional climate. I. An aerological study of blocking. *Tellus,* **2,** 196–211.

——, 1950b: Blocking action in the middle troposphere and its effects on regional climate. II. The climatology of blocking action. *Tellus,* **2,** 275–301.

Rogers, J. C., 1981: Spatial variability of seasonal sea-level pressure and 500 mb height anomalies. *Mon. Wea. Rev.,* **109,** 2093–2106.

Ropelewski, C. F., and M. S. Halpert, 1987: Global and regional scale precipitation patterns associated with the El Niño–Southern Oscillation. *Mon. Wea. Rev.,* **115,** 1606–1626.

——, and ——, 1989: Precipitation patterns associated with the high index phase of the Southern Oscillation. *J. Climate,* **2,** 268–284.

——, ——, and X. Wang, 1992: Observed tropospheric biennial variability and its relationship to the Southern Oscillation. *J. Climate,* **5,** 594–614.

Rossby, C. G., and Coauthors, 1939: Relations between variations in the intensity of the zonal circulation of the atmosphere and the displacements of the semi-permanent centers of actions. *Tellus,* **2,** 275–301.

Salby, M. L., R. R. Garcia, and H. H. Hendon, 1994: Planetary-scale circulations in the presence of climatological and wave-induced heating. *J. Atmos. Sci.,* **51,** 2344–2367.

Sanders, F., 1973: Skill in forecasting daily temperature and precipitation—Some experimental results. *Bull. Amer. Meteor. Soc.,* **54,** 1171–1179.

——, 1979: Trends in skill of daily forecasts of temperature and precipitation, 1966–78. *Bull. Amer. Meteor. Soc.,* **60,** 763–769.

——, 1988: Life history of mobile troughs in the upper westerlies. *Mon. Wea. Rev.,* **116,** 2629–2648.

——, and J. R. Gyakum, 1980: Synoptic-dynamic climatology of the ''bomb.'' *Mon. Wea. Rev.,* **108,** 1589–1606.

Sardeshmukh, P. D., 1993: The baroclinic chi problem and its application to the diagnosis of atmospheric heating rates. *J. Atmos. Sci.,* **50,** 1099–1112.

——, and B. J. Hoskins, 1988: The generation of global rotational flow by steady idealized tropical divergence. *J. Atmos. Sci.,* **45,** 1228–1251.

——, M. Newman, and M. D. Borges, 1997: Free barotropic Rossby

wave dynamics of the wintertime low-frequency flow. *J. Atmos. Sci.,* **54,** 5–23.
——, G. P. Compo, and C. Penland, 2000: Changes of probability associated with El Niño. *J. Climate,* **13,** 4268–4286.
Sawyer, J. S., 1970: Observational characteristics of atmospheric fluctuations with a time scale of a month. *Quart. J. Roy. Meteor. Soc.,* **96,** 610–625.
Schonher, T., and S. E. Nicholson, 1989: The relationship between California rainfall and ENSO events. *J. Climate,* **2,** 1258–1269.
Schubert, S. D., 1986: The structure, energetics, and evolution of the dominant frequency-dependent three-dimensional atmospheric modes. *J. Atmos. Sci.,* **43,** 1210–1237.
——, Y. Chang, M. Suarez, and P. Pegion, 2005: On the relationship between ENSO and extreme weather over the contiguous U. S. *U.S. CLIVAR Variations,* **3,** 1–4.
Shapiro, M. A., H. Wernli, N. A. Bond, and R. Langland, 2001: The influence of the 1997–99 El Niño–Southern Oscillation on extratropical baroclinic life cycles over the eastern North Pacific. *Quart. J. Roy. Meteor. Soc.,* **127,** 331–342.
Shutts, G. J., 1986: A case study of eddy forcing during an Atlantic blocking episode. *Advances in Geophysics,* Vol. 29, Academic Press, 135–162.
Simmons, A. J., 1982: The forcing of stationary wave motion by tropical diabatic heating. *Quart. J. Roy. Meteor. Soc.,* **108,** 503–534.
——, and A. Hollingsworth, 2002: Some aspects of the improvement in skill of numerical weather prediction. *Quart. J. Roy. Meteor. Soc.,* **128,** 647–677.
——, J. M. Wallace, and G. W. Branstator, 1983: Barotropic wave-propagation and instability, and atmospheric teleconnection patterns. *J. Atmos. Sci.,* **40,** 1363–1392.
Stainforth, D., J. Kettleborough, M. Allen, M. Collins, A. Heaps, and J. Murphy, 2002: Distributed computing for public-interest climate modeling research. *Comput. Sci. Eng.,* **4,** 82–89.
Straus, D. M., and J. Shukla, 2002: Does ENSO force the PNA? *J. Climate,* **15,** 2340–2358.
Sumner, E. J., 1954: A study of blocking in the Atlantic-European sector of the Northern Hemisphere. *Quart. J. Roy. Meteor. Soc.,* **80,** 402–416.
Thompson, D. W. J., and J. M. Wallace, 1998: The Arctic Oscillation signature in the wintertime geopotential height and temperature fields. *Geophys. Res. Lett.,* **25,** 1297–1300.
——, and ——, 2000: Annular modes in the extratropical circulation. Part I: Month-to-month variability. *J. Climate,* **13,** 1000–1016.
——, and ——, 2001: Regional climate impacts of the Northern Hemisphere annular mode. *Science,* **293,** 85–89.
——, M. P. Baldwin, and J. M. Wallace, 2002: Stratospheric connection to Northern Hemisphere wintertime weather: Implications for prediction. *J. Climate,* **15,** 1421–1428.
Thorncroft, C. D., B. J. Hoskins, and M. F. McIntyre, 1993: Two paradigms of baroclinic-wave life-cycle behavior. *Quart. J. Roy. Meteor. Soc.,* **119,** 17–55.
THORPEX, 2004: A global atmospheric research programme for the beginning of the 21st century. *WMO Bulletin,* Vol. 54, No. 3.
Tracton, M. S., 1990: Predictability and its relationship to scale interaction processes in blocking. *Mon. Wea. Rev.,* **118,** 1666–1695.
——, and E. Kalnay, 1993: Operational ensemble prediction at the National Meteorological Center—Practical aspects. *Wea. Forecasting,* **8,** 379–398.
Trenberth, K. E., 1976: Fluctuations and trends in indexes of Southern Hemispheric circulation. *Quart. J. Roy. Meteor. Soc.,* **102,** 65–75.
——, 1986: An assessment of the impact of transient eddies on the zonal flow during a blocking episode using localized Eliassen–Palm flux diagnostics. *J. Atmos. Sci.,* **43,** 2070–2087.
——, 1997a: Short-term climate variations: Recent accomplishments and issues for future progress. *Bull. Amer. Meteor. Soc.,* **78,** 1081–1096.
——, 1997b: The definition of El Niño. *Bull. Amer. Meteor. Soc.,* **78,** 2771–2777.
——, and D. J. Shea, 1987: On the evolution of the Southern Oscillation. *Mon. Wea. Rev.,* **115,** 3078–3096.
——, and D. P. Stepaniak, 2001: Indices of El Niño evolution. *J. Climate,* **14,** 1697–1701.
——, G. W. Branstator, D. Karoly, A. Kumar, N. C. Lau, and C. Ropelewski, 1998: Progress during TOGA in understanding and modeling global teleconnections associated with tropical sea surface temperatures. *J. Geophys. Res.,* **103C,** 14 291–14 324.
Tung, K. K., and R. S. Lindzen, 1979a: A theory of stationary long waves. Part I: A simple theory of blocking. *Mon. Wea. Rev.,* **107,** 714–734.
——, and ——, 1979b: A theory of stationary long waves. Part II: Resonant Rossby waves in the presence of realistic vertical shears. *Mon. Wea. Rev.,* **107,** 735–750.
van Loon, H., and J. C. Rogers, 1978: the seesaw in winter temperatures between Greenland and Northern Europe. Part I: General description. *Mon. Wea. Rev.,* **106,** 296–310.
Vitart, F., and T. N. Stockdale, 2001: Seasonal forecasting of tropical storms using coupled GCM integrations. *Mon. Wea. Rev.,* **129,** 2521–2537.
Walker, G. T., 1924: Correlation in seasonal variations of weather. IX. A further study of world weather. *Memo. Indian Meteor. Dept.,* **24,** 275–332.
——, and E. W. Bliss, 1932: World Weather V. *Memo. Roy. Meteor. Soc.,* **4,** 53–84.
Waliser, D. E., C. Jones, J. K. E. Schemm, and N. E. Graham, 1999: A statistical extended-range tropical forecast model based on the slow evolution of the Madden–Julian oscillation. *J. Climate,* **12,** 1918–1939.
——, K. M. Lau, W. Stern, and C. Jones, 2003: Potential predictability of the Madden–Julian oscillation. *Bull. Amer. Meteor. Soc.,* **84,** 33–50.
Wallace, J. M., and D. S. Gutzler, 1981: Teleconnections in the geopotential height field during the Northern Hemisphere winter. *Mon. Wea. Rev.,* **109,** 784–812.
——, and N. C. Lau, 1985: On the role of barotropic energy conversions in the general circulation. *Advances in Geophysics,* Vol. 28, Academic Press, 33–74.
——, and D. W. J. Thompson, 2002a: Annular modes and climate prediction. *Phys. Today,* **55,** 28–33.
——, and ——, 2002b: The Pacific center of action of the Northern Hemisphere annular mode: Real or artifact? *J. Climate,* **15,** 1987–1991.
——, G. H. Lim, and M. L. Blackmon, 1988: Relationship between cyclone tracks, anticyclone tracks, and baroclinic wave-guides. *J. Atmos. Sci.,* **45,** 439–462.
——, E. M. Rasmusson, T. P. Mitchell, V. E. Kousky, E. S. Sarachik, and H. von Storch, 1998: The structure and evolution of ENSO-related climate variability in the tropical Pacific: Lessons from TOGA. *J. Geophys. Res.,* **103** (C7), 14 241–14 259.
Wang, B., and T. Li, 1994: Convective interaction with boundary-layer dynamics in the development of a tropical intraseasonal system. *J. Atmos. Sci.,* **51,** 1386–1400.
Webster, P. J., 1981: Mechanisms determining the atmospheric response to sea surface temperature anomalies. *J. Atmos. Sci.,* **38,** 554–571.
——, and J. R. Holton, 1982: Cross-equatorial response to middle-latitude forcing in a zonally varying basic state. *J. Atmos. Sci.,* **39,** 722–733.
——, and C. Hoyos, 2004: Prediction of monsoon rainfall and river discharge on 15–30-day time scales. *Bull. Amer. Meteor. Soc.,* **85,** 1745–1765.
Weickmann, K., 1983: Intraseasonal circulation and outgoing longwave radiation modes during Northern Hemisphere winter. *Mon. Wea. Rev.,* **111,** 1838–1858.
——, 2003: Mountains, the global frictional torque, and the circulation over the Pacific–North American region. *Mon. Wea. Rev.,* **131,** 2608–2622.

——, and P. D. Sardeshmukh, 1994: The atmospheric angular momentum cycle associated with a Madden–Julian oscillation. *J. Atmos. Sci.,* **51,** 3194–3208.

——, and E. Berry, 2007: A synoptic–dynamic model of subseasonal atmospheric variability. *Mon. Wea. Rev.,* **135,** 449–474.

——, G. R. Lussky, and J. E. Kutzbach, 1985: Intraseasonal (30–60 day) fluctuations of outgoing longwave radiation and 250 mb streamfunction during northern winter. *Mon. Wea. Rev.,* **113,** 941–961.

——, G. N. Kiladis, and P. D. Sardeshmukh, 1997: The dynamics of intraseasonal atmospheric angular momentum oscillations. *J. Atmos. Sci.,* **54,** 1445–1461.

Wheeler, M., and G. N. Kiladis, 1999: Convectively coupled equatorial waves: Analysis of clouds and temperature in the wavenumber-frequency domain. *J. Atmos. Sci.,* **56,** 374–399.

——, and K. M. Weickmann, 2001: Real-time monitoring and prediction of modes of coherent synoptic to intraseasonal tropical variability. *Mon. Wea. Rev.,* **129,** 2677–2694.

——, G. N. Kiladis, and P. J. Webster, 2000: Large-scale dynamical fields associated with convectively coupled equatorial waves. *J. Atmos. Sci.,* **57,** 613–640.

Whitaker, J. S., and R. M. Dole, 1995: Organization of storm tracks in zonally varying flows. *J. Atmos. Sci.,* **52,** 1178–1191.

——, and P. D. Sardeshmukh, 1998: A linear theory of extratropical synoptic eddy statistics. *J. Atmos. Sci.,* **55,** 237–258.

——, and K. M. Weickmann, 2001: Subseasonal variations of tropical convection and week-2 prediction of wintertime western North American rainfall. *J. Climate,* **14,** 3279–3288.

Wilks, D. S., 2006: *Statistical Methods in the Atmospheric Sciences.* 2d ed. Academic Press, 627 pp.

Willett, H. C., 1949: Long-period fluctuations of the general circulation of the atmosphere. *J. Meteor.,* **6,** 34–50.

Winkler, C. R., M. Newman, and P. D. Sardeshmukh, 2001: A linear model of wintertime low-frequency variability. Part I: Formulation and forecast skill. *J. Climate,* **14,** 4474–4494.

Wyrtki, K., 1975: El Niño—The dynamic response of the equatorial Pacific Ocean to atmospheric forcing. *J. Phys. Oceanogr.,* **5,** 572–584.

Zebiak, S. E., and M. A. Cane, 1987: A model El Niño–Southern Oscillation. *Mon. Wea. Rev.,* **115,** 2262–2278.

——., 2005: Madden–Julian oscillation. *Rev. Geophys.,* **43,** RG2003, doi: 10.1029/2004RG000158.

Zhang, C., and J. Gottschalck, 2002: SST anomalies of ENSO and the Madden–Julian Oscillation in the Equatorial Pacific. *J. Climate,* **15,** 2429–2445.

Zhang, Y., and I. M. Held, 1999: A linear stochastic model of a GCM's midlatitude storm tracks. *J. Atmos. Sci.,* **56,** 3416–3435.

Zhu, Y., and R. E. Newell, 1998: A proposed algorithm for moisture fluxes from atmospheric rivers. *Mon. Wea. Rev.,* **126,** 725–735.

——, ——, and W. G. Read, 2000: Factors controlling upper-troposphere water vapor. *J. Climate,* **13,** 836–848.